Project

Validation of coastal forecasts

Reference: MyWave-xxxxxxxxx

Project N°: FP7-SPACE-2011-284455	**Work programme topic:** SPA.2011.1.5.03 – R&D to enhance future GMES applications in the Marine and Atmosphere areas
Start Date of project : 01.01-2012	**Duration**: 36 Months

WP leader: Deltares	**Issue:**
Contributors : KNMI, HZG, CNR, ISMAR, AEMET and PdE	
MyWave version scope : <all project versions> or <version x>	
Approval Date :	**Approver:**
Dissemination level: PU	

DOCUMENT

VERIFICATION AND DISTRIBUTION LIST

	Name	Work Package	Date
Checked By:			
Distribution			

CHANGE RECORD

Issue	Date	§	Description of Change	Author	Checked By
0.1	3-9-2014	all	First draft of table of contents	Martin Verlaan	
0.2	19-12-2014		Contributions from all partners	Gert-Jan Marseille, Paolo Pezzutto, Marta Gomez, Joanna Staneva, Sofia Caires	Martin Verlaan
1.0	27-2-2015		Draft version	Gert-Jan Marseille, Paolo Pezzutto, Marta Gomez, Joanna Staneva, Sofia Caires Martin Verlaan, Ad Stoffelen	
1.1	2-3-2015		Final version	Gert-Jan Marseille, Paolo Pezzutto, Marta Gomez, Cristina Toledano Lozano, Sofia Caires, Ad Stoffelen	Martin Verlaan

TABLE OF CONTENTS

LIST OF FIGURES

LIST OF TABLES

GLOSSARY AND ABREVIATIONS

3D-Var	Three-dimensional variational analysis
4D-Var	Four-dimensional variational analysis
ARPAL	Liguria (Italy) Regional Environmental Protection agency
CNR	National (Italy) Research Council
DA	Data assimilation
EnKF	Ensemble Kalman Filter
HARMONIE	Hirlam Aladin Research on Meso-scale Operational Nwp In Euromed
HCMR	Hellenic Centre Marine Research
HZG	Helmholtz-Zentrum Geesthacht
H_s or H_{m0}	Significant wave height
ISMAR	(CNR) MARine Sciences Institute
ISPRA	Istituto Superiore PRotezione Ambiente
KNMI	Koninklijk Nederlands Meteorologisch Instituut (Royal Dutch Meteorological Institute)
NN	Neural Network
PdE	Puertos de l'Estado
RON	Italian National wave sensors network
SWAN	Simulating Waves Nearshore
$T_{m-1,0}$ or T_{m1}	Mean wave period
WAM	WAve Modelling

APPLICABLE AND REFERENCE DOCUMENTS

Applicable Documents

	Ref	Title	Date / Issue
DA 1	MyWave-A1	MyWave: Annex I – “Description of Work	September 2011

Reference Documents

	Ref	Title	Date / Issue
DR 1	MyWave-D2.1	Near-shore scatterometer wind product	28/3/2014
DR 2	MyWave-D2.2	Assimilation Methodologies, MyWave Report D2.2	10/1/2014

I INTRODUCTION

I.1 Framework

Work package 2 (WP2) of the MyWave project focusses on increasing the use of earth observations by improving data processing algorithms and data assimilation systems for ocean waves. Aiming at the exploration of new methodologies in data assimilation, improvement of the use of near-shore satellite data and connection of large-scale forecast and near-shore forecasts. Its ultimate goal is to use improved data processing and data assimilation methods to obtain better wave forecasts from regional or coastal high-resolution models.

I.2 Motivation

Many off-shore and coastal activities are influenced by wind-generated waves. Since a relatively large part of these activities are near the coast, wave forecasts in these areas are crucial for safety at sea and optimal economic use. This work package (WP2) of the MyWave project studies a number of methods to further increase the accuracy and reliability of coastal wave forecasts. The activities can roughly be divided in three groups:

1. Assimilation of observations
2. Use of high-resolution wind forecasts and use of wave models with a high resolution near the coast
3. Improving our understanding of the largest uncertainties in the forecasts through the use of triple collocation.

Data assimilation has seen a strong development of new methods recently. Application of these new insights, mainly from meteorology and oceanography, to wave forecasting can improve the amount of information extracted from observations. Here, we consider a number of different types of observations: in-situ observations by downward looking radars or wave buoys, coastal HF-radar and space-borne scatterometer observations of wind speed. Space-borne observations by altimeter and SAR were used for validation and triple collocation (WP 2.1 and 2.2.2).

Regional wind and wave forecasts for the considered study areas have been compared with scatterometer winds, altimeter wave heights, wave-buoy observations and in-situ wind observations to make a realistic assessment of the accuracy of each, to identify inconsistencies and to suggest potential improvements. Special attention has been given to particularly difficult areas as the Northern Adriatic Sea. Here the surrounding mountains make the wind forecast particularly challenging, while the proximity of coastlines challenges the satellite capability.
Furthermore, the impact of high-resolution wind forcing, e.g., as provided by the HARMONIE model, has been studied to assess the impact on accuracy of the wind forecasts, as well as wave forecasts from wave models forced with these data. The

higher resolution potentially leads to a higher accuracy, but the variability increases at the same time, which makes high-resolution forecasting far from trivial.

Unstructured grids can be more easily adapted to increase resolution locally than structured grids, which makes them very attractive for coastal wave-forecasting. Here the unstructured-grid approach is compared to the more traditional nesting of refined local structured grids.

In general differences between model forecasts and observations can be caused both by errors in the model and its forcing as well as errors in the observations. Triple collocation is a technique that can help further our understanding of the remaining uncertainties in the wave forecasts. By making use of at least three sources of data for the same locations and times, and assuming that the errors of these sources are independent, one can estimate the contributions for each source. Although some care has to be used to verify these assumptions, this technique has the potential to further our understanding and help guide future efforts on error analysis.

I.3 Objectives

The objectives of WP2 are to assess the current accuracy of high-resolution coastal wave forecast and to test various options for further improvement of the accuracy and reliability of these forecasts. This report contains all main WP2 results and may contain some repetition of the previous deliverables ([DR1] and [DR2]).

The main contents of the report follow the structure of the MyWave workpackage 2, i.e.:

- Data-assimilation (Task 2.1)
- Coastal wind products and their impact on wave forecasts (Task 2.2)
- Connecting large-scale forecasts to near-shore forecasts (Task 2.3)

I.4 Contributors to the report

The MyWave WP2 team members that have contributed to this report are Gert-Jan Marseille and Ad Stoffelen from KNMI on assimilation of scatterometer data in a non-hydrostatic atmospheric model (sections III.2, IV.3.1 and V.3.3), Martin Verlaan and Sofia Caires from Deltares on Ensemble Kalman Filter data assimilation on a coastal wave model (sections II.3, III.3, IV.2.2, V.3.4 and V.3.5), Kathrin Wahle, Heinz Günther and Joanna Stavena, from HZG on neural networks data assimilation on a coastal wave model (sections II.4.1, II.4.2, III.4, IV.2.3 and V.4), Marta Gómez and Cristina Toledano from PdE-AEMET on the North Atlantic and Cantabrian Sea studies (sections II.4.3, IV.2.4 and V.5) and Paolo Pezzutto and Luigi Cavaleri from ISMAR on the Adriatic study (sections IV.2.1, IV.3.2 and V.2).

II WAVE AND ATMOSPHERIC MODELS

II.1 Introduction

This chapter gives a short introduction of the atmospheric and wave models that have been applied in this study. These are 1) HARMONIE, the Numeric Weather Prediction (NWP) model used operationally at KNMI, 2) SWAN, the wave model used in the operational Dutch North Sea forecasts and 3) WAM the wave model used operationally by Puertos del Estado and by HZG. These models are presented in this order in the following sections.

II.2 HARMONIE

KNMI is currently in the transition phase from moving from the operational hydrostatic model HirLAM (High resolution limited area model) to the non-hydrostatic HARMONIE (Hirlam ALADIN Research on Mesoscale Operational NWP in Euromed) model. The grid size of the latest HirLAM model version is 11 km, where HARMONIE is operated typically at 2.5 km grid size. Besides the smaller grid size, a major difference of both models is that HARMONIE explicitly resolves convective processes, where HirLAM uses sub-grid-scale parameterizations to simulate convection. The HARMONIE model is available since early 2012. The model domain covers mainly Western Europe and part of the North Atlantic, see Figure II.1. The number of grid points is 800x800, meaning that the domain covers a 2000x2000 km^2 area. The model top is at 10 hPa (~26 km) and the number of model levels equals 60. The operational HARMONIE model version at KNMI is nested in the HirLAM model. Experimental tests indicated that nesting within the ECMWF model gives slightly better results. The results discussed in this report are all based on HARMONIE nesting with the ECMWF model.

Observations are assimilated in the model, initially four times a day, i.e., with a 6-hour assimilation window. In the current operational setting, a 3-hour assimilation window is used and analyses performed 8 times per day. Operationally observations are used from radiosondes, synop stations, buoys and aircraft (AMDAR). Experimental tests are performed with high spatial and temporal resolution radar, Mode-S (Euro Control radar-tracked aircraft) and GPS humidity observations. Section V.3.3 reports on the introduction of scatterometer winds in HARMONIE assimilation.

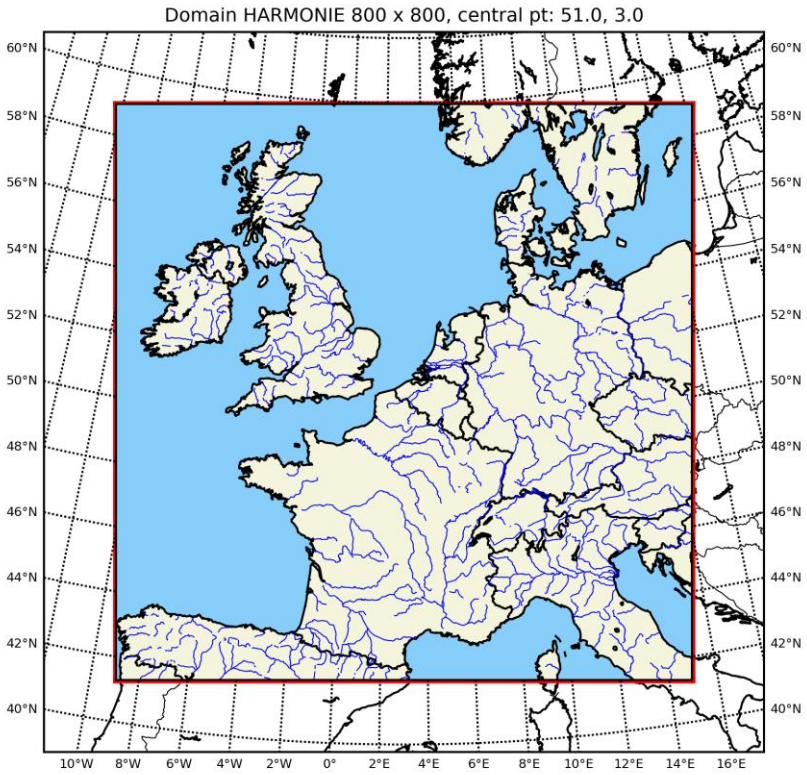

Figure II.1 HARMONIE mesoscale model domain, used operationally by KNMI (The Netherlands). The domain is centered at 51 degrees latitude, 3 degrees longitude and is composed of 800x800 grid points covering a 2000x2000 km area.

II.3 SWAN

Deltares is responsible for the operational model used to forecast the wave conditions in the Dutch North Sea. The model used for the operational wave forecasts is SWAN. SWAN is a state-of-the-art third generation shallow water phase-averaging wave model. It can account for:

- Wave propagation in time and space, shoaling, refraction due to current and depth, frequency shifting due to currents and non-stationary depth.
- Wave generation by wind.
- Three- and four-wave interactions.
- Whitecapping, bottom friction and depth-induced breaking.
- Dissipation due to vegetation.
- Wave-induced set-up.
- Transmission through and reflection (specular and diffuse) against obstacles.
- Diffraction.

Furthermore, SWAN computations can be made on a regular, a curvi-linear grid and a triangular mesh in a Cartesian or spherical co-ordinate system. Nested runs, using input, namely two-dimensional wave spectra, from other (larger scale) models can be made with SWAN.

The SWAN model has been validated and verified successfully under a variety of field cases and is continually undergoing further development. It sets today's standard for nearshore wave modelling. For more information on SWAN, reference is made to http://swanmodel.sourceforge.net/online_doc/online_doc.htm from where the SWAN scientifical/technical documentation and used manual can be downloaded.

In short, the model solves the action balance equation, in Cartesian or spherical coordinates, without any ad hoc assumption on the shape of the wave spectrum. In Cartesian coordinates the equation is

$$\frac{\partial N}{\partial t}+\frac{\partial}{\partial x}(c_x N)+\frac{\partial}{\partial y}(c_y N)+\frac{\partial}{\partial \sigma}(c_\sigma N)+\frac{\partial}{\partial \theta}(c_\theta N)=\frac{S_{tot}}{\sigma}, \quad (1)$$

where N is the action density, t is the time, σ is the relative angular frequency, and θ the wave direction. The first term on the left-hand side of Eq. (1) represents the local rate of change of action density in time. The second and third terms represent propagation of action in geographical space. The fourth term represents shifting of the relative frequency due to variation in depth and currents. The fifth term represents depth-induced and current-induced refractions. The quantities c_x, c_y, c_θ and c_σ are the propagation speeds in the geographical x- and y-space, and in the θ- and the σ-space, respectively. The expressions of these propagation speeds are taken from linear wave theory. In (1) S_{tot} is the energy source term. This source term is the sum of separate source terms representing different types of processes: wave energy growth by wind input, wave energy transfer due to non-linear wave-wave interactions (both quadruplets and triads), and the decay of wave energy due to whitecapping, bottom friction, and depth induced wave breaking. For some source terms more than one formulation is implemented in SWAN, see http://swanmodel.sourceforge.net/ online_doc/online_doc.htm.

As to SWAN's numerical approach, the integration of the propagation and of the source terms of Eq. (1) has been implemented with finite difference schemes in all four dimensions (geographical space and spectral space). A constant time increment is used for the time integration. The model propagates the wave action density of all components of the spectrum across the computational area using implicit schemes in geographical and spectral space, supplemented with a central approximation in spectral space. In geographical space the scheme is upwind and applied to each of the four directional quadrants of wave propagation in sequence. Three of such schemes are available in SWAN: a first-order backward space, backward time (BSBT) scheme, a second-order upwind scheme with second order diffusion (the SORDUP scheme) and a second order upwind scheme with third order diffusion (the S&L scheme). The numerical schemes used for the source term integration are

essentially implicit. In order to match physical scales at relatively high frequencies and to ensure numerical stability at relatively large time steps, a limiter controlling the maximum total change of action density per iteration at each discrete wave component is imposed.

II.3.1 Dutch North Sea operational wave model

The operational SWAN North Sea model used for wave forecasts in the Dutch waters consists of two grids. The first grid, the SWAN Dutch Continental Shelf (SWAN-DCSM) model covers a large area and computes boundary conditions for the nested detailed model domain. In this study we only consider the SWAN-DCSM grid and model and shall refer to it as SWAN-DCSM. The characteristic of the SWAN-DCSM grid are given in *Table II.1* and its domain and bathymetry are shown in Figure II.2.

Shape	ΔX	ΔY	number of cells (active grid points)	Xmin;Xmax	Ymin;Ymax
rectangular	1/20° ≈ 3.6 km	1/30° ≈ 3.6 km	420 x 480 (136,892)	-12° ; +9° ≈ 1500 km	+48° ; +64° ≈ 1700 km

Table II.1 Grid characteristics of SWAN-DCSM.

The directional domain of the model covers the full circle, divided into 45 bins of 8° each. The frequency range is from 0.03 Hz to 0.6 Hz (1.7 s – 33.3 s). SWAN divides this into 31 frequency bins. The time step of the computations is 1 hour.

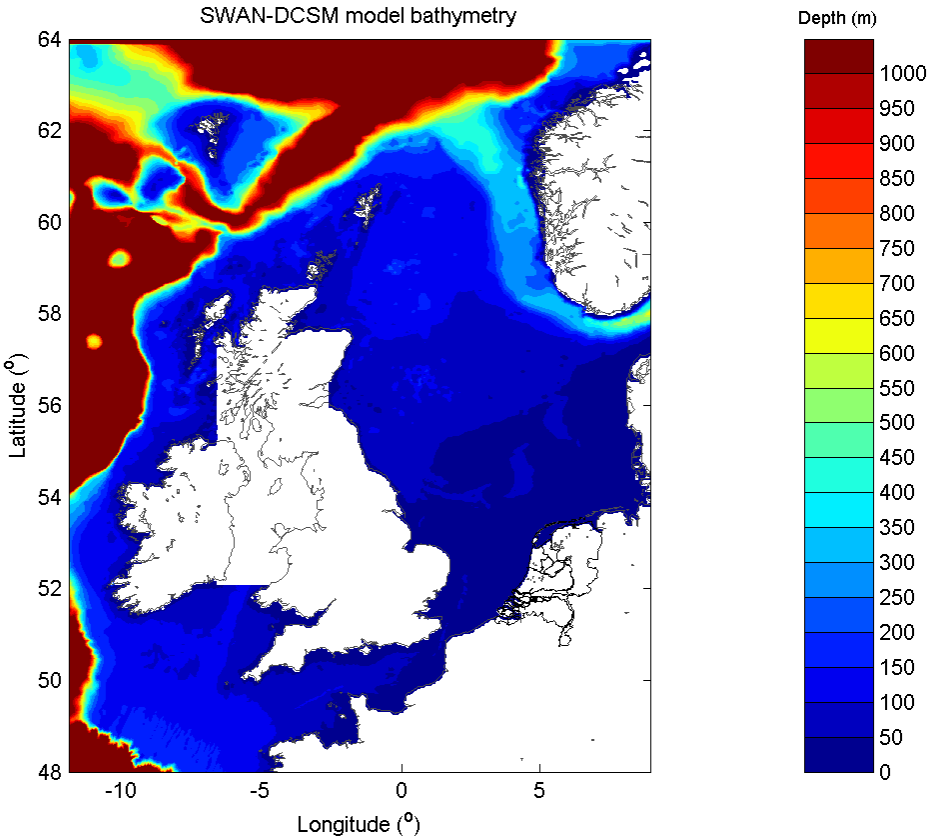

Figure II.2 SWAN-DCSM model domain and bathymetry.

The offshore wave boundary conditions of the SWAN-DCSM model come from the global ECMWF-WAM (ECMWF, 2011) and are available on a regular grid with 0.25 x 0.25 degrees resolution. The SWAN boundaries can thus in principle be chosen freely. However, ECMWF-WAM contains only limited shallow water physics and SWAN should cover the regions where shallow water effects are considered relevant. The SWAN domain was selected such that it should be expected – mainly due to resolution and added physics - to achieve better results than those of ECMWF-WAM. A larger domain than the one chosen will probably not improve the quality of the forecasts in the area of interest near shore.

II.4 WAM

II.4.1 Model Description

WAM is a third generation wave model which solves the wave transport equation explicitly without any presumptions on the shape of the wave spectrum. It represents the physics of the wave evolution in accordance with our knowledge today for the full set of degrees of freedom of a 2d wave spectrum. WAM computes the 2d wave variance spectrum through integration of the transport equation in spherical coordinates:

$$\frac{\partial F}{\partial t}+(\cos\varphi)^{-1}\frac{\partial}{\partial\varphi}(\dot{\varphi}\cos\varphi F)+\frac{\partial}{\partial\lambda}(\dot{\lambda}F)+\sigma\frac{\partial}{\partial\sigma}\left(\dot{\sigma}\frac{F}{\sigma}\right)+\frac{\partial}{\partial\theta}(\dot{\theta}F)=S$$

with

$F(\lambda,\phi,\sigma,\theta,t)$ wave energy density spectrum
(λ, ϕ) Longitude, Latitude
(σ, θ) intrinsic frequency, wave direction

$$\dot{\varphi}=\left(c_g\cos\theta+u_{North}\right)/R$$

$$\dot{\lambda}=\left(c_g\sin\theta+u_{East}\right)/(R\cos\varphi)$$

$$\dot{\theta}=c_g\sin\theta\tan\varphi/R+\dot{\theta}_D+\dot{\theta}_C$$

$$\dot{\sigma}=\dot{\sigma}_C$$

The source functions on the right of the transport equation comprise the contributions of wind input (S_{in}), nonlinear interaction (S_{nl}), dissipation (S_{dis}), bottom friction (S_{bf}) and wave breaking (S_{br}) : $S = S_{in} + S_{nl} + S_{ds} + S_{bf} + S_{br}$.

The last release of the third generation wave model WAM Cycle 4.5.4 is an update of the WAM Cycle 4 wave model, which is described in Komen et al. (1994) and Guenther et al. (1992). The basic physics and numerics are kept in the new release. The source function integration scheme made by Hersbach and Janssen (1999), and the up-dates model (Bidlot, et al., 2005) are incorporated. Other main improvements introduced in WAM Cycle 4.5.4 are technical improvements, which take into account the new possibilities of Fortran 95 and the MPI (**M**essage **P**assing **I**nterface) for parallelization purposes. On request from the user community a number of additional options are added in the model. A big advantage of the new state-of-the-art version WAM Cycle 4.5.4 is its high-grade modular composition which allows an easy replacement of individual parts of the code.

II.4.2 German Bight Set-up

The nested-grid wave model system for the German Bight is been implemented at HZG The system includes a regional WAM model for the North Sea (spatial resolution: $\Delta\varphi * \Delta\lambda = 0.05° * 0.08333°$ ~ 5 km) and a finer meshed local model for the German Bight ($\Delta\varphi * \Delta\lambda = 0.00928° * 0.015534°$ ~ 900 m). The driving wind fields for both are provided by the German Met Service (DWD: Deutscher Wetterdienst), computed as U_{10}-fields by the atmospheric model COSMO_EU. The model area of the COSMO_EU is shown in Figure 1 (upper left). It provides forecast results for 78 hours with a spatial resolution of about 7 km.

The required boundary information used at the open boundaries of the North Sea model is derived from the regional wave model EWAM for Europe that is running twice a day in the operational wave forecast routine of the DWD. The depth distribution in the model grid for EWAM is given in Figure 1 (upper right). The local model for the German Bight receives its boundary values from the North Sea wave model. The model grids and the depth distributions (Figure 1, North Sea on the lower

left and German Bight on the lower right side) for the two wave models correspond to those used in the setup for the GETM circulation model in order to simplify the coupling of both for the German Bight. The complete setup of the nested-grid model system for the German Bight is concentrated in Figure II.3.

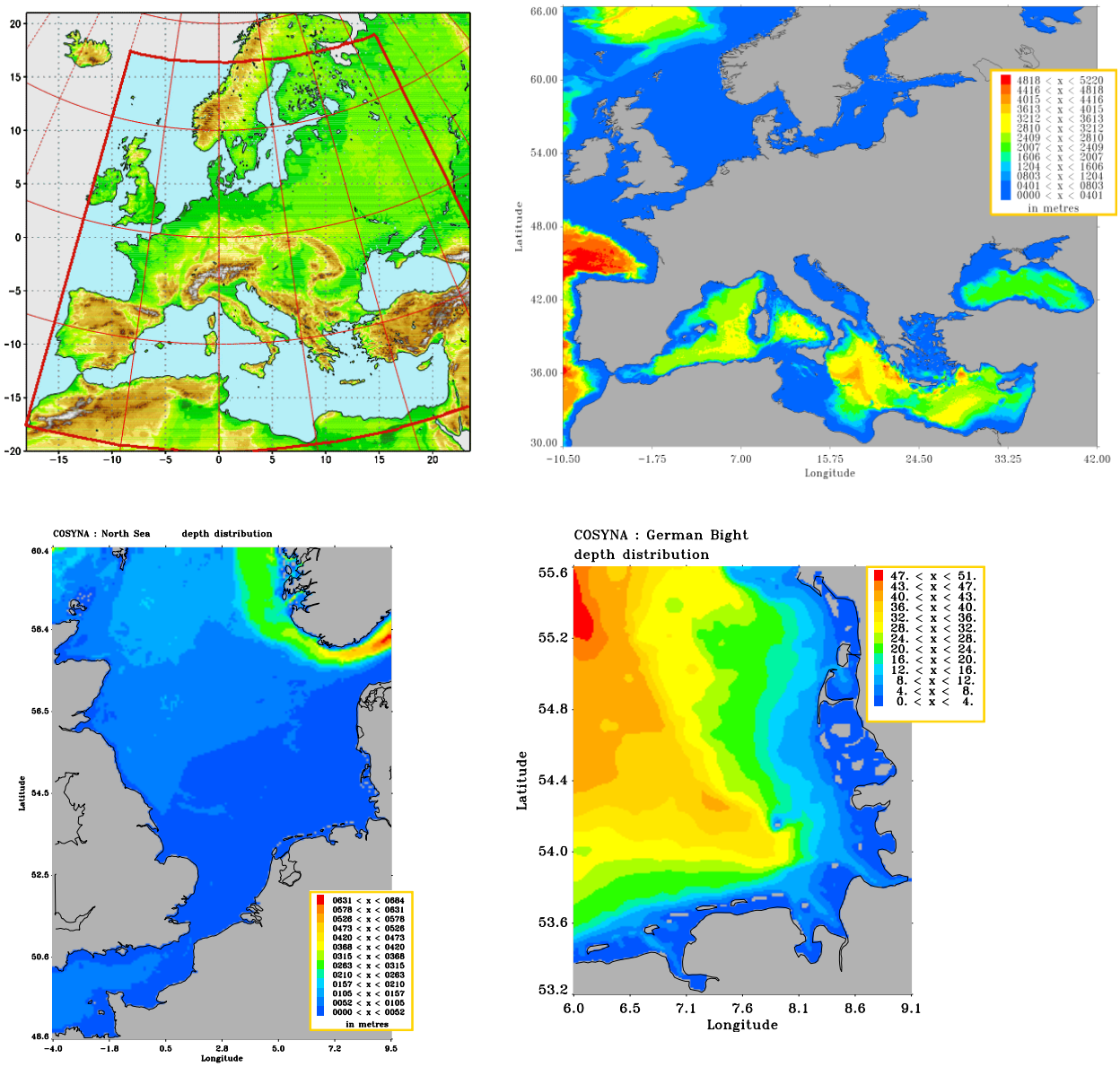

Figure II.3 Setup of the nested-grid wave model system for North Sea and German Bight.

Driving wind fields are provided by the COSMO_EU model (upper left, the red line denotes the location of the EWAM in COSMO_EU), boundary values by the regional European wave model EWAM (upper left: EWAM depth distribution). Depth distribution of the model for the North Sea (lower left) and for the German Bight (lower right).

The wave models run in shallow water mode including depth refraction and wave breaking and calculate the two dimensional energy density spectrum at the active

model grid points in the frequency-/direction space. The solution of the WAM transport equation is provided for 24 directional bands at 15^o each with the first direction being 7.5^o measured clockwise with respect to true north and 30 frequencies logarithmically spaced from 0.042 Hz to 0.66 Hz at intervals of $\Delta f/f = 0,1$.

The driving wind fields for all wave model runs discussed in this report are provided by the atmospheric COSMO_EU model of the DWD. This regional non-hydrostatic model with its integration domain shown in Figure II.3 (upper left) runs at the DWD since September 2005. It uses 40 vertical levels with the lowest level 10 meter above ground and performs forecasts for 78 hours (at 00 and 12 UTC). For the specification of the used rotated grid, the south pole has been shifted to 40^oS and 10^oE. The spatial resolution is 7 km. The rotated lat-lon coordinates of the lower left and the upper right corner of the integration domain are lon=- 18.0^o, lat=-20.0^o and lon= 23.5^o, lat= 21.0^o, respectively. The integration domain includes 665x657 model grid points and boundary values at its open boundary are provided by the global DWD model GME. For all wave model runs the U_{10} COSMO_EU wind fields are used. Those are available in hourly intervals. As an example of wind variability we show the wind speed and direction during the storms Christian and Xavier that took place in October and December, 2013, see Figure II.4. The horizontal distribution of the wind field for the German Bight is shown on Figure II.5.

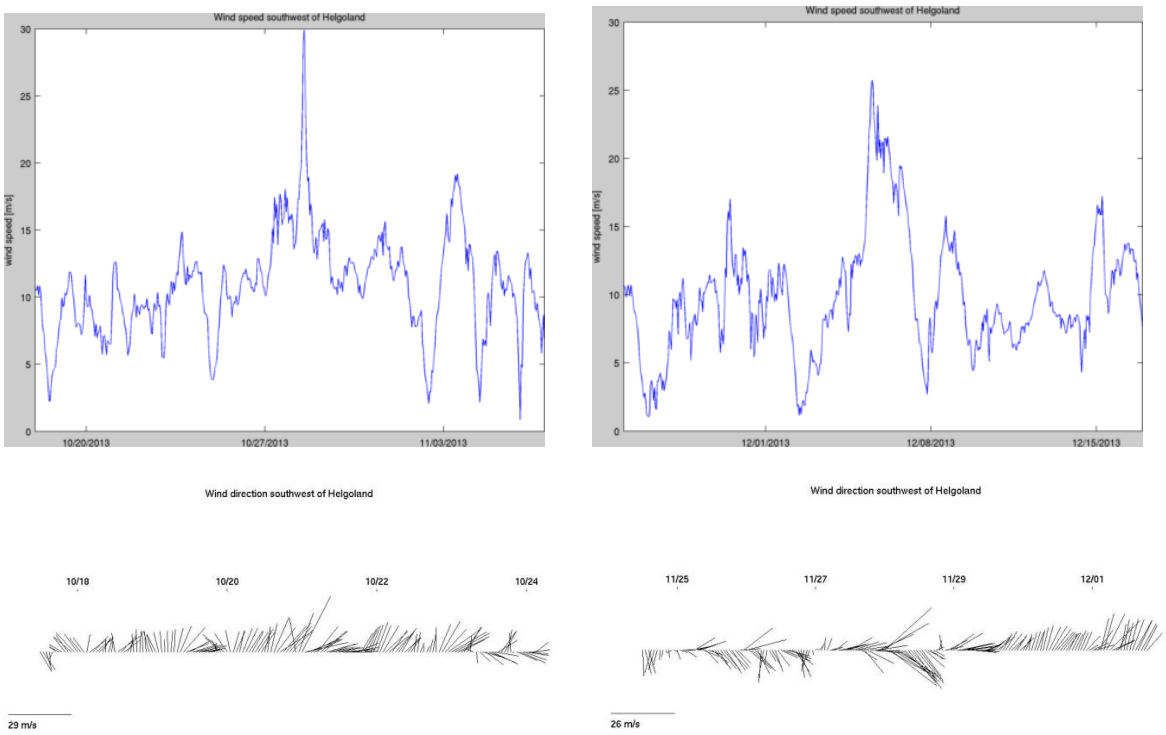

Figure II.4 Wind speed and wind direction for Helgoland Station during the storm events Christian in October, 2013 (left) and storm Xavier in December, 2013 (right).

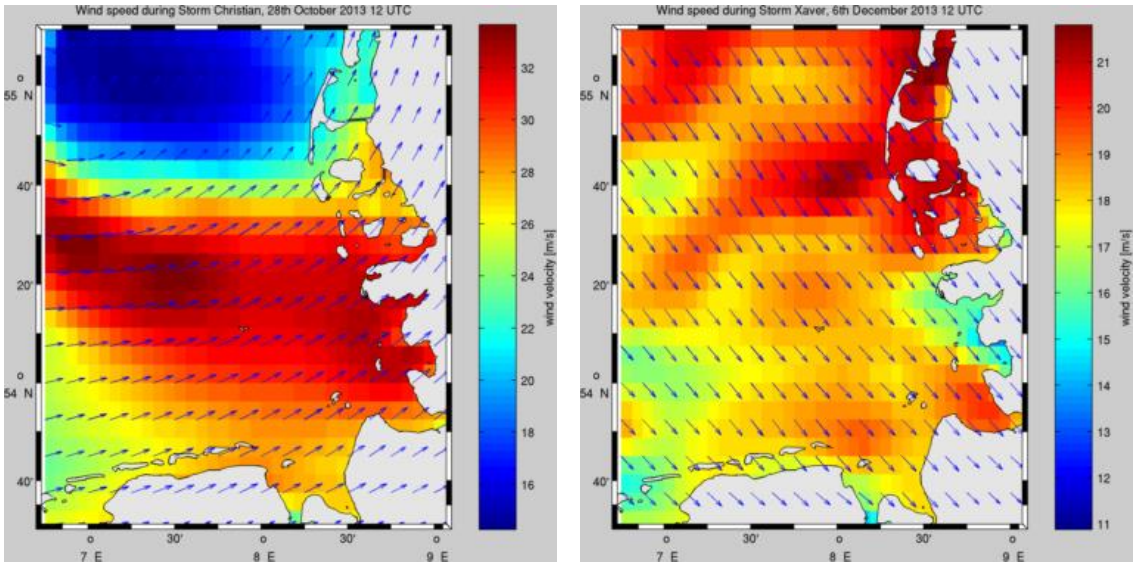

Figure II.5 Horizontal distribution of wind fields for the German Bight region during the storm events Christian on 24. October, 2013 (left) and storm Xavier on 6. December, 2013 (right).

Figure II.6 shows an example of the horizontal distribution of the significant wave height in the North Sea and in the nest for the German Bight on the 15th of February 2012 at 06 UTC with significant wave heights up to 6.8 m.

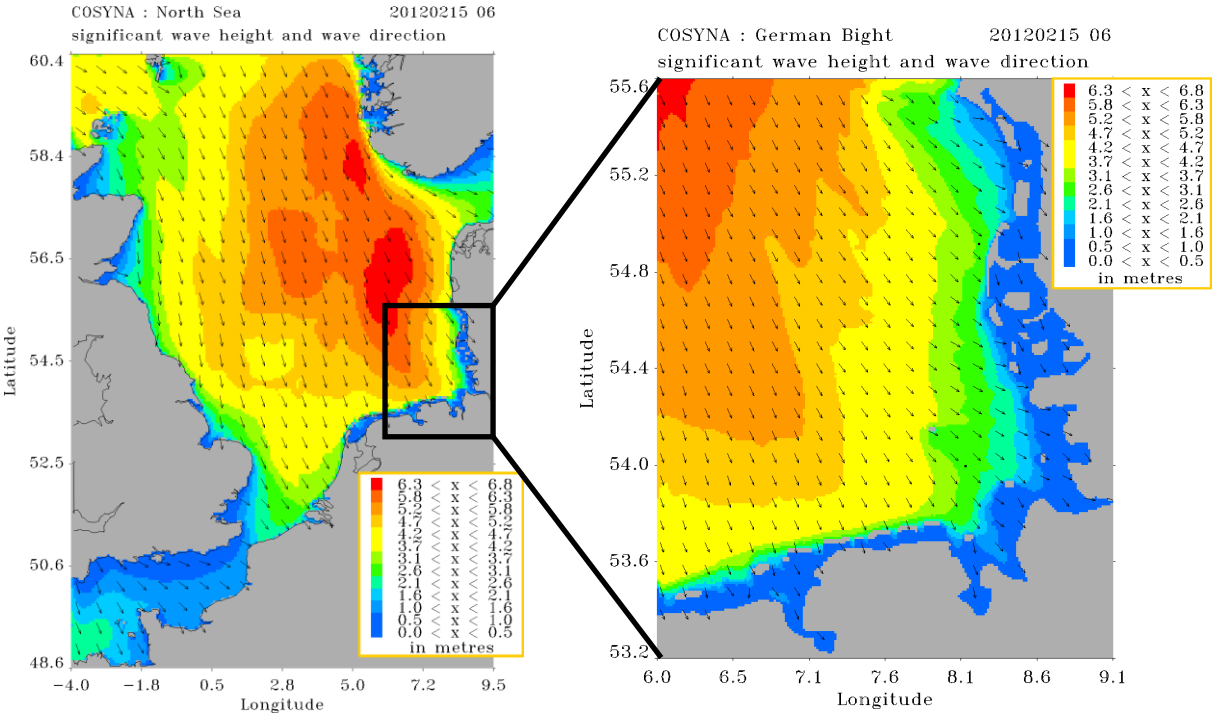

Figure II.6 Nested-grid wave system for North Sea and German Bight (right).

The results of both wave models include the full two dimensional spectral information and 29 integrated parameters which are included in Table II.2.

Parameter No.	Parameter	Dimension
1	Wind speed U10	m/s
2	Wind direction	Degree from North (towards)
3	Friction velocity	m/s
4	Drag coefficient	
5	Water depth	m
6	Current speed	m/s
7	Current direction	Degree from North (towards)
8	Dummy	
9	Significant wave height	m
10	Wave peak period	s
11	Wave mean period	s
12	Wave Tm1 period	s
13	Wave Tm2 period	s
14	Wave direction	Degree from North (towards)
15	Directional spread	Degree
16	Normalized wave stress	%
17	Sea significant wave height	m
18	Sea peak period	s
19	Sea mean period	s
20	Sea Tm1 period	s
21	Sea Tm2 period	s
22	Sea direction	Degree from North (towards)
23	Sea directional spread	Degree
24	Dummy	
25	Swell significant wave height	m
26	Swell peak period	s
27	Swell mean period	s
28	Swell Tm1 period	s
29	Swell Tm2 period	s
30	Swell direction	Degree from North (towards)
31	Swell directional spread	Degree
32	Dummy	

Table II.2 Integrated parameters of the wave model output.

The wave model results (integrated parameters) are validated against buoy data available in the area of the model grids.

II.4.3 Puertos del Estado WAM model versión

An improvement on the original WAMDI numerical spatial integration scheme was introduced at Puertos del Estado. This consisted of using a two-way nesting scheme which allows the definition of different grid resolutions in various subregions of the model domain. Along the boundary, between these subregions of different resolutions, there are two types of points, those receiving energy by advection and those receiving energy by interpolation. Those points are alternated within the advection algorithm and modified accordingly to minimise the computational cost.

With this two-way nesting scheme the resolution of the Atlantic application is increased from 1 degree, in the open deep water, to 0.25 degrees close to the continental shelf. The Mediterranean application has also a variable grid spacing of 10 and 5 minutes.

III DATA ASSIMILATION TECHNIQUES

III.1.1 Introduction

Even though numerical wave models are becoming more and more accurate, forecasts can to some extent deviate from the available observations. The process for correcting forecasts such that they better match the observations is known as Data assimilation (DA). For chaotic models that are very sensitive to changes in the initial conditions, such as meteorological models this is a crucial step in any forecast system. For wave models, the significance is smaller, but still significant improvements through the use of data-assimilation have be shown in a number of studies.
Over the past decades a large number of algorithms have been developed for data-assimilation. 3D-VAR, 4D-VAR and the Ensemble Kalman Filter (EnKF) are among the more popular. The use of Neural Networks on the other hand is a quite new an promising technique.

III.2 3D-VAR

Three-dimensional variational analysis (3D-Var) is an incremental DA method where the analysis increment is found by iteratively finding the minimum of a cost function that is composed of background and observation penalty terms. The former measures the deviation of the model (analysis) state to the background (short term forecast from the previous analysis) and the latter measures the deviation from observations. As such the model state is drawn to recent observations, taking into account the model state history through the background state (and thus past observations). This is done in a statistical consistent way, taking into account the characteristics of background and observation errors. More details are found in [DR 1].

In data assimilation observations are gathered over a certain time period: the assimilation window. The aim is to find the model state that best fits the background state and observations at analysis time, that is generally set at the window centre. This model state is called the analysis. In 3D-Var it is assumed that all observations within the assimilation window are measured at analysis time. This is generally true for observations from conventional observing systems like radiosondes, synop stations and buoys. However, aircraft and satellite overpasses are asynoptic, introducing a time shift between observation and model background state.

As an example, for a 6-hour assimilation wind, the 18 UTC analysis uses all observations between 15 and 21 UTC. Conventional observing systems measure hourly (buoys, synop stations) or 6/12-hourly (radiosondes). HARMONIE uses only those observations measured within 30 minutes from analysis time. Aircraft observations are available over the complete assimilation window and in principle are all used in the analysis. Satellite overpasses generally do not coincide with the exact

analysis time. The current setting in HARMONIE DA is to ignore the time discrepancy between the model simulation at analysis time and the satellite measurement. Figure III.1shows an example of this so-called timing issue where the satellite observation is almost 2.5 hours after analysis verification time. Both the model and the scatterometer have the front at the correct location, yet assimilating scatterometer winds as if they were observed at 18 UTC may shift the front position incorrectly. In practice the background departure check will remove most of the observations near the front, which is correct in the current 3D-Var implementation, but also removes valuable observational information near the frontal zones that is relevant for mesoscale forecasting in particular. Currently most NWP centres use a 3-h assimilation window operationally which partly resolves the timing issue. The trend is to further reduce the assimilation window to 1 hour, the so-called rapid update cycle, which is useful in particular in extreme weather events. This is further discussed in section V.3.3.2. In addition NWP centres work on implementing 4D-Var assimilation schemes, but its current status within the HirLAM/HARMONIE consortium is still experimental.

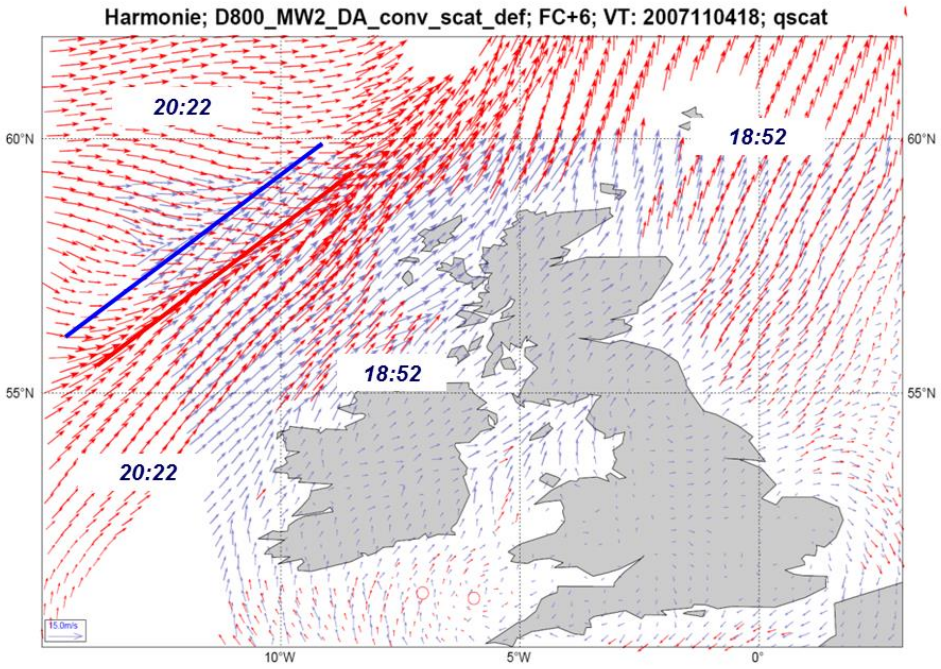

Figure III.1 HARMONIE 6-h forecast valid at 4 November 2007 18 UTC (blue arrows) and overlaid scatterometer winds from 2 QuikScat overpasses near 18:52 and 20:22 UTC (red). The solid blue/red line mark the location of the front by the model (at 18UTC) and scatterometer (at 20:22 UTC) respectively.

III.3 ENKF

The key difference between the Ensemble Kalman filter (EnKF) and the other methods used in MyWave is that the model uncertainty, mainly the covariance, is computed from an ensemble of model forecasts in a procedure very similar to Monte

Carlo methods. Starting from an initial ensemble of model states $\xi_i^a(t_0)$ the model M is used to compute a forecast for each ensemble member:

$$\xi_i^f(t_{k+1}) = M\xi_i^a(t_k) + w_i(t_k),$$

where $w_i(t_k)$ denote the system noise, used to model uncertainties in the model. From this one can compute the sample mean as

$$x^f(t_k) = 1/n\sum_{i=1}^{n}\xi_i^f(t_k)$$

and covariance

$$\mathbf{P}^f(t_k) = 1/(n-1)\sum_{i=1}^{n}(\xi_i^f(t_k) - x^f(t_k))(\xi_i^f(t_k) - x^f(t_k))'.$$

The Kalman gain is expressed as

$$\mathbf{K}(t_k) = \mathbf{P}^f(t_k)\mathbf{H}'(\mathbf{H}\mathbf{P}^f(t_k)\mathbf{H}' + \mathbf{R})^{-1},$$

where $\mathbf{H}$ denotes the observation operator that maps the model state to values that match the observations. $\mathbf{R}$ is the error covariance of the observations at time t_k.

The analysis or measurement-step of the EnKF uses a perturbation of the observations $v_i(t_k)$ and a separate analysis for each of the ensemble members to obtain a consistent ensemble of states that incorporate the observations $y(t_k)$,

$$\xi_i^a(t_k) = \xi_i^f(t_k) + \mathbf{K}(t_k)(y(t_k) - H\xi_i^f(t_k) - v_i(t_k))$$

If required one can obtain the mean and covariance of the model state after the analysis, that can be computed from

$$x^a(t_k) = 1/n\sum_{i=1}^{n}\xi_i^a(t_k),$$

and

$$\mathbf{P}^a(t_k) = 1/(n-1)\sum_{i=1}^{n}(\xi_i^a(t_k) - x^a(t_k))(\xi_i^a(t_k) - x^a(t_k))'.$$

Note that the classical EnKF formulation requires the model simulations to stop each time an observation is available. In the asynchronous EnKF (Sakov et al., 2010) this restriction is relaxed. The observations are accumulated over a predefined time interval $]t_k, \ldots, t_{k+m}]$. During the model forecast for each member the matching values $\mathbf{H}\xi_i^f(t_k), \ldots, \mathbf{H}\xi_i^f(t_{k+m})$ are collected. Finally the observations are assimilated all at once as if they occurred at time t_{k+m}, but with the predicted values that were collected at the appropriate times.

Spectral wave models like SWAN are stable forced systems and it is therefore crucial to include system noise or model uncertainty when applying EnKF. Without system noise or covariance inflation the Kalman filter will diverge, i.e., the error covariance matrix $\mathbf{P}^f(t_k)$ will become smaller and smaller and the observations will effectively be ignored.

Two likely sources of uncertainty in a spectral wave model are the uncertainty in the wind forcing and uncertainty for the wave parameters that are specified at the open-boundary.

III.3.1 OpenDA

OpenDA is a generic toolbox for data assimilation. It includes, among several other algorithms, an implementation of the EnKF with the option for asynchronous filtering as described above. The easiest and most flexible way to connect a model to OpenDA is with what is called a black-box wrapper. The characteristics of a black-box wrapper are that the model remains a separate executable with interaction by the input and output files of the model, see Figure III.2. For this purpose one needs to supply subroutines for reading and writing of these model specific file formats. These routines have been implemented for SWAN and are made available through the official OpenDA release (http://www.openda.org).

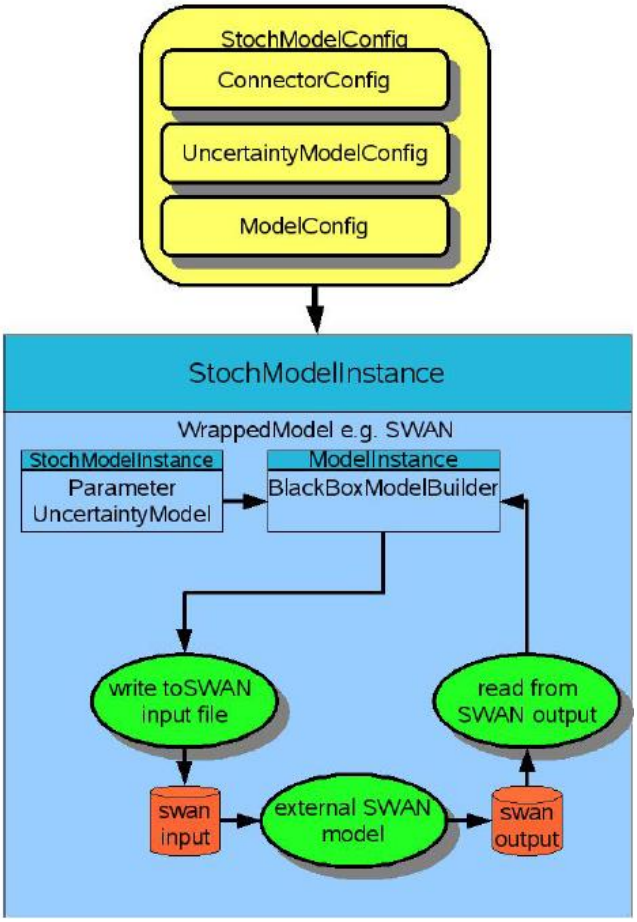

Figure III.2 Schematic diagram of the black box connection between SWAN and OpenDA.

The OpenDA implementation for SWAN uses the full spectra at all grid-cells as the state of the model. This is similar to the contents of a restart file. Most previous work on Kalman filtering for spectral wave models has used a reduced state, often consisting of the significant wave-height and wave-period. The difference in memory consumption between the two approaches is substantial (order 100x), but the reduced parametric space does not allow for assimilation of other wave parameters or spectral data. In addition changes of the parameter fields by the assimilation need a ad-hoc step to adjust the full spectra that the model requires. The computationally

more expensive approach used here allows for assimilation of all available data in a natural manner and can update the full spectra in a consistent manner.

III.4Neural networks

The neural networks (NNs) approach is a novel method for data assimilation into the wave models. In general the NN aims to explore an extensive parallel network of simple elements in order to obtain result in a very short time and, at the same time, with insensitivity to loss and failure of some of the elements of the network. These unique properties make possible to use the NN in a wide range of applications, e.g. remote sensing (e.g. Schiller, 2007), financing, engineering, image processes, recognition of patterns, etc. Detailed description of the NN method can be found in Haykin (1994) and Bischop (1995).

Neural Networks can be used to approximate an arbitrary non-linear function that maps a vector of input variables to a vector of output variables. It is also possible to use previous outputs of the NN as input for a next step of the computation, but these recursive NN are not considered here. The application of a NN can be divided into a training phase and a forecasting phase. During the training phase a large dataset of input and output vectors are used to train the NN, i.e., to estimate the coefficients and structure of the NN. The training phase consists of adjusting the weights for the best performance of the network in establishing the mapping of many input/output vector pairs.

Contrary to physically-based models, with the NN it is not necessary that the relation between inputs and outputs is causal, a statistical correlation is sufficient. This gives an additional freedom to decide which variables are inputs and which variables are outputs. This unique property of NN makes it possible to perform data assimilation by simply changing the input and output variables for the NN. Where physically-based wave models, such as WAM (http://www.hzg.de/institute/coastal_research/structure/system_analysis/KSD/topics/developments/003136/index_0003136.html), require wind and boundary conditions as inputs and provide computed wave parameters on the grid-points as outputs, a NN can in principle accept observed wave parameters as inputs and wind and boundary conditions as outputs. The technical changes for this are very small. The challenge is to select the right input and output variables that work well with the objective (learning) function, since a NN will always provide an answer, but some choices can result in much more accurate results than others.

To understand the performance of NNs for data assimilation in the wave models it is difficult to estimate both wind and boundary conditions together. One first has to use the new methodology either for optimizing the wind forcing or the boundary conditions and then combine both forcings.

NNs provide a statistical estimation procedure and thus have similar properties to e.g. multiple linear regression methods. For example, if too many input variables are selected, with a limited set of training data, then the training may overfit the data. It is

therefore necessary to reserve part of the available data for validation. The most obvious indication for overfitting is when the NN has a much higher accuracy for the training data than for the validation data. Another property is generalization, i.e. a NN may sometimes generate good estimates for new inputs (i.e. data with properties not well captured by the training data set), but there is no guarantee.

An extreme example is if the training data only covers calm weather, then the NN may perform poorly for storms. An important technique to reduce overfitting is to reduce the number of inputs. One way to do this is with Principal Component Analysis (PCA), sometimes also called POD, POP or EOF. Another way is to lump a variable e.g. for a whole boundary instead of allowing spatial variation.

A NN is usually trained for each scalar output variable separately. This makes it cumbersome to compute output for many output variables. The approach proposed here is to use an 'inverse' NN to estimate the wave parameters at the open boundary of the wave model from the observations. Next, these estimated boundary conditions can be used as input for a run with a physically-based model, here WAM. It is also possible to train a forward NN to generate output for a limited number of output locations.

The combined procedure that we are developing works as follows: First train a forward NN, with wind forecasts and boundary conditions from a larger scale model, e.g. significant wave height (H_s), mean wave period, etc. at a number of locations along the open-boundary. To reduce the number of inputs for wind and boundary conditions, a PCA is used.

The outputs of the forward model are given by the outputs of the wave model corresponding to the actual observations. This implies that the forward model will mimic the behaviour of the physically based wave model.

An additional inverse NN is trained with the same data, but with a reversed role. Here WAM-output matching the observations as input of the inverse-NN and boundary and wind PCA values are obtained as outputs. Note that the experiments with a preliminary version in this report use winds as an input for the inverse-NN. Note that the training procedure does not require any real observations, but it does require model output for a reasonably long WAM run. In general, it is also possible to use the same training procedure, but with real observations.

After training of the forward-NN and inverse-NN one can perform a forecast by first running the inverse-NN with real observations, which results in an estimate for the open-boundary (and wind forcing). The forward-NN and/or the WAM model can then be used to compute the forecast. To forecast more than a few hours ahead the boundary-conditions and wind fields are complemented with forecasted boundary-conditions from a larger model and wind fields from a meteorological model.

The experiments in this report are performed with a synthetic dataset. The first-guess uses $H_s = 0$ at the open-boundary and the 'truth' model, that is used to generate

training data and synthetic observations, uses wave parameters from the large scale North Sea WAM model for the boundary conditions.

This is a rather extreme case, which was chosen to clearly show the impact of the data-assimilation procedure. It is important to mention that after training NN has a lower computational cost than extended and linear KF, variational method, and particle filter.

Within the MyWave Project a new methodology based on the use of NN for data assimilation in the wave models is developed. The following assimilation schemes have been developed:

1. apply inverse WAM NN for each (point) measurement → ensemble of boundary values and / or wind ensemble
2. apply forward WAM NN for each ensemble member → emulated measurements in each point error (quality) estimate
3. from these 'ensemble' of boundary and / or wind values chooses the best one in terms of error.

The basic idea and first results have already been described in detail in [DR2].

In summary, Neural Networks were used to emulate the WAM model and its adjoint in the German Bight area. Given (synthetic) measurements $\overrightarrow{r_M}$of integrated parameters (significant wave height, period and mean wave direction) a first estimate of variables $\vec{c}$ (wind forcing, boundary values) are derived by the NN emulating the adjoint wave model $\overrightarrow{c_1} = N^{-1}(\overrightarrow{r_M})$. Subsequent application of the forward NN gives an error χ_1^2 which is minimised using the Levenberg-Marquardt algorithm:

$$\chi_k^2 = (\overrightarrow{r_M} - \overrightarrow{r_k})^T C (\overrightarrow{r_M} - \overrightarrow{r_k})$$
$$\overrightarrow{c_{k+1}} = \overrightarrow{c_k} + (M^T C^{-1} M + \lambda 1)^{-1} M^T C^{-1} (\overrightarrow{r_M} - \overrightarrow{r_k})$$

where C is the covariance matrix and $M$is the Jacobian matrix with

$$(M_{ni}) = (\partial\, m_n / \partial\, c_i)_{\vec{c}=\overrightarrow{c_k}}$$

which is known since using feedforward backpropagation NNs. λ is a control parameter allowing to gently adjust between a Gauss-Newton (0) and a gradient descent (1) scheme.

Data from the pre-operational wave forecast system at HZG served as data base for training and testing the NNs (see [DR2]). The two leading Principal Components (PC) of wind fields and of boundary values were supplied to the forward NN to derive integrated parameters in a sub-area of the German Bight (synthesising measurements by an HF-radar). Analyses of forward NN showed a very good overall performance except for very shallow areas, which is probably due to the wave breaking processes.

The inverse (adjoint) NN showed errors that are of one order of magnitude larger than the corresponding forward NN experiment. These large errors were explained

by the non-bijectivity of a wave model: one and the same sea state might have been caused by different combinations of swell and wind sea. Thus we decided to reduce the complexity of the inversion problem by dividing the adjoint model into two parts: one for deriving boundary values where PC's of wind fields serve as additional input for the inverse NN and a second working *vice versa.* The retrieval of boundary values was thereby significantly improved and reconstructed wave heights compared well with target values (see [DR2]).

Missing in [DR2] was the wind retrieval and a validation of the adjoint model in an assimilation experiment which is demonstrated in this report.

The idea for the data assimilation based on NN is schematically presented in Figure III.3.

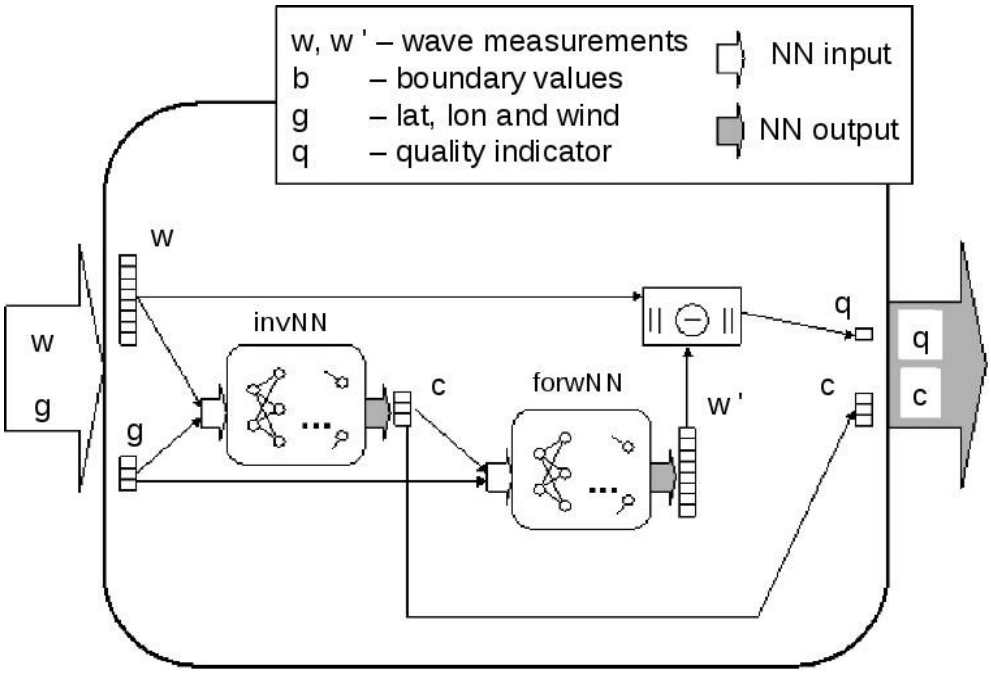

Figure III.3 Idea of assimilation scheme, w, w' are the wave measurements, b-boundary values, g-latitude, longitude and wind values, c-other parameters, q-quality indicator.

One big advantage of using NNs in data assimilation is its computational speed: once you have the NNs trained its further application costs little time. Additionally, the NNs scheme implies a quality/ out of scope check. These aspects make the use of NNs attractive compared to direct inversion of numerical models, like AdWAM by Hersbach (1998).

The methodology and preparation of data for the NNs data assimilation is described in the next section.

III.4.1 Neutral Network for wind retrieval

The Neural Network for wind retrieval was trained using wave integrated parameters (significant wave height H_s, wave period tm1, and mean direction thq) at given locations (indicated by latitude- and longitude indices) at present time, three and six hours back in time and northern and western boundary values (first two PC's of H_s, tm1 and thq at one location)

reaching three to twelve hours back in time as input parameters (the time range is motivated by the average time duration for wind waves passing the German Bight area). Wind fields (first two PCs of u- and v-component) reaching zero, three and six hours back in time are derived by this NN.

The performance of the NN when applied to independent (not used during training) testing data is demonstrated on Figure III.4.

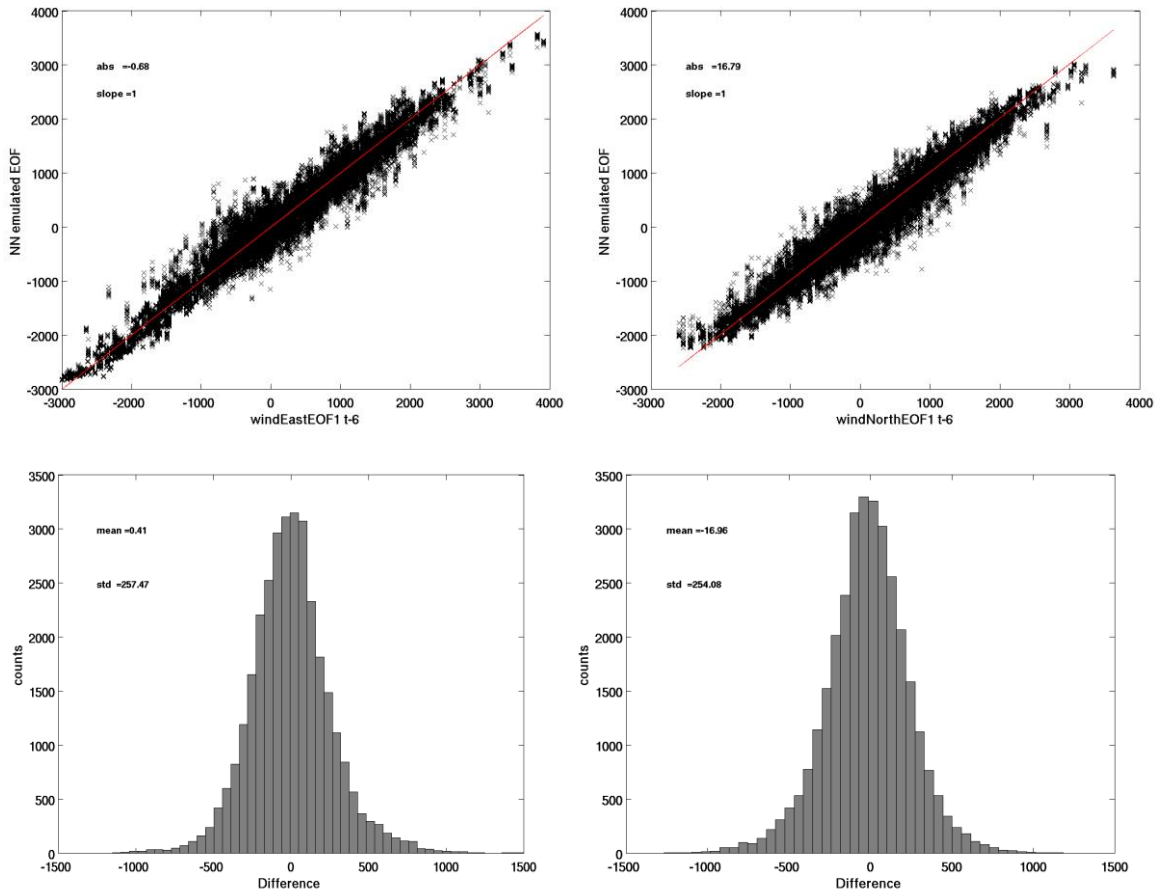

Figure III.4 Performance of NN for wind retrieval when applied to testing dataset. Left: leading PC of east wind component six hours ago. Right: same for north wind component.

IV WIND AND WAVE DATA

IV.1Introduction

This chapter describes the considered sources of wind and wave data. Next section deals with in-situ data and Section IV.3 with satellite data.

IV.2 In-situ

IV.2.1 Mediterranean Sea

All the available data over the Mediterranean Sea are hosted on a dedicated CNR-ISMAR server, provided by various institutions on a monthly basis, starting from July 2013. This storage area is accessible operationally by all the interested partners, in order to perform WP3 forecast validations. ISPRA gathers the information from 30 WMO coded buoy stations in the Mediterranean Region (see Table IV.1), while ISMAR has managed to obtain the data from two buoys from the Israel Ports Development and Assets Company Ltd and Coastal (IPC) and Marine Engineering Research Institute Ltd (CAMERI). This has been possible through a specific agreement signed by ISMAR in order to get the data for MyWave Project research purposes.

Each time-series is quality checked (see MyWave D3.2) in order to guarantee reliability of the observations. Cameri provides high frequency sampled wind data, which have been filtered and under-sampled on 30 minutes basis, and 30 minutes wave spectra, from which we derive the necessary spectral moments. The parameters of interest collected for this subtask (2.2.3) are significant wave height (H_S, m) and wind speed at 10 m above ground (U_{10}, m/s). All series are stored in NetCDF4 self-describing format, adding proper metadata, therefore providing overall uniformity.

Name	WMO id	°E	°N	Source	Provider
RonSV	*61200*	8.18	43.92	ARPAL	ARPAL
Ashdod	-	34.65	31.88	Cameri	Cameri
Haifa	-	34.94	32.84	Cameri	Cameri
Athos	*6101003*	24.72	39.97	HCMR	MyOcean
Iraklio	*61277*	25.12	35.73	HCMR	MyOcean
Methoni	*68422*	21.60	36.82	HCMR	MyOcean
Saron	*6101001*	23.57	37.60	HCMR	MyOcean
Rhone	*61284*	4.87	43.32	Ifremer	MyOcean
Lion	*61002*	4.70	42.10	MeteoFrance	MeteoFrance
Nice	*61001*	7.89	43.42	MeteoFrance	MeteoFrance
C. Begur	*61196*	3.63	41.91	PdE	MyOcean
C. Gata	*61198*	-2.33	36.57	PdE	MyOcean
C. Palos	*61417*	-0.33	37.65	PdE	MyOcean
Dragonera	*61430*	2.10	39.56	PdE	MyOcean
Mahon	*61197*	4.44	39.72	PdE	MyOcean
Tarragona	*61280*	1.47	40.68	PdE	MyOcean
Valencia	*61281*	0.20	39.52	PdE	MyOcean
Alghero	*61213*	8.11	40.55	RON	ISPRA
Ancona	*61218*	13.72	43.83	RON	ISPRA
Cagliari	*61221*	9.45	39.11	RON	ISPRA
Catania	*61207*	15.15	37.44	RON	ISPRA
Cetraro	*61211*	15.91	39.45	RON	ISPRA
Civitavecchia	*61216*	11.69	42.13	RON	ISPRA
Crotone	*61210*	17.22	39.02	RON	ISPRA
La Spezia	*61219*	9.83	43.93	RON	ISPRA
Mazara	*61208*	12.53	37.52	RON	ISPRA
Monopoli	*61215*	17.38	40.98	RON	ISPRA
Palermo	*61209*	13.34	38.26	RON	ISPRA
Ponza	*61214*	12.95	40.87	RON	ISPRA
Venezia	*61220*	12.52	45.34	RON	ISPRA

Table IV.1 List of moored buoys, limited to the ones that have been sufficiently operational (meaning at least 100 qc data) between July 1st and Dec 31st 2013.

IV.2.2 Southern North Sea

For the validation of the Dutch North Sea wave results and forcing winds in-situ measurements maintained by the Dutch Government have been used. Figure IV.1 shows the locations for which results are presented in this report. At some of the locations measurements from more than one wave measuring device are available.

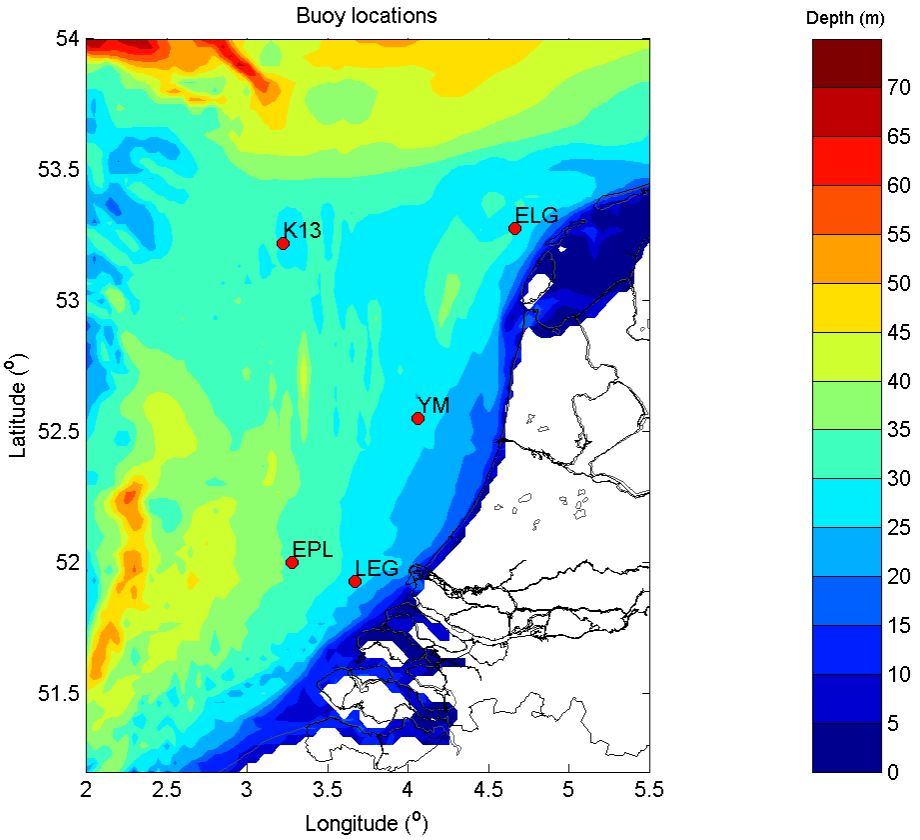

Figure IV.1 Location of in-situ measurement stations maintained by the Dutch Government and from which data were used in this study.

IV.2.3 German Bight

The measurements for validation of the German Bight North Sea model results are obtained from the GTS (Global Telecommunications System) net that provides continuously wind and wave data worldwide. The wave model simulations of the fine resolution German Bight set-up have been validated with measurements recorded by the buoys of the BSH (Bundesamt für Seeschifffahrt und Hydrographie, Hamburg) and by the buoys of the HZG. The main focus of directed on the conditions in the German Bight, therefore the discussion of the comparisons between the wave model results with measurements will be more detailed for that area. Figure IV.2 indicates the location of the buoy locations in the German Bight where wave measurements are available.

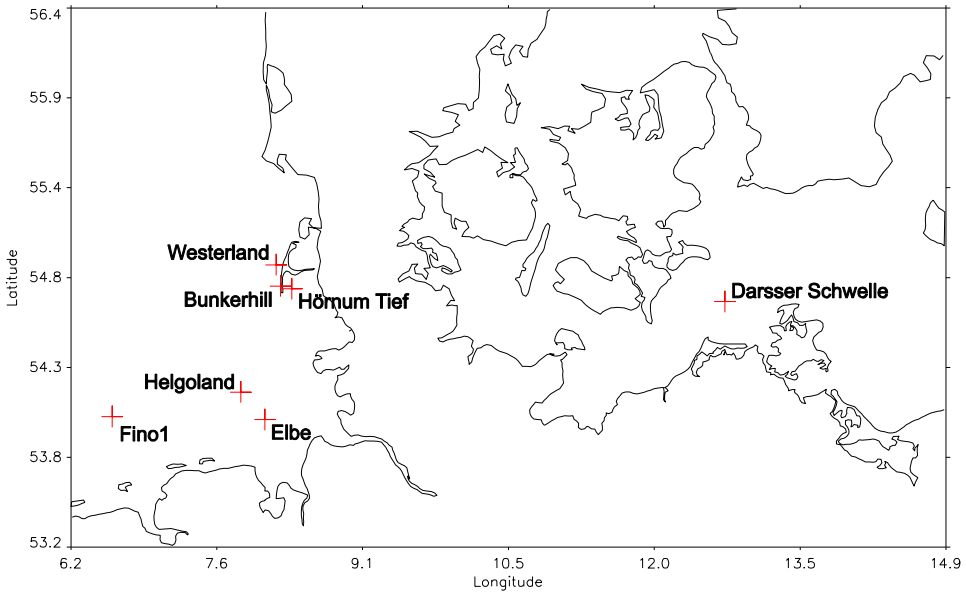

Figure IV.2 Buoy locations with measurements in the German Bight.

IV.2.4 Atlantic Ocean and Cantabrian Sea

The buoy data used for the tasks Cantabrian cross validation and the comparison of unstructured grid versus regular in Canary Islands come from 2 PdE netwoks: coastal and deep sea buoy.

The Deep Sea Buoy network is based on 12 Seawatch and 3 WaveScan buoy stations. The instruments are located at points with depths between 200 and 800 m and measure atmospheric and oceanographic parameters. Measurements are transmitted every hour via satellite to Puertos del Estado and directly posted to the web.

The Coastal Buoy Network is providing real time data in some specific points located at shallow waters. The main objective of the measurements is to complement those of the Deep Sea Network at those locations of special interest for the port operations or wave modeling validation. The buoys employed are directional Tryaxis.

The buoys used from the Deep Sea Network are 7: Estaca de Bares, Cabo de Peñas, Santander IEO, Bilbao-Vizcaya, Villano-Sisargas, Cabo Silleiro and Tenerife Sur. All of them are Seawatch buoys. The oceanographic parameters measured are calculated over periods of 10 min and depth of 3 m. The wave parameters are calculated over 26 min periods. The meteorological parameters measured are over 10 min periods at 3 m height.

The two buoys used from the Coastal Buoy Network are Santa Cruz de Tenerife and Las Palmas Este. These buoys only measure the directional wave and water temperature.

Buoy	Network	Lat	Lon	Depth
Estaca de Bares	Deep Sea	44.12ºN	7.67ºW	1800 m
Cabo de Peñas	Deep Sea	43.75ºN	6.16ºW	615 m
Santander – IEO	Deep Sea	43.85ºN	3.77ºW	2500 m
Bilbao-Vizcaya	Deep Sea	43.64ºN	3.05ºW	2136 m
Villano-Sisargas	Deep Sea	43.50ºN	9.21ºW	386 m
Cabo Silleiro	Deep Sea	42.12ºN	9.43ºW	600 m
Santa Cruz de Tenerife	Coastal	28,46ºN	16,23ºW	56m
Las Palmas Este	Coastal	28,05ºN	15,39ºW	30m
Tenerife Sur	Deep Sea	27,99ºN	16,58ºW	710m

Table IV.2 Buoys used for Cantabrian triple colocation and SWAN unstructured validation in Canary island.

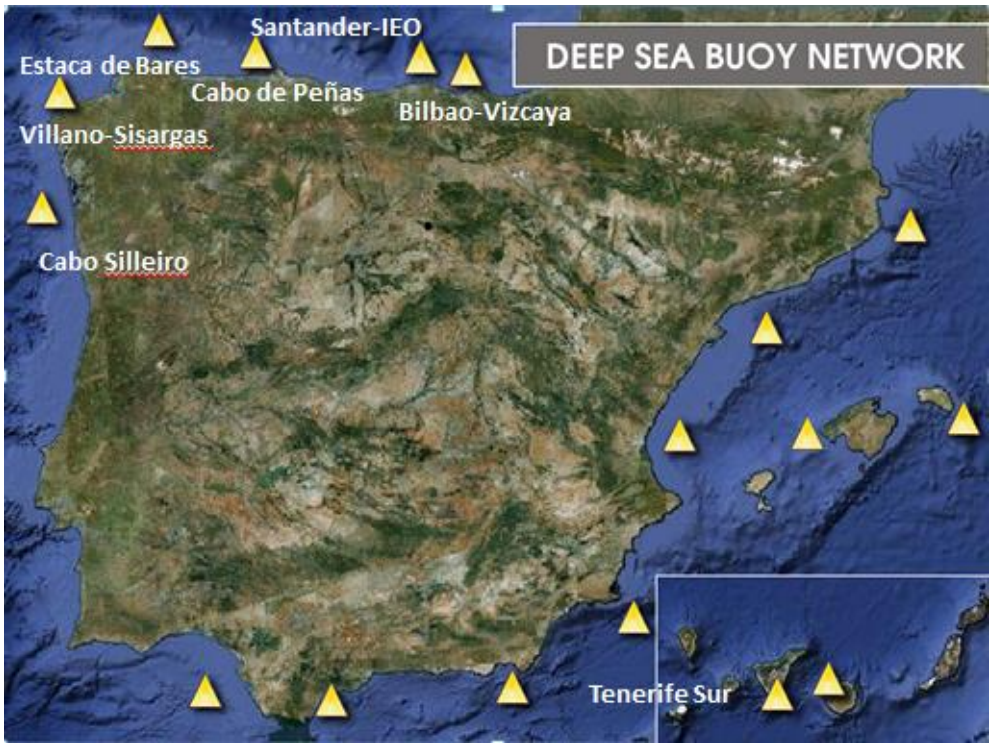

Figure IV.3 Deep Sea Buoy Network.

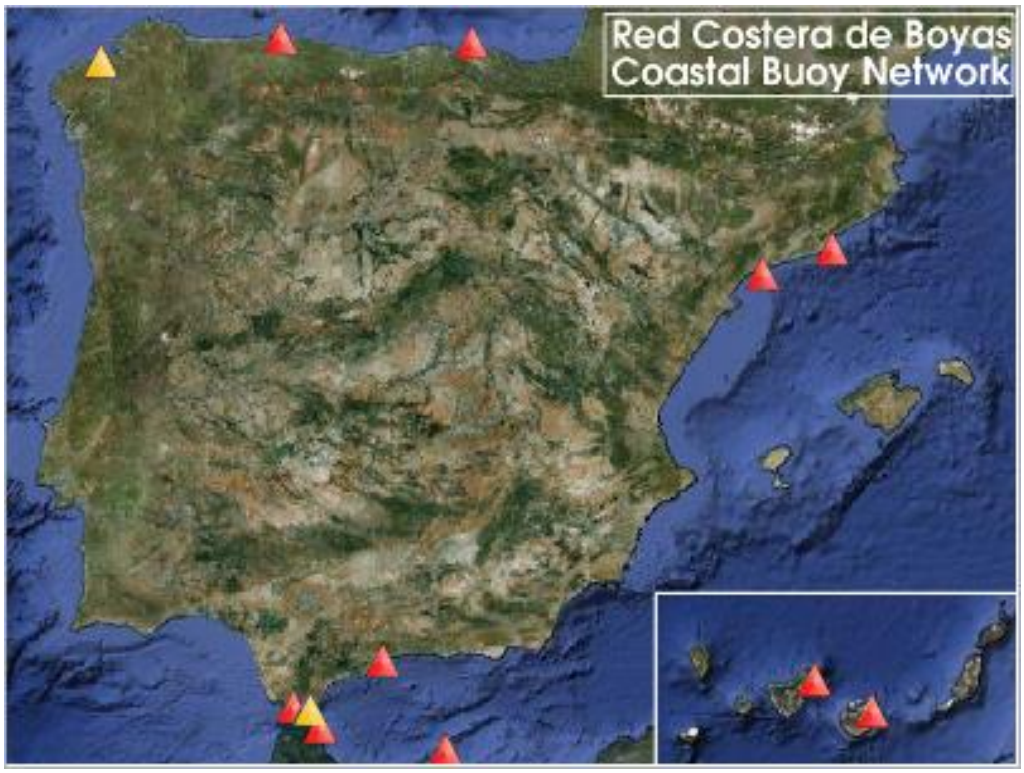

Figure IV.4 Coastal Buoy Network.

IV.3 Satellite

IV.3.1 Scatterometer

A scatterometer is a satellite radar instrument, which provides a measure of wind speed and direction near the sea surface. Scatterometers measure the electromagnetic microwave backscatter by the wind-roughened ocean surface (Figa-Saldaña et al., 2002). Scatterometer wind information is organised on a grid of Wind Vector Cells (WVCs) projected on the earth swath of the instrument. The number of across-swath WVCs determine the sampling resolution of the surface wind field and the wind information is considered to be Nyquist sampled, with modest correlation between neighbouring WVCs. Each WVC contains between two and four ambiguous local wind vector solutions that are the result of the inversion of the CMOD5 wind Geophysical Model Function (GMF), for a given set of backscatter values and a given scanning geometry (Stoffelen and Anderson, 1997; Portabella and Stoffelen, 2004). Each wind ambiguity is characterised by a solution probability that is determined based on the distance-to-cone residual after the inversion.

The wind ambiguities, solution probabilities and prior information from the ECMWF model 10-m background wind are used in a 2D variational (2D-Var) ambiguity removal procedure (Vogelzang et al., 2009) to produce an analysed surface wind field. This wind field is then used to select the wind vector ambiguity in each WVC that is closest to the analysis, based on vector difference, as the solution for the observed surface wind. A wind vector solution flag is set to the index of the selected

wind ambiguity in each WVC. Finally, the backscatter measurements, wind ambiguities, scanning geometry and wind vector solution flag, among others, are made available as a scatterometer wind product[1] in BUFR and NetCDF format. A detailed overview of past and current operational scatterometer is provided in Verhoef et al. (2012). Here we summarize the main characteristics of the scatterometers used in the MyWave study:

- SeaWinds. US Ku-band (sensitive to rain) scatterometer on QuikScat satellite. Launched in 1999 and operational until November 2009;
- ASCAT. European C-band (rain insensitive) scatterometer on Metop-A satellite. Launched 19 October 2006 and instruments A and B still operational;
- OSCAT. Indian Ku-band (rain sensitive) scatterometer on OceanSat-2. Launch June 2011 and operational until February 2014.

Seawinds (QSCAT) and OSCAT 10-m wind vector observations are representative for 25 km areas (25-km product), ASCAT provides a 12.5-km product. A relatively new product developed at KNMI as part of the EUMETSAT OSI-SAF activities is the ASCAT coastal product. Away from coastal regions this product is almost identical to the nominal 12.5 km product. However, an enhanced processing is applied to the beam footprints to calculate the wind in coastal WVCs (Verhoef et al., 2012). As such it is possible to compute winds as close as ~15 km from the coast, while in the nominal 12.5-km product, WVCs closer than ~35 km from the coast are flagged because of land contamination, see (Verhoef et al., 2012, Verhoef and Stoffelen, 2011). Verhoef et al. (2012) show that the quality of coastal winds is similar to that in the open ocean. Figure IV.5 shows the locations of the coastal product in red and overlaid the 12.5 km ASCAT product in grey. Away from the coastal regions, the locations of the coastal and 12.5 km product overlap, but near the coasts, the coastal product produces substantially more winds than the 12.5 km product. For instance, the coverage is about doubled in the Irish Sea.

[1] See http://www.knmi.nl/scatterometer

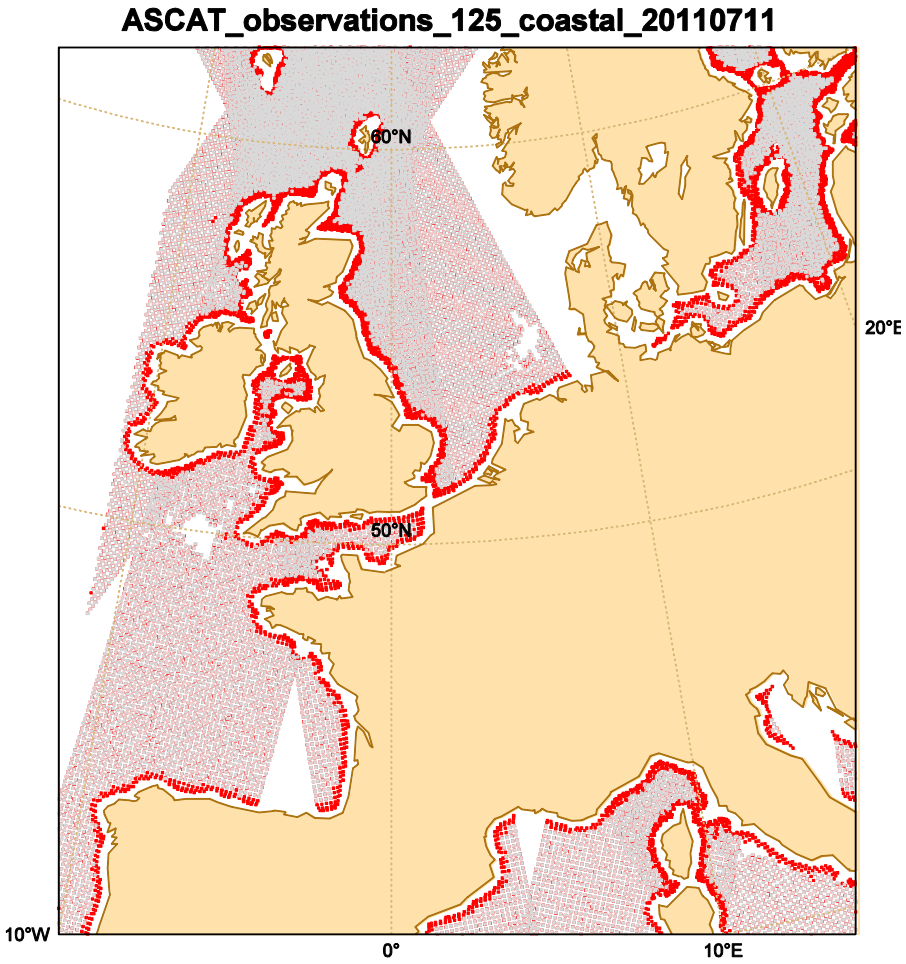

Figure IV.5 ASCAT observation locations over sea for the coastal product (red) and overlaid the 12.5 km product (grey) for all satellite overpasses on 11 July 2011 in the HARMONIE domain. The red band following the European coastline shows the additional ASCAT observations of the coastal product relative to the 12.5 km product.

Figure IV.6 zooms in to North Sea between the UK and The Netherlands. The distance of adjacent observations near the coast is clearly smaller than 12.5 km, due to the advanced processing near the coast. On average the distance of observations from the coast has been reduced from about 50 km to about 35 km by evolving from the 12.5 km to the coastal product. The additional observations are potentially very useful for collocation with buoys that are positioned close to the coasts. Moreover, these additional observations may improve the modelled wind field near the coast to better forecast storm surge.

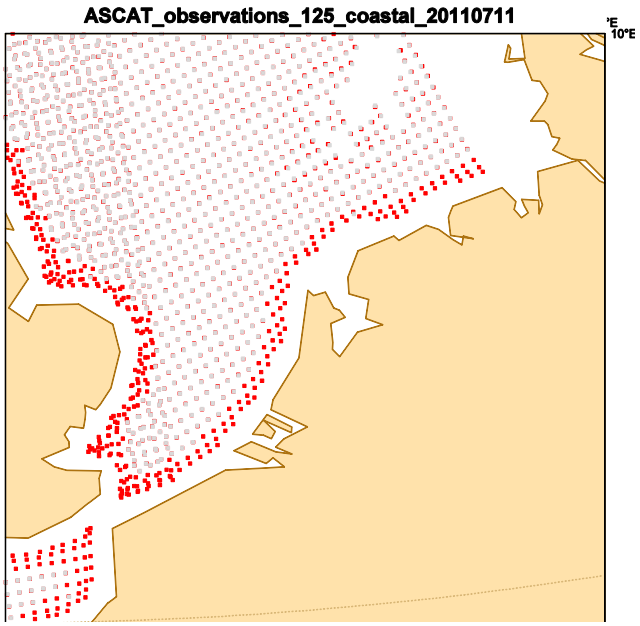

Figure IV.6 Same as Figure IV.5 but now zoomed in to the North Sea region between the UK and the Netherlands. White spots, e.g. at the top of the figure, indicate data void regions where the quality control procedure has flagged the corresponding observations as low quality.

IV.3.1.1.1 QuikScat re-processing

The GMF for QuikScat processing was improved in 2014. As a result, the complete 10-year QuikScat data has been re-processed at KNMI. Figure IV.7 shows that statistics of the old and re-processed QuikScat product are similar for low wind speeds, but the bias was reduced substantially for large wind speeds. These statistics are preliminary as evaluations are still on-going at the time of writing.

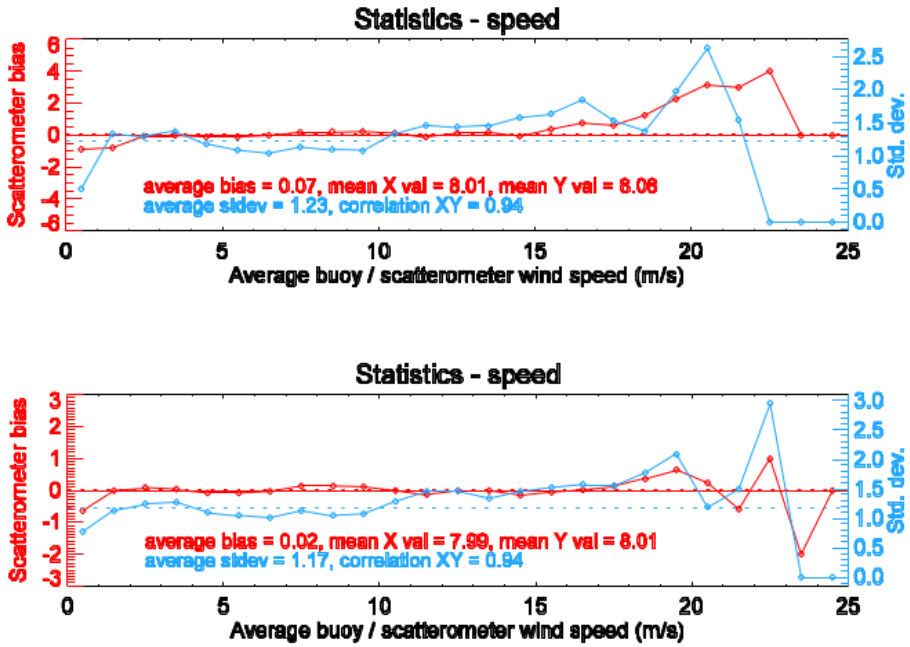

Figure IV.7 Statistics of QuikScat minus buoys wind speed before (top) and after (bottom) QuikScat reprocessing. Red/cyan lines show the bias and standard deviation respectively.

Comparing Figure IV.8 and Figure IV.9 shows that the wind speed over the North Sea has reduced substantially from a maximum of 10 Bft to a maximum of 9 Bft, after re-processing. Regions of more calm winds are largely unaffected.

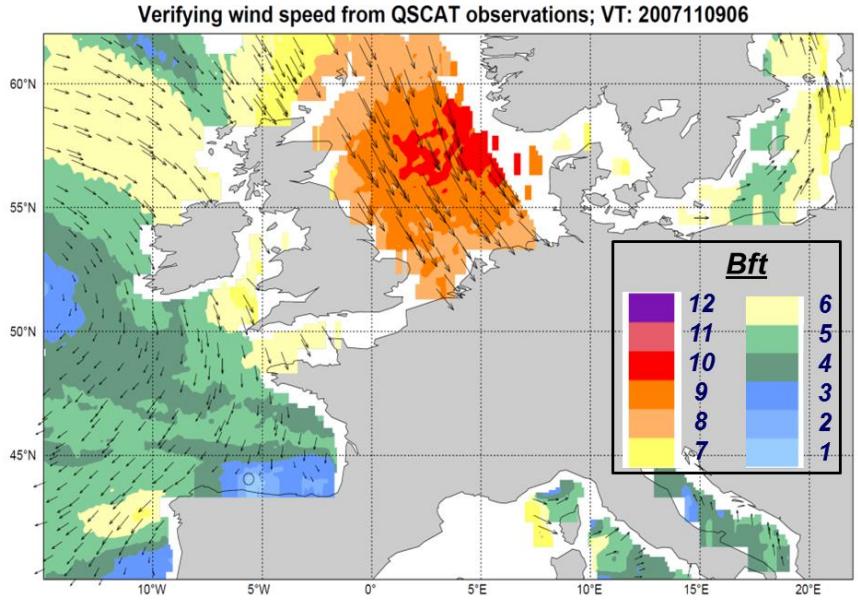

Figure IV.8 QuikScat 10-m wind speed measured at 9 November 2007, obtained from the previous version of the GMF. Combined plot of 2 QuikScat overpasses near near 04:30 UTC and 6:12 UTC.

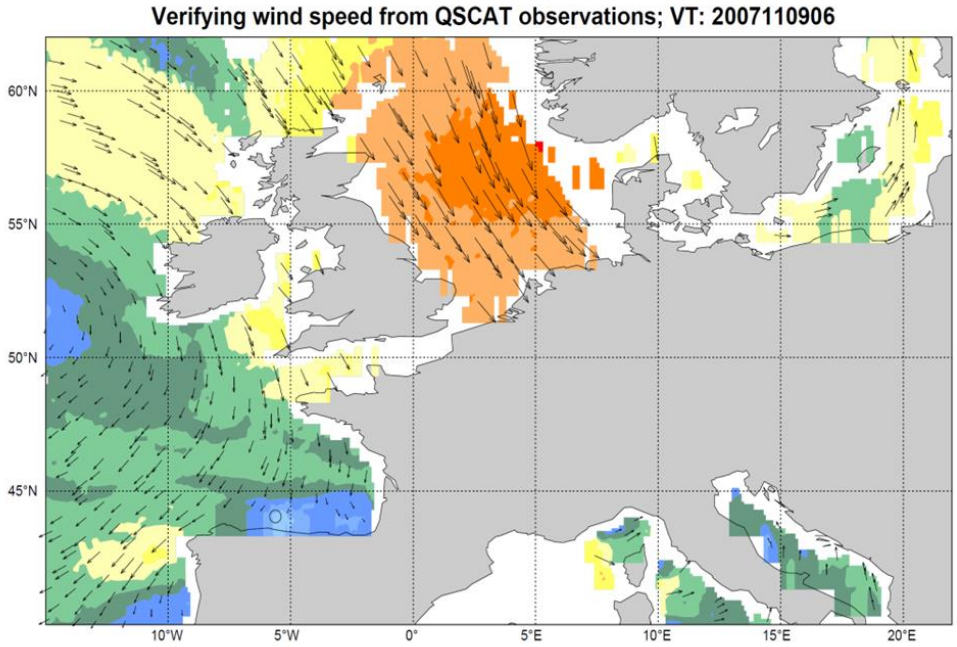

Figure IV.9 Same as Figure IV.8 but now after re-processing.

Figure IV.10 shows an intercomparison of re-processed QuikScat winds with 10-m HARMONIE model background winds. The proximity of the cyan and red curve illustrates the general close correspondence between the model and scatterometer winds. The large deviations between model and observations are mainly due to time mismatch between model analysis time and observation time, see section III.2, and the model positive bias for strong winds. The latter is confirmed by other studies, e.g. Baas (2014).

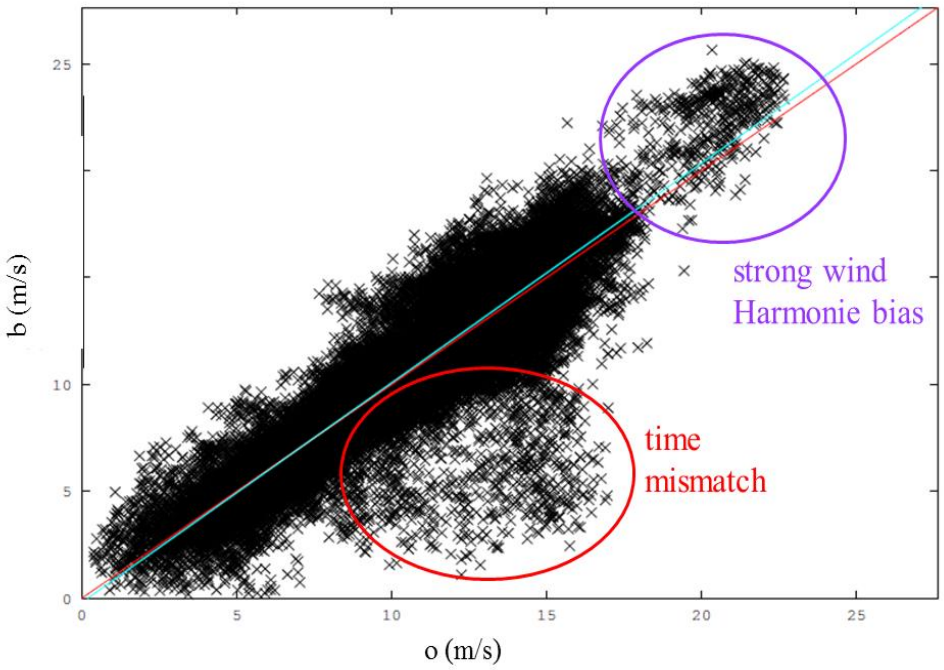

Figure IV.10 Scatter plot of the intercomparison of HARMONIE (y-axis) and QuikScat scatterometer (x-axis) wind speed over the 1 week period 4-11 November 2007. The red solid line is the diagonal, the cyan line the best match to the scatter points. Large deviations between model and observations are mainly due to time mismatch between model analysis time and observation time, see section III.2, and the positive model bias for strong winds.

IV.3.2Altimeter

Wave altimeter data over the North Sea and Mediterranean Sea have been extracted from the RADS (Doornbos, 2013, http://rads.tudelft.nl/rads/) archive and processed in order to provide controlled numerical fields to be used in OI procedures. This archive is DEOS' effort in establishing a harmonised, validated and cross-calibrated sea level data base from satellite altimeter data. It operates within the framework of the Netherlands Earth Observation NETwork NEONET, an internet facility, funded by the Dutch government (BCRS and SRON), for exploitation of remote-sensing expertise and data. The retrieved altimeters are listed in Table IV.3.

Handling of the altimeter data via the RADS system after the web retrieval consists in selecting the available data, within all available satellite cycles, with reference to a certain area and time interval, as well as to a certain number of parameters.

For the project purpose, in the Mediterranean Sea significant wave height and wind speed data were considered with an overall quality check based on the following parameters: norm std dev of range (threshold 0.15), norm std dev of significant wave height (1.00) and, wherever available, off-nadir angle squared from waveform (0.40).In the North Sea only significant wave height data were considered.

Mission Name	id	Launched	Provider
ERS-2	23560	21 Apr 1995	TuDelft
GFO-1	25157	10 Feb 1998	TuDelft
ENVISAT1	27386	1 Mar 2002	TuDelft
Jason 2	*33105*	*20 Jun 2008*	TuDelft
CryoSat 2	36508	8 Apr 2010	TuDelft
Saral-Altika	*39086*	*25 Feb 2013*	TuDelft

Table IV.3 List of considered satellite missions altimetry data.

V COASTAL WAVE FORECAST

V.1Introduction

This chapter is dedicated to the validation of the considered Mediterranean Sea, North Sea and North Atlantic wave forecasts. Each section deals with one region. Effects of 3D-Var EnKF and NN data assimilation are considered separately in sections V.3.3, V.3.5 and V.4. A detailed triple collocation study is reported in the next section and in Section V.5.2. The final section of this chapter compares the unstructed gridding with the grid nesting ways of obtaining high resolution coastal wave forecasts.

V.2 Mediterranean Sea

In this section we present the results of MyWave subtask 2.2.3, which aim is to cross validate *in-situ* and satellite measurements, together with wind speed and wave height forecasts. In particular the target is a realistic assessment of the accuracy of in situ and satellite measurements in the Mediterranean Sea.

V.2.1 Introduction

Observations are affected by errors. In a statistical sense, this means that a single observation is a realization of the convolution of the true climate distribution and the error distribution. These errors are helpful for a number of operations along the forecast process. For example, the design and the verification of an ensemble system does strongly depend on them. The exclusion of errors in the validation process would indicate a somehow “fake” reliability for the considered Ensemble Prediction System (EPS). For example, if the EPS were perfectly reliable, then it would lack of reliability if verified against pure observations.

V.2.1.1Available Data

In MyWave we have the opportunity to make use of high resolution forecast for the estimate of in situ and satellite instrument error uncertainties. The work done so far in WP3 has made an extensive set of co-located observations in Mediterranean Sea available to MyWave partners. The data set covers the six months period ranging from July 1st to December 31st 2013. Thanks to the cooperation between UKMO, ISMAR and USAM, each observation is co-located with both UKMO and Nettuno (nearest neighbour) forecast systems. In the following we make use of the (supposed) independence of the two forecast errors in order to extensively asses the error uncertainties for all the available observations set.

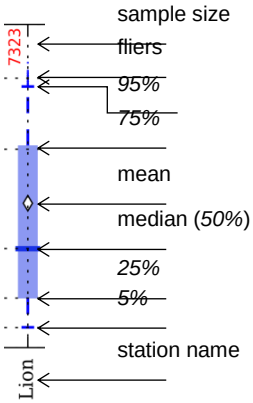

Figure V.1 Schematic representation of an instrument dataset.

For each instrument we present here the statistical characterization of the observed data. The representations are given graphically, and can be read with the help of Figure V.1. Buoys wind speed and significant wave height sets are depicted in Figure V.2 and Figure V.3, respectively. We must add that the stations list is restricted to those which turned out to be useful for the present work. That is, stations with a very small number of points are flagged as unreliable for that particular variable, therefore not considered. Altimeter (U_{10} and H_S) are given in Figure V.4, and Scatterometer wind speed distributions are rendered in Figure V.5.

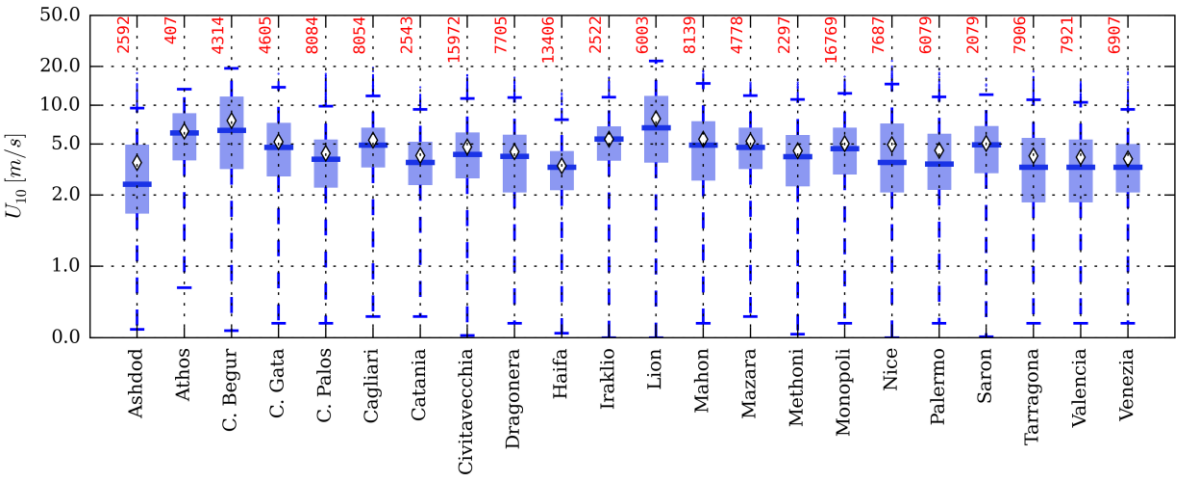

Figure V.2 Buoy observations. Distributions of wind speed measurements.

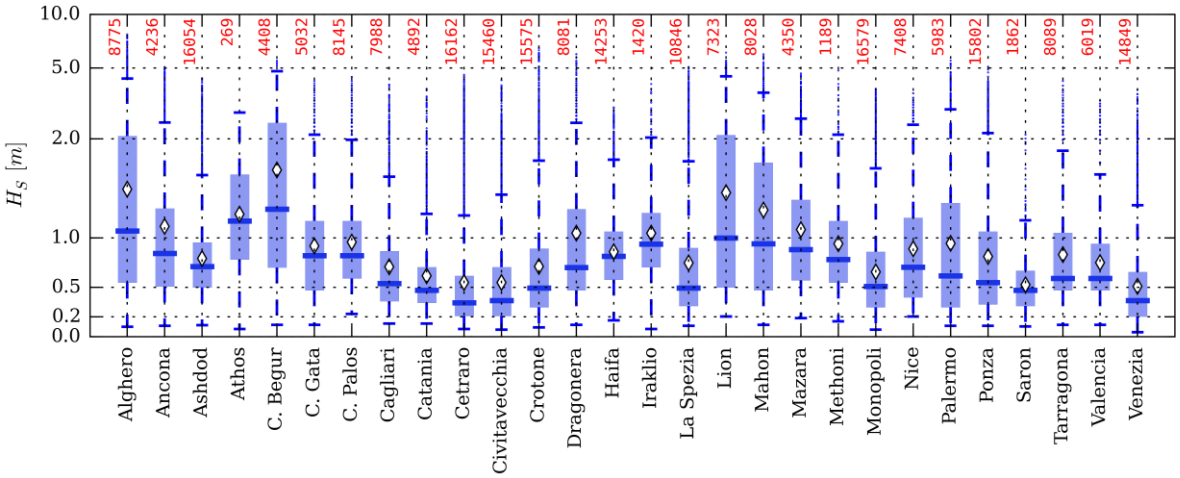

Figure V.3 As Figure V.2 but for significant wave height measurements.

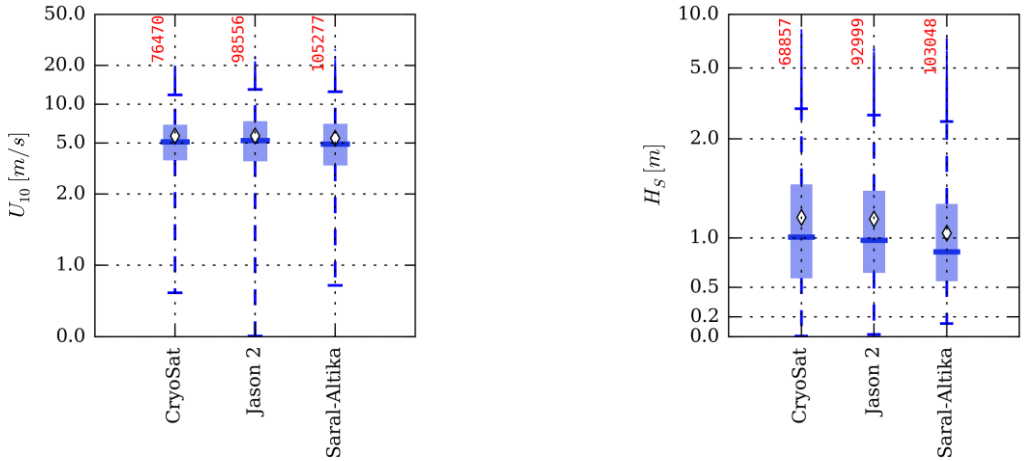

Figure V.4 Altimeter observations. Distributions of wind speed (left) and significant wave height (right) measurements.

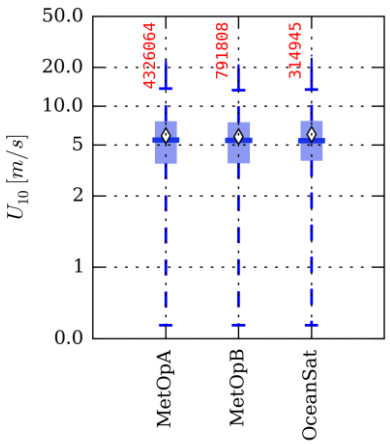

Figure V.5 Scatterometer observations. Distributions of wind speed measurements.

V.2.1.2 Methodology

The estimate of the accuracy of a signal (observation or forecast) can be assessed by means of the cross estimation between three signals, via triple collocation (Stoffelen, 1998; Janssen, et al. 2007). This technique requires that the three signals ($\mathbf{x}_i$) are estimators of the true signal **s**:

$$\mathbf{x}_i = \beta_i \mathbf{s} + \mathbf{e}_i \quad i = 1,2,3 \tag{2}$$

The fundamental hypothesis states that the errors ($\mathbf{e}_i$) associated to the signals are mutually independent, *i.e.*:

$$\mathbf{e}_i^T \mathbf{e}_j = 0 \quad i \neq j \tag{3}$$

and that they are not correlated with the true signal. The output of the procedure are the absolute estimates of the three error 2-norms (root mean squared errors), together with the estimates of two relative slopes, that is the set:

$$\Omega = \left\{ \|\mathbf{e}_i\|_2, \|\mathbf{e}_j\|_2, \|\mathbf{e}_k\|_2, \frac{\beta_j}{\beta_i}, \frac{\beta_k}{\beta_i} \right\} \tag{4}$$

with arbitrary choice of the indices.

In the present work, due to the limited extension of some subsamples, the confidence intervals are retrieved via a Monte Carlo bootstrap algorithm. Moreover, prior to each triple collocation, we make sure that each subsample is unbiased by subtracting the subsample mean value. In this way, the error estimates are actually the error standard deviations, *i.e.,* the measure of the error uncertainties. In other words, we replace the hypotheses on error orthogonality with the same condition applied to unbiased errors. That is

$$\left(\mathbf{e}_i - \langle \mathbf{e}_i \rangle\right)^T \left(\mathbf{e}_j - \langle \mathbf{e}_j \rangle\right) = 0 \quad i \neq j \tag{5}$$

and

$$\left(\mathbf{e}_i - \langle \mathbf{e}_i \rangle\right)^T s = 0 \,. \tag{6}$$

V.2.2Observations Accuracies

In this paragraph we present the results of triple collocation assessment for each one of the available (and consistent) data set. Following figures (Figure V.6 to Figure V.9) give, instrument by instrument, the estimated error uncertainties together with error bars. These indicate the 90% confidence intervals as estimated from the plain bootstrap procedure. For sake of uniformity with literature results, the results are given as scatter index, that is the error uncertainties are normalized dividing them by the observations sample mean.

There might be the case of a low energetic sample in which the truncation errors become very important. In the scatter index fashion, the errors are therefore amplified. For example, most of the RON buoys are provided by the same producer, same model, and operate with the same software. But observing Figure V.7 alone there seems to be a huge difference in performance between Alghero and Mazara buoys. With an eye to Figure V.3 one can argue that the reason of performance difference may come from the fact that Alghero climate is much more energetic than Mazara's. The differences in normalized error uncertainties between buoys may therefore strongly depend on the observed climate due to the speed scaling and the spatial representativeness errors (Stoffelen, 1998).

In the case of satellite measurements, their behaviour is very similar to what previously reported in literature (see *e.g.* Janssen, et al. 2007) with few differences between instruments. Altimeter wind speed scatter index (Figure V.8) varies between 22% (CryoSat) and 24% (Jason 2), while scatterometer (Figure V.9) relative uncertainty varies between 19% (MetOpB) and 22% (MetOpA). The altimeter errors on H_S do strongly depend on the mission: CryoSat uncertainty is approximately 24% of the sample mean, Jason' is 21% and Altika is 18% (Figure V.8).

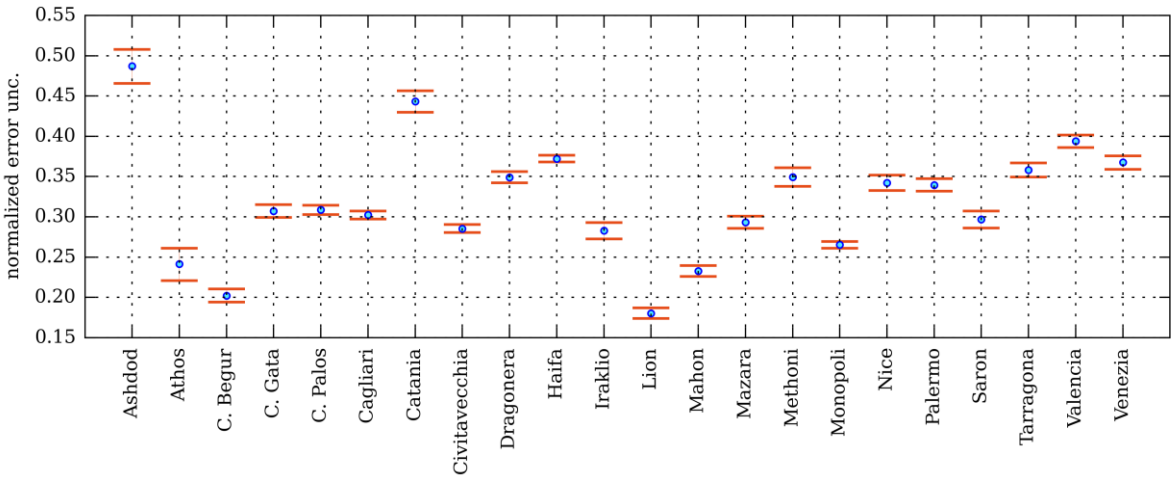

Figure V.6 Accuracy of wind speed buoy observations. Results are dressed with 90% bootstrap confidence intervals.

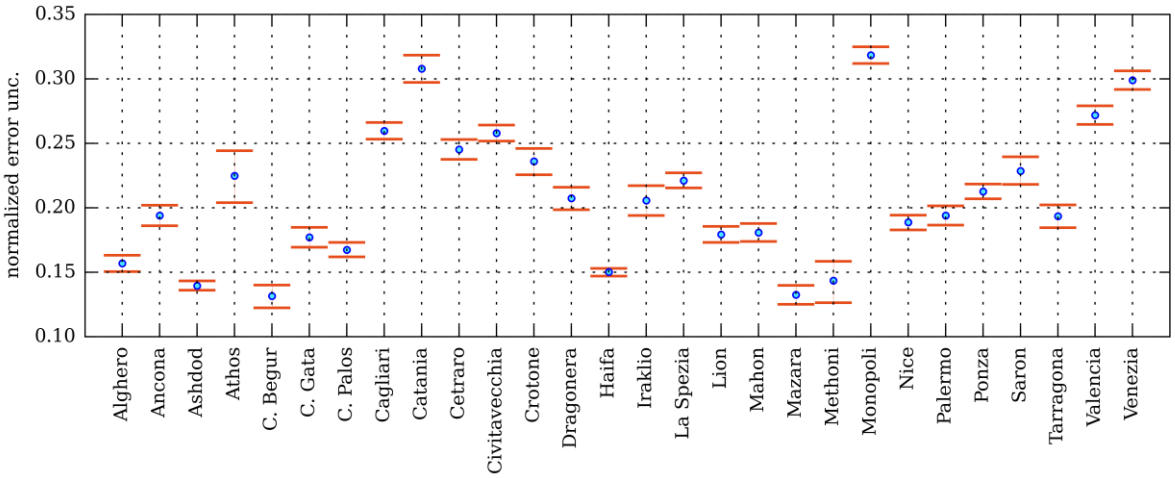

Figure V.7 *As Figure V.6 but for significant wave height measurements.*

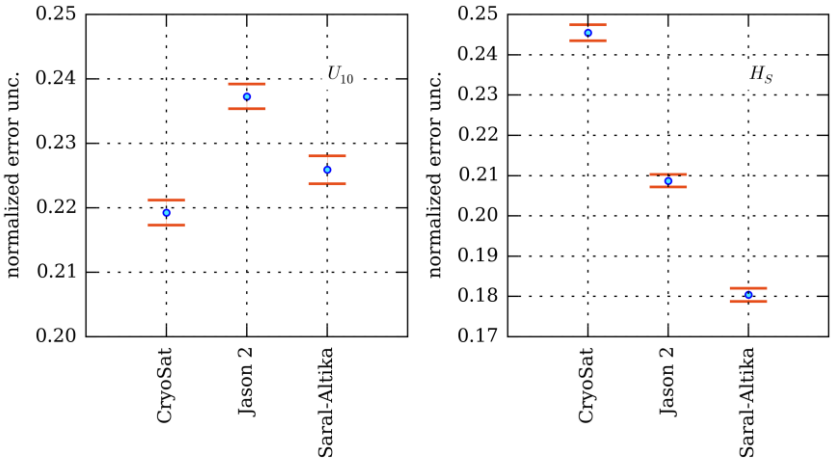

Figure V.8 *Altimeter normalized errors. Wind speed (left) and significant wave height (right).*

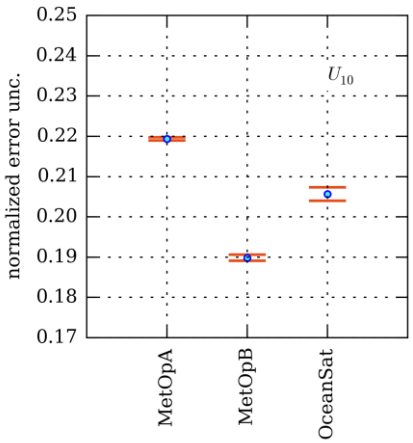

Figure V.9 *Normalized errors of scatterometer wind speed observations.*

V.2.3 Overall Accuracies

In this paragraph we give the results of the triple collocation procedure for the overall dataset. We persist with the distinction instrument type by instrument type, but we consider them as a whole, in order to evaluate the somehow averaged uncertainties in the Mediterranean Sea. In this case, we also give the regression slopes of the model control forecasts (relative to the instrument) and the models associated uncertainties.

Since the model errors, true signal and amplifications are expected to vary along forecast lead time, we perform triple collocation on 6 hours overlapping time windows. In the case of scatterometers, the number of observations are not evenly distributed over the day. In fact there are few hours when none of the three considered instruments passes over the Mediterranean Sea. In this case, the results are given for first and second forecast day only.

In the case of buoys both wind speed (U_{10}, Figure V.10) and significant wave height (H_S, Figure V.11) error uncertainties of the instruments appear to be relatively stable along forecast lead time. This partially confirms the triple collocation hypotheses. That is to say that there's no correlation between some of the couples formed by the errors and the true signal, or that all correlation effects cancel each other. On the other side, errors grow for both models with forecast lead time. We must underline that the error uncertainties of both Nettuno and UKMO control runs are practically coincident at buoy locations.

In the case of altimeters, some of the non-correlation hypotheses seems to fail. We can observe the effect in the bottom panels of Figure V.12 (U_{10}) and Figure V.13 (H_S). Instrument error uncertainties seem to grow along forecast lead time, due to reduced correlation with the degraded model fields. The buoy and altimeter errors that both resolve more small-scale signal that the model, become increasingly correlated when the signal (in the model) decreases, therefore invalidating the simple triple collocation procedure. A spatial representativeness error may be considered to improve the interpretation (Vogelzang et al., 2011; Stoffelen, 1998). The same is observed in Figure V.14 for scatterometer wind speed.

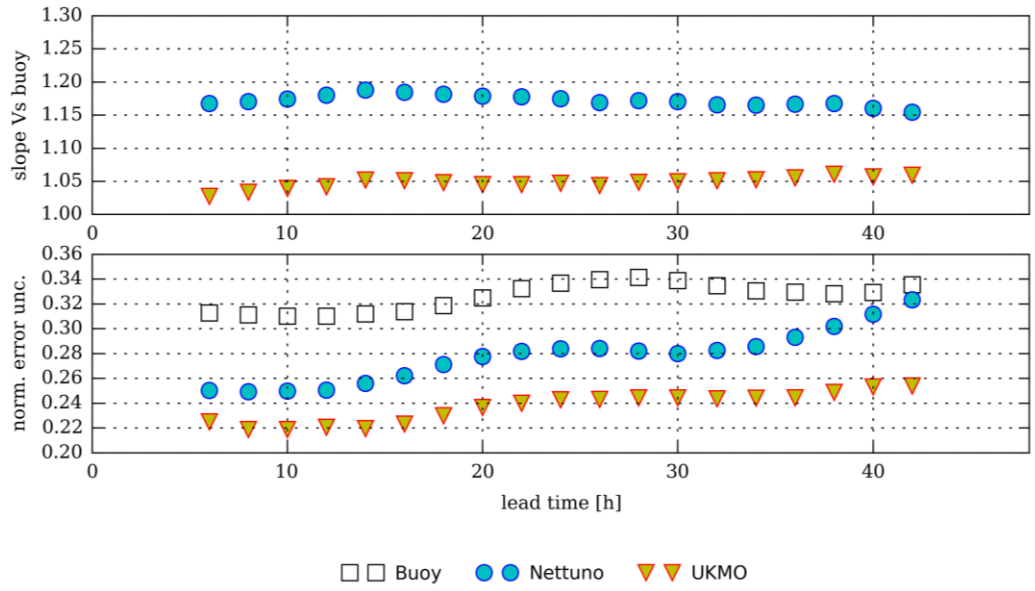

Figure V.10 Relative slope (top) and accuracy (bottom) of UKMO and Nettuno wind speed control forecast. The slopes are evaluated with respect to buoy observations.

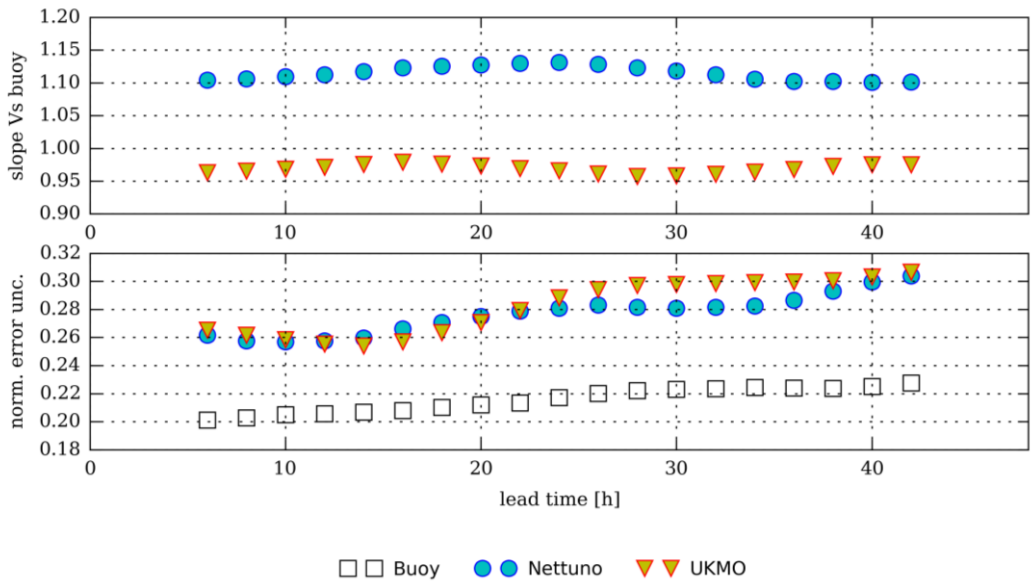

Figure V.11 Same as Figure V.10 but for significant wave height.

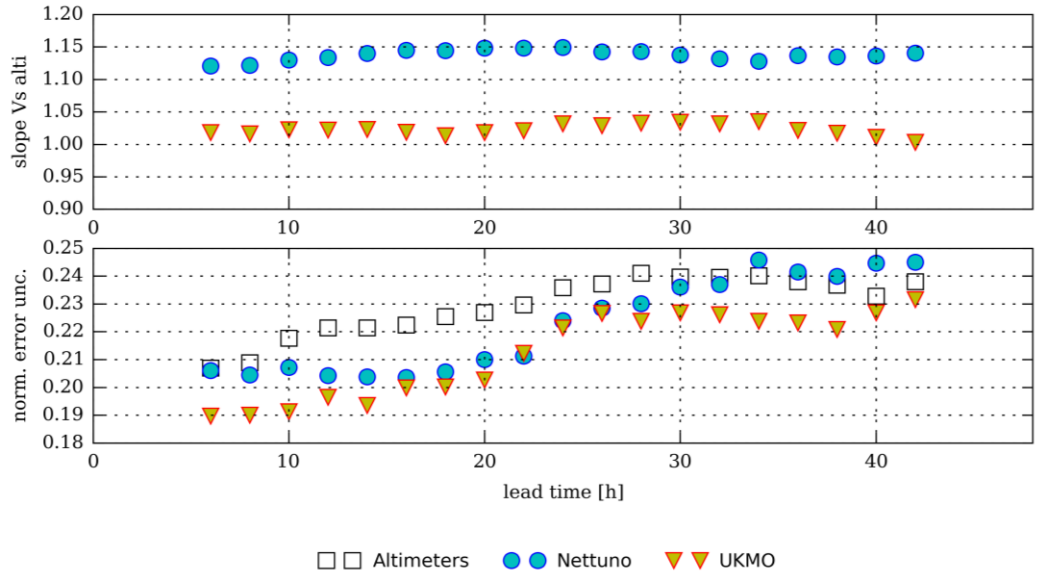

Figure V.12 As Figure V.10 but for altimeter wind speed observations.

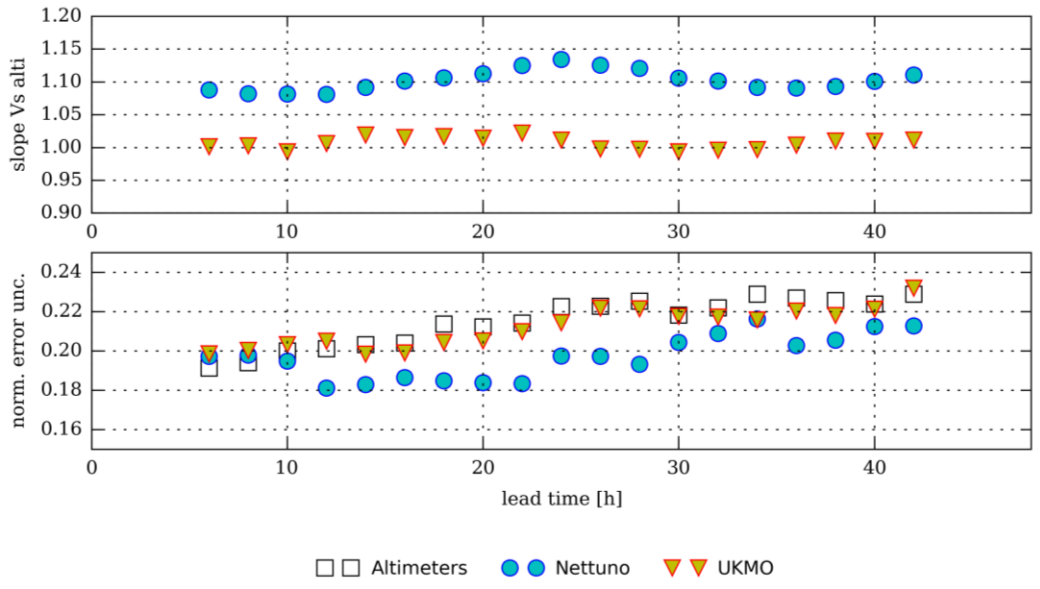

Figure V.13 As Figure V.10 but for altimeter significant wave height observations.

Let's add a few words about the control forecasts behaviour. These have been extensively validated in WP3 (D3.4), but here we present a different point of view, which should be seen as a pre-validating process. The above figures describe the overall errors of the de-biased models, if triple collocation hypotheses were true. We hereby confirm that Nettuno, with respect to UKMO, presents a higher tendency to amplify the true signal. Regarding significant wave heights, Nettuno errors are slightly less uncertain than UKMO ones. The opposite occurs in the forecast wind speed field.

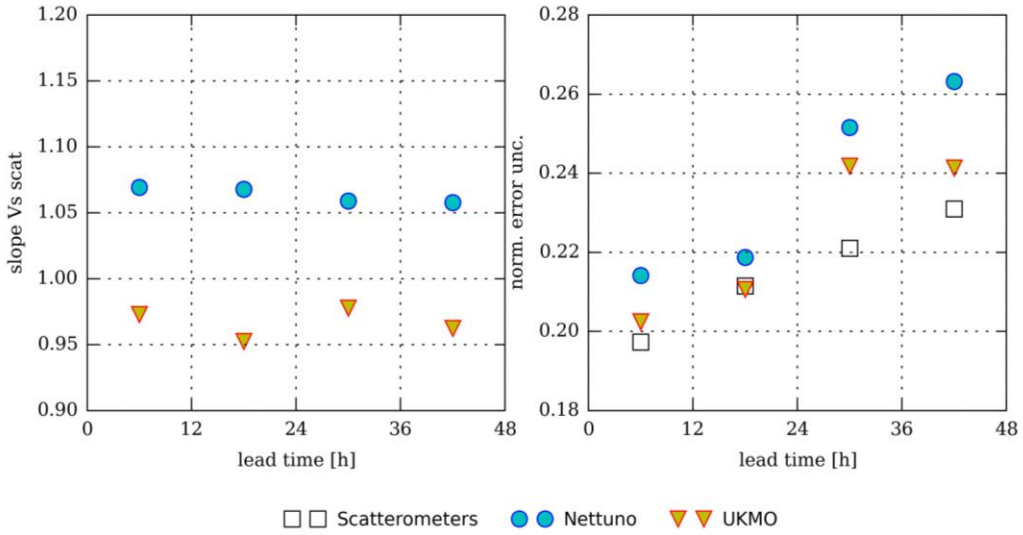

Figure V.14 Relative slope (left) and accuracy (right) of UKMO and Nettuno wind speed control forecast. The slopes are evaluated with respect to scatterometer observations.

V.3 Southern North Sea

V.3.1 Introduction

In this section the results of the Southern North Sea forecast and data assimilation experiments are reported. Both atmospheric model and wave model results are presented. The atmospheric model experiments have been carried out by KNMI using their HARMONIE model. The wave modelling experiments have been carried out by Deltares using the SWAN North model (SWAN-DCSM). Four periods have been considered in the experiments and they are briefly described in the next section. In Section V.3.3 the HARMONIE experiments are described. In Section V.3.4 the wave model results are assessed using a different forcing winds, including those resulting from the HARMONIE experiments. At last, a SWAN-DCSM data assimilation experiment is presented in Section V.3.5.

V.3.2 Storm periods

Four storm periods have been agreed upon the MyWave partners for the verification of model wind and wave predictions in the Southern North Sea. These four periods are:

- Period 1 – from 28 October until 3 November 2006 – This period is characterized by a NW-W storm. On the 1st of November 2006 a sharp trough (convergence zone in cold air) circles over the North Sea to the south, steered by a rapid eastward moving storm low in the northern North Sea. Wind variations (increase and decrease, as well as direction changes) are large during the day, temperature variations small (cold air event). The storm is marked as a surge- and SWL record in Delfzijl and well known as Allerheiligenvloed or the “Horses storm”, because 227 horses were isolated

due to flood in Marrum, 25 horses drowned, the rest was saved in a spectacular rescue operation.

- Period 2 – from 4 until 11 November 2007 – On 08 November 2007 an intensifying low moves over the southern Norwegian Sea to Skagerak, the next day with decreasing intensity to the central Baltic. In its intensifying period it causes a north-westerly storm field over the central North Sea with a long fetch over water on the 9th. As a cold-air-mass-event the temperature changes at 1.5 km are small, about max. 5 ºC, the air mass is unstable (in November with relative warm seawater). This NW storm is the first since the building of the Nieuwe Waterweg (Dutch for "New Waterway") and the Maeslantkering (Dutch for "Maeslant barrier", http://en.wikipedia.org/wiki/Maeslantkering) that led to the closure/activation of the Maeslantkering storm surge barrier.
- Period 3 – from 11 until 17 July 2011 - This period is characterized by a NE storm which is not very common but interesting. It is one of the periods used in the benchmark assessment of the operational SWAN model for the North Sea.
- Period 4 – from 6 December until 6 January 2012 - A 1 month period that includes storm Ulli (http://en.wikipedia.org/wiki/Cyclone_Ulli). This longer period is considered in order to obtain more robust statistics of the models performances.

V.3.3 Data assimilation in HARMONIE

V.3.3.1 HARMONIE data assimilation period 2

Period 2 extends from 4-11 November 2007. A brief description of the event is found above and in [DR1]. Four experiments with the HARMONIE model were conducted for this period:

1. No data assimilation, i.e., downscaling from ECMWF model forecasts (*NODA*)
2. Data assimilation of conventional observations only (*CONV*). A 3-hour assimilation window was used.
3. Same as (2) but with additional assimilation of scatterometer winds from ASCAT and QuikScat (*CONV+SCAT*). The default settings for scatterometer assimilation were used. These are related to ECMWF's strategy of scatterometer assimilation: ASCAT thinning to 100 km distance between adjacent observations and no thinning applied to QSCAT.
4. Same as (3) but without ASCAT thinning (*CONV+SCAT-NOTHIN*)

Figure V.15 shows a typical example of the coverage of used observations by HARMONIE for two assimilation cycles. The coarse coverage of ASCAT winds in the left panel clearly shows the thinning when default settings are applied (experiment 3 (CONV+SCAT) mentioned above). In the "no-thinning" experiment 4 ASCAT observations at all grey dots are used. The right panel of Figure V.15 shows that most QSCAT observations are used. Missing data are mainly related to quality control checks, e.g., removing observations affected by rain or too large background departures.

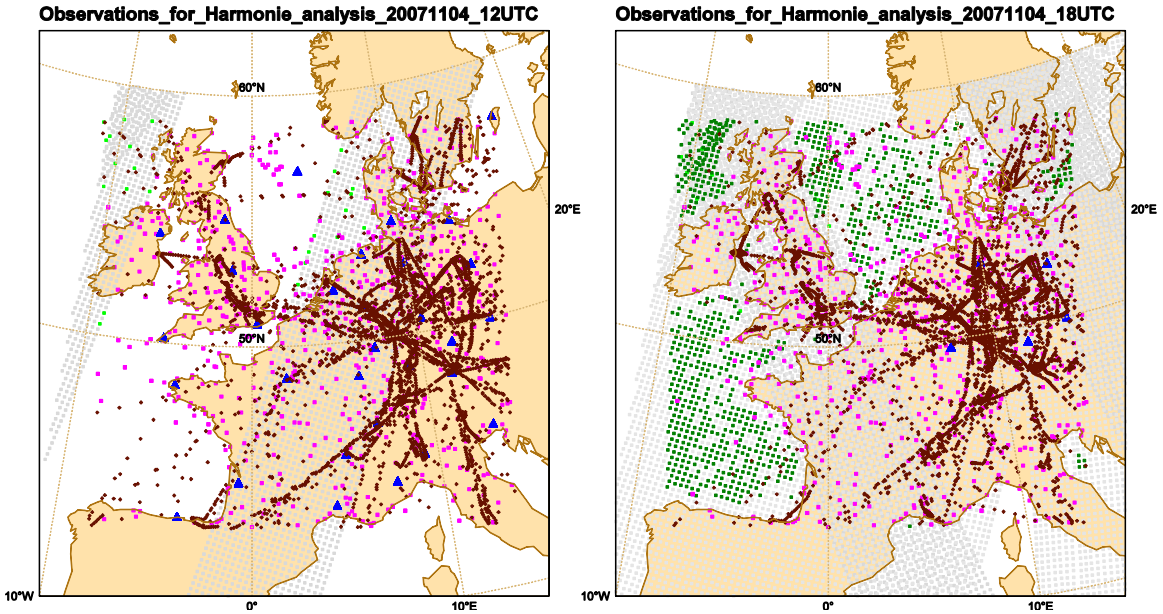

Figure V.15 Observations used by HARMONIE on 4 November 2007 for the 12 UTC analysis (left) and 18 UTC analysis (right). Colours indicate the different observing systems: SYNOP stations (magenta), radiosonde (blue triangle), AMDAR (brown), ASCAT (light green) and QSCAT (dark green). The grey spots indicate all scatterometer locations.

The Maeslantkering (part of the Dutch coastal flooding defense system) was closed for the first time on 9 November 2007. Figure V.16 and Figure V.17 show 4 HARMONIE forecasts, corresponding to the 4 experiments defined above, valid on 9 November 2007 at 06 UTC. For comparison, Figure V.18 shows the ECMWF forecast valid at the same time. ECMWF shows maximum wind speeds of 9 Bft over the North Sea in agreement with observations from QuikScat measured around the same time, see Figure IV.9. The maximum wind speed in all HARMONIE runs is 10 Bft, i.e., larger than ECMWF and as observed by QuikScat, confirming the positive wind speed bias of HARMONIE for strong winds, see also Figure IV.10.

The differences between the 4 HARMONIE runs in Figure V.16 and Figure V.17 are rather subtle. When zooming in to the Dutch coastal area in Figure V.19, the experiment including scatterometer winds shows increased winds in the South-Westerly part of the Netherlands (Zeeland). Validation with independent observations from e.g. wind masts is needed to conclude which experimental set up performs best, see Section V.3.4.2.

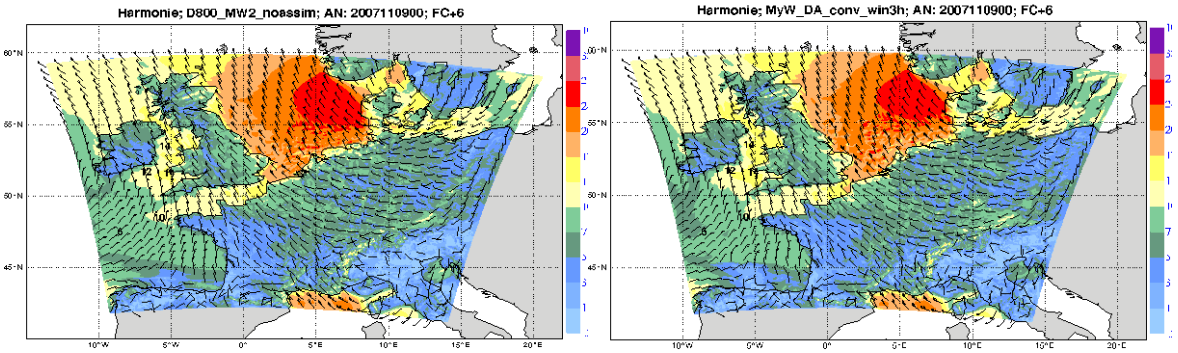

Figure V.16 6-hour HARMONIE forecasts valid at 9 November 2007 06 UTC from experiment 1 (NODA) (left) and experiment 2 using conventional observations only (CONV). The colours in the legend on the right hand side go from 1-12 Bft.

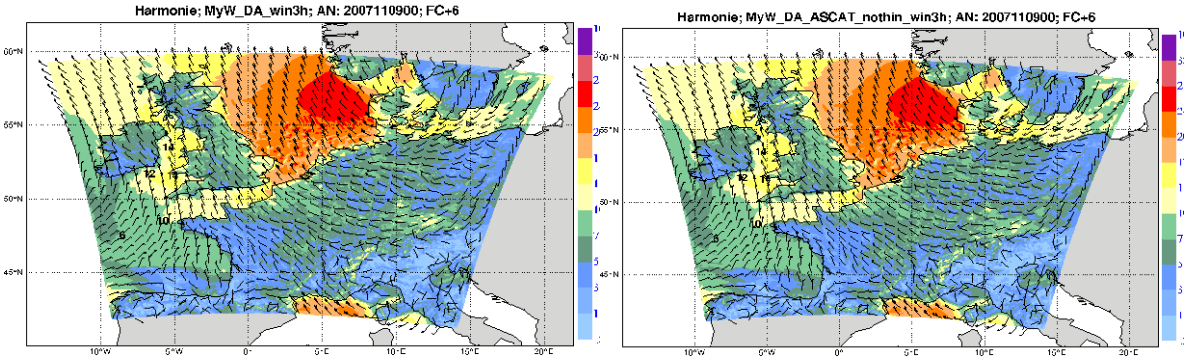

Figure V.17 Same as Figure V.16 but now for experiment 3 (CONV+SCAT) (left) and experiment 4 (CONV+SCAT-NOTHIN) (right).

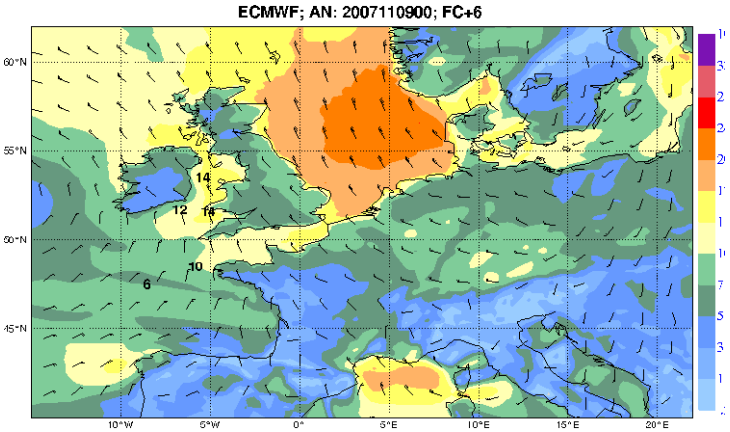

Figure V.18 Same as Figure V.16 but now for the ECMWF model.

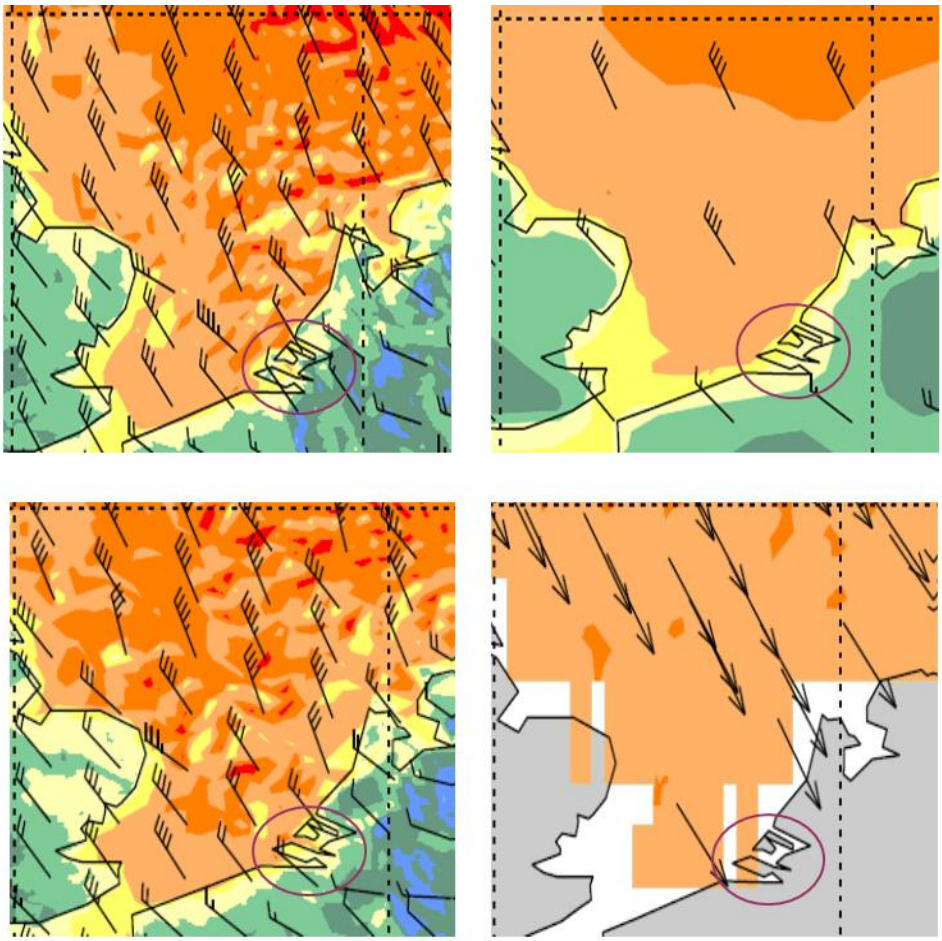

Figure V.19 6-hour HARMONIE forecasts valid at 9 November 2007 06 UTC, with focus on the Dutch coastal area, from the NODA (upper left), ECMWF (upper right) and CONV+SCAT-NOTHIN (bottom left) experiments. The bottom right panel shows QuikScat, i.e., zoomed in from Figure IV.9.

Comparing the HARMONIE forecasts with ECMWF and QuikScat observations in Figure V.19 it is clear that HARMONIE generates much more small-scale structures than ECMWF and observed, an indication that HARMONIE is too excessive on convective processes and/or rain; it was verified that the model produced rain around 06 UTC. This was further evaluated by considering satellite imagery from the MeteoSat 2nd generation geostationary platform. Figure V.20 in combination with the flow pattern from e.g. Figure V.18 indicates a large scale flow pattern from the North Pole area moving towards Europe. Cold air flow over relatively warm ocean surface water triggers convection and up-and-down drafts, so called rolls. These rolls grow with distance from the origin of the flow. Well-developed rolls are separated over longer distances and have deepened, visualized by the darker clouds over the Southern part of the North-Sea in the infrared image. The satellite figures show strong convective activity over the North-Sea, but from these figures it is not clear whether this produced rain around 06 UTC. The rain flags in the QuikScat product were off, indicating that no rain was observed by QuikScat. We note that the QuikScat effective footprint is about 50 km (for the used 25-km product), i.e., much lower than the HARMONIE model grid size. The scatterometer observations thus

give no clue on the actual occurrence and realism of the small-scale model structures.

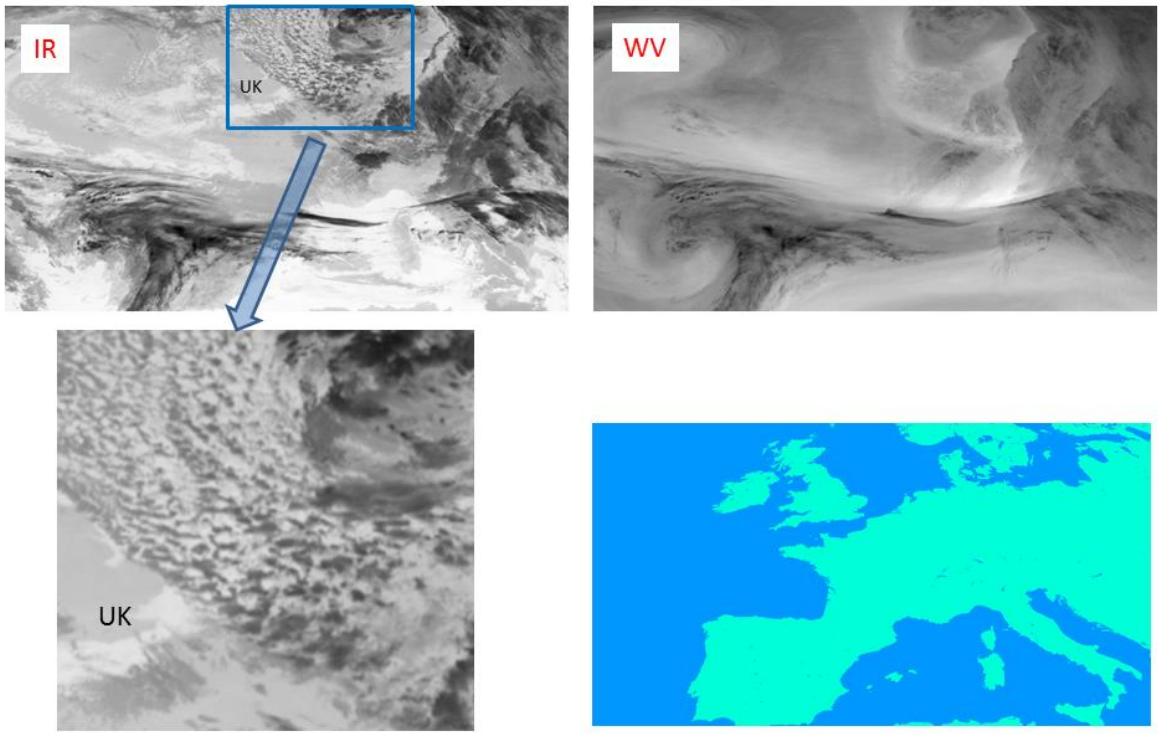

Figure V.20 Imagery from the geostationary MeteoSat Second Generation satellite on 9 November 2007 06 UTC from the Infrared (IR) channels (top left) and water vapour (WV) channel (top right). The lower left panel zooms in on the UK and North-Sea area. The bottom right panel shows the domain of the top panel figures. White/black spots in the IR figure correspond to relatively cold/warm regions. The temperature over the UK was around 3 degrees, while the ocean temperature was about 9 degrees Celsius.

Figure V.21 is another way of showing the small-scale features present in the model but not found in the QuikScat observations. It is noted that data assimilation systems assume all observations as point observations, also for area average observation like scatterometer. For global models with a typical grid size of 10-20 km and an effective model resolution of 100-200 km or lower this assumption may be approximately valid. However, this assumption breaks down for mesoscale models with grid sizes in the order of 3 km and smaller. Figure V.22 shows that averaging in the model domain equal to the observation footprint size makes the model state more representative for the observation, i.e., the cyan vectors, rather than the blue vectors, are better in agreement with the red vectors. Mesoscale data assimilation will therefore profit from more advanced observation operators that take into account the observation footprint size.

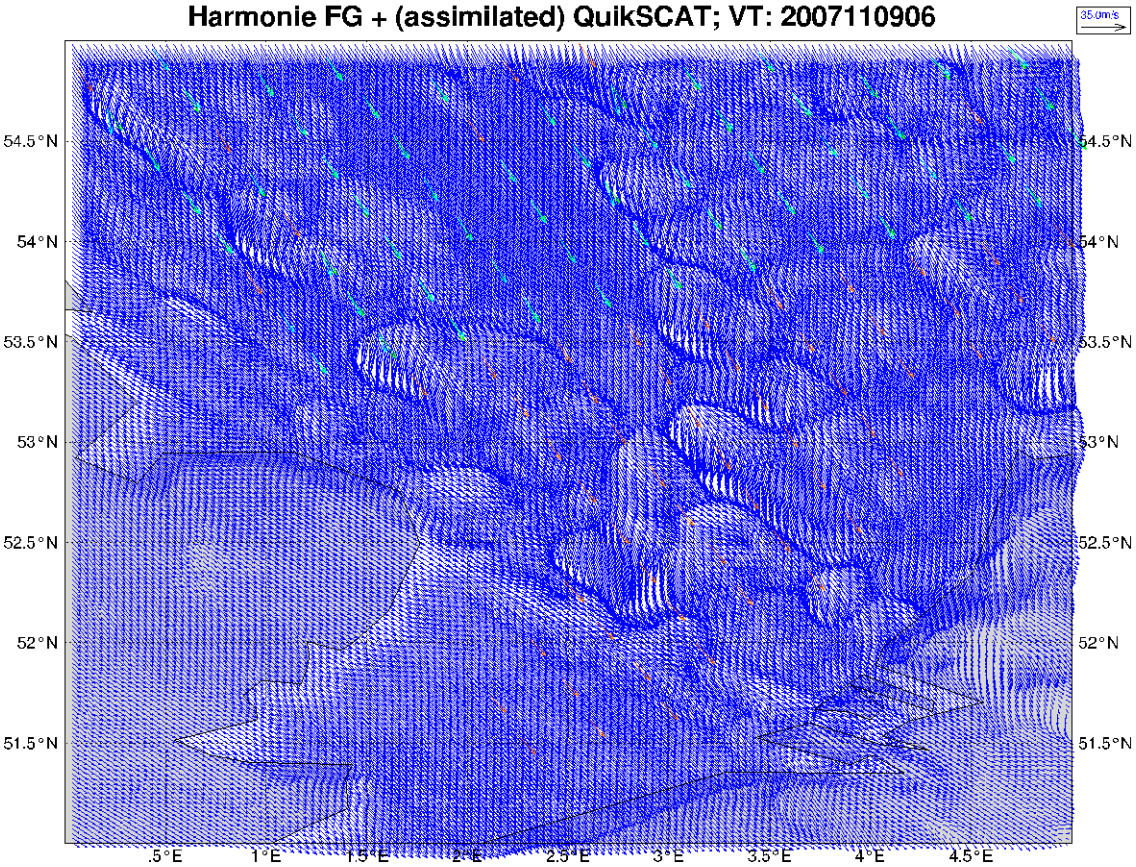

Figure V.21 HARMONIE 6-hour 10-m wind forecast valid on 9 November 2007 06 UTC (dark blue). Wind vectors are plot on the 2.5 km HARMONIE grid. Overlaid, QuikScat observations used (cyan) and not used (red) by data assimilation.

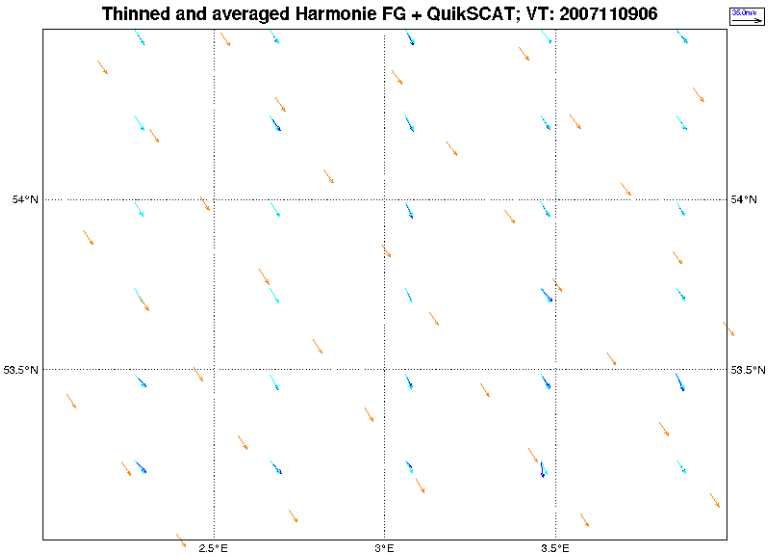

Figure V.22 Same as Figure V.21 but zoomed in and the HARMONIE model wind (dark blue) thinned to 25-km distance separation, i.e., the distance of neighboring QuikScat observations. The cyan vectors are the result of averaging HARMONIE winds over 25x25 km boxes.

Finally, we would emphasize that data assimilation cannot compensate for model deficiencies, such as biases. The left panel of Figure V.23 shows the background state of the 06 UTC analysis in the right panel. Clearly, QuikScat has been able to reduce the too strong background winds North of Germany, near Denmark. However, the subsequent forecasts in Figure V.24 and Figure V.25 show that the model tends to strengthen the wind field again. Already, after 3 hours the wind field bias is at the same level as before the assimilation of QuikScat.

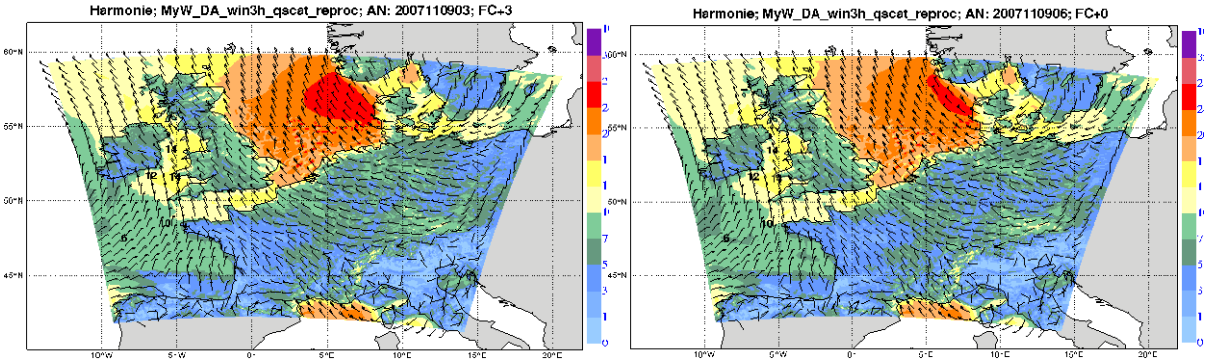

Figure V.23 HARMONIE 3-hour forecast valid at 9 November 2007 06 UTC (left) and HARMONIE analysis valid for the same time (right).

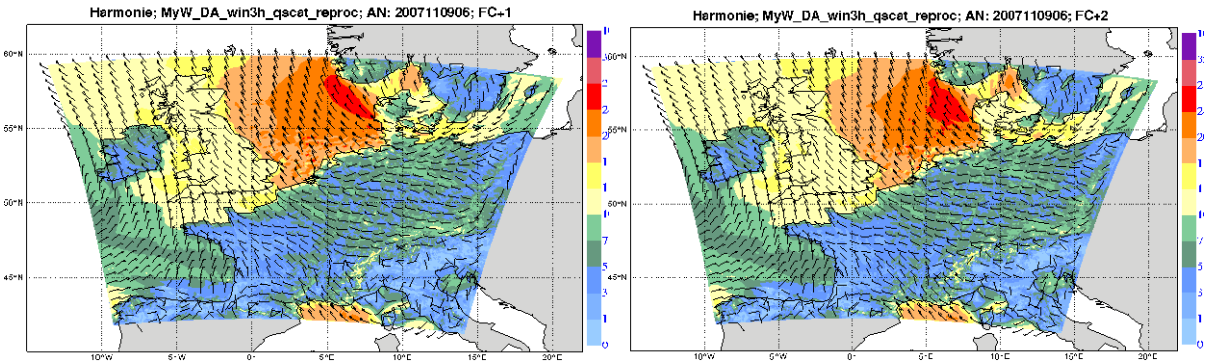

Figure V.24 Left: 1-hour forecast initiated from the 06 UTC analysis in the right panel of Figure V.23. Right: similar but now for a 2-hour forecast

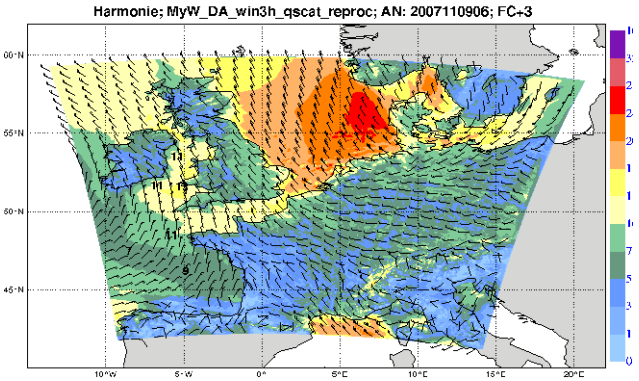

Figure V.25 Same as Figure V.24, but now the 3-hour forecast initiated from the 06 UTC analysis.

V.3.3.2 HARMONIE data assimilation period 4

Period 4 extends from 6 December 2011 until 6 January 2012 and covers the period before and at the moment that storm Ulli hit West Europe and gave high water levels in the Netherlands on 5 January 2011. A more complete description of the event is found in [DR1]. Three experiments with the HARMONIE model were conducted for this period:

1. Data assimilation of conventional observations only. The assimilation window is 3 hours. (*CONV-3h*)
2. Same as (1) but with additional assimilation of scatterometer winds from ASCAT and OSCAT (*CONV+SCAT-3h*). Scatterometer observations were used at their maximum resolution, i.e., no data thinning was applied
3. Same as (2) but for a 1-hour assimilation window (*CONV+SCAT-1h*)

The 3rd experiment with a 1-hour assimilation window was used for the first time in HARMONIE and motivated by the findings from the earlier experiments of period 2, see section V.3.3.1, that a 3 hour window may be too large for high-impact weather events discussed in this report.

An advantage of 1-hour over 3-hour cycling is that about 3 times more observations from SYNOP stations and buoys are used. Second, the timing mismatch between asynoptic observations and the analysis time as discussed in III.2 is less prominent. Table V.1 and Table V.2 show that both the bias and standard deviation of the background departures are smaller for 1-hour assimilation window. The number of used observations is expected to be slightly larger because of reduced time-mismatch and subsequent denial of observations through quality control (background departure check). This is true indeed for ASCAT, but surprisingly not for OSCAT. Further study is needed here.

(m/s)	ASCAT-u	ASCAT-v	OSCAT-u	OSCAT-v
3-h window	0.06/0.01	-0.77/-0.14	0.40/0.29	-0.33/-0.01
1-h window	-0.03/-0.00	-0.66/-0.11	0.31/0.18	-0.56/-0.29

Table V.1 Background departures (o-b) bias (m/s) for the 10-m wind components of ASCAT and OSCAT for the experiment with a 3-hour and 1-hour assimilation window. Statistics are based on the 1-month period: 6/12/2011 – 6/1/2012.

(m/s)	ASCAT-u	ASCAT-v	OSCAT-u	OSCAT-v
3-h window	2.02/1.11	1.86/1.00	2.17/1.61	1.9/1.61
1-h window	1.79/1.01	1.72/0.93	1.76/1.24	1.84/1.31

Table V.2 Same as Table V.1 but now for the standard deviation (m/s).

#	ASCAT-u	ASCAT-v	OSCAT-u	OSCAT-v
3-h window	56087	56087	9994	9994
1-h window	58810	58810	8634	8634

Table V.3 The number of used observations over the 1-month period in the 3-hour and 1-hour experiments.

Model forecast output of all 3 HARMONIE experiments has been compared to independent wind and surface pressure observations measured by buoys (from standard averaging over a 10-minute period) and ships. Observation quality control was limited to removing duplicate observations at a single time step but reported at different locations. More strict quality control by removing observation outliers was not implemented. Presented statistics below should therefore be considered as relative, comparing the various experiments, rather than as absolute measures. The location of the buoys and ships over the 1-month period is displayed in Figure V.26.

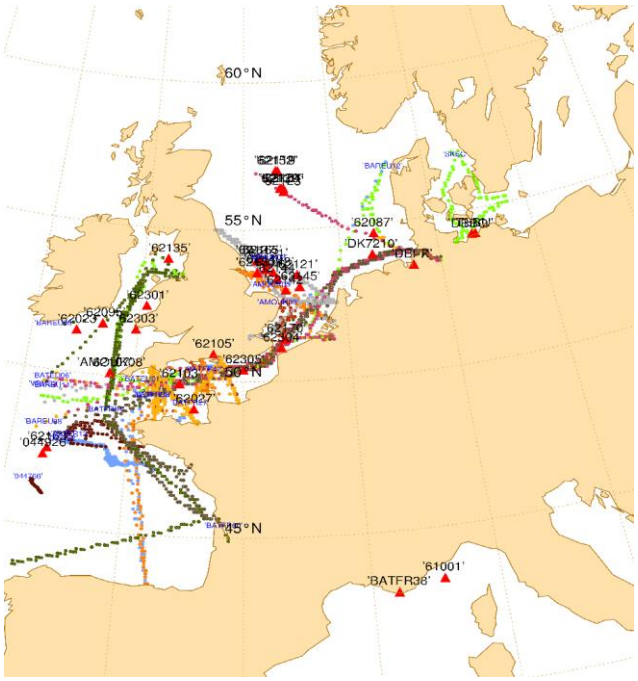

Figure V.26 Locations of buoys (red triangle) and ships (colored tracks) over the 1-month period 6/12/2011 – 6/1/2012.

Next, for each of the 3 experiments the nearest forecast to observation location time is used and interpolated to the observation location. For each experiment forecasts were generated at 1 hour intervals. Experiments CONV-3h and CONV+SCAT-3h have 3-hour assimilation cycles and either 1-h, 2-h or 3-h forecasts used for the comparison with observations. For the CONV+SCAT-1h experiment only 1-hour forecasts are used. In addition ECMWF model forecasts are used in the evaluation. These are available at hourly interval but only starting from 00 and 12 UTC. This means that for the comparison with observations 1-h, 2-h, …., 12-h forecasts are used for ECMWF. Figure V.27 and Figure V.28 show a typical example for a buoy located in the North-Sea.

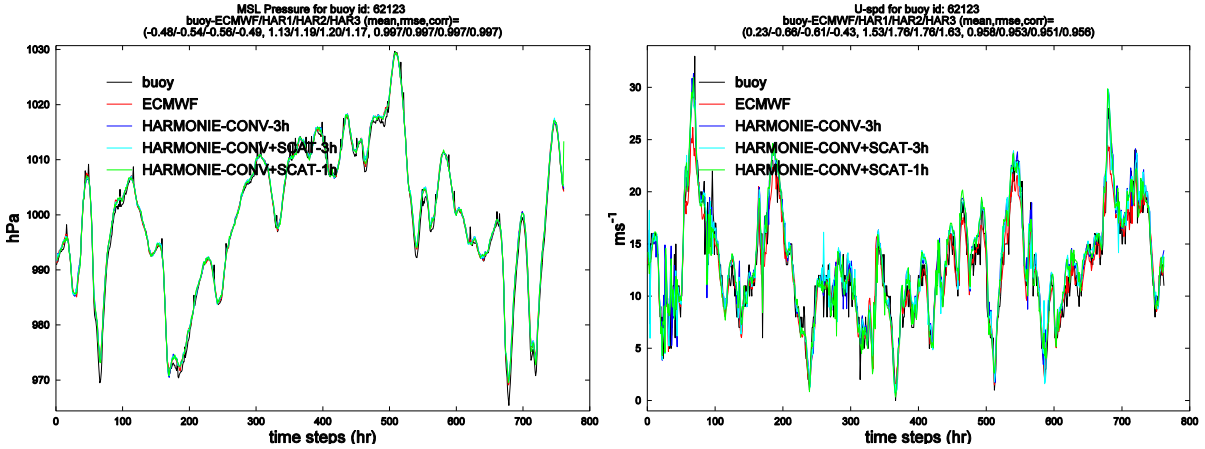

Figure V.27 Time series of buoy (black) mean sea level pressure (hPa) (left) and wind speed (right) for buoy number 62123 located at latitude 56.30 degrees and longitude 2.20 degrees. Model winds from nearest available forecasts are obtained from ECMWF (red) and the 3 HARMONIE runs: CONV-3h (blue), CONV+SCAT-3h (cyan) and CONV+SCAT-1h (green). See text for details of these experiments. The title provides statistics of (o-b), including bias and RMSE and the correlation value between time series.

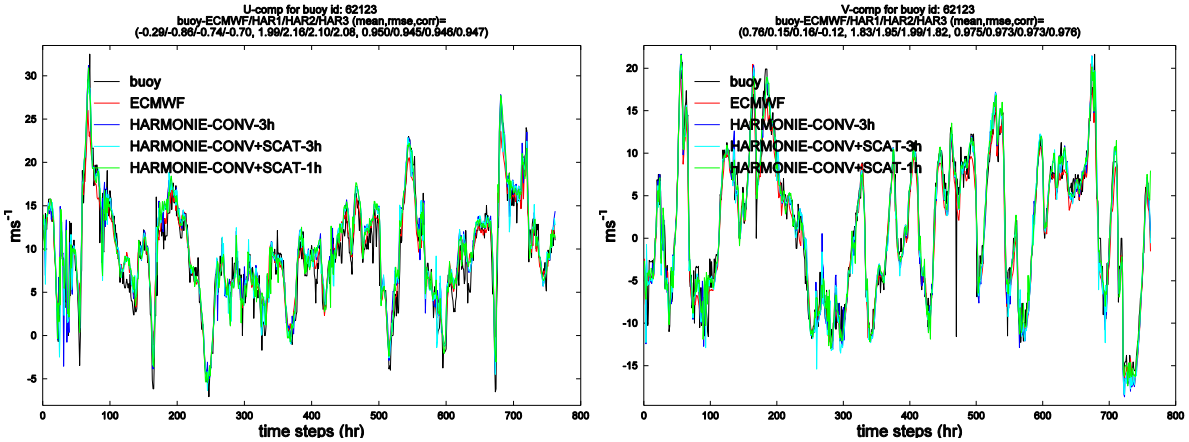

Figure V.28 Same as Figure V.27 but now for the 10-m zonal (left) and meridional (right) wind components.

For each buoy and ship statistics of the background departures, (o-b), have been calculated. Buoy observations were obtained from standard averaging over a 10-

minute period. In addition the correlation values of the observation and model time series were calculated for the 3 HARMONIE model runs and ECMWF. Combining the statistics of all buoys and ships in a single plot in Figure V.29 and Figure V.30 shows the added value of using a 1-hour assimilation cycle for HARMONIE: the model wind for the 1-hour cycle is closer to the observations for both wind components and wind speed. Also the correlation value is generally larger. However, mean sea level pressure becomes slightly worse in the 1-hour cycling experiment. Also, ECMWF generally outperforms all HARMONIE experiments except for the meriodonal wind component of ships. Also the correlation value is generally higher for CONV+SCAT-1h than ECMWF. As mentioned above, the RMSE errors in Figure V.29 and Figure V.30 do include representativeness errors, that are larger for ECMWF than HARMONIE given the 10-minute integration period of buoy observations. In addition, outliers may have entered the statistics. Given these limitations, the presented absolute values should be treated with care and focus should be on the relative intercomparison of the various experiments.

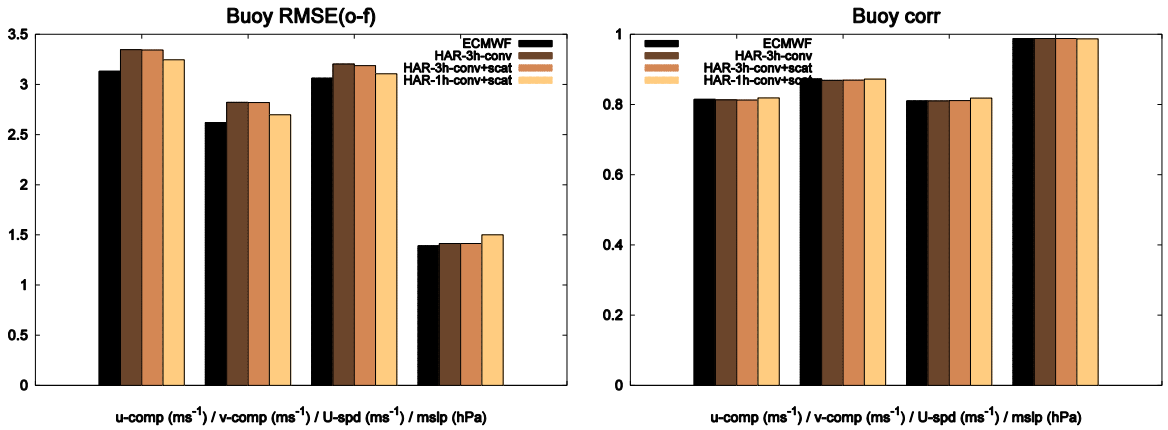

Figure V.29 Mean of RMSE of observation minus forecast for all buoys. Same for the correlation value (right). Each coloured bar corresponds to the experiment as provided by the legend. The 4 groups in each plot correspond to the zonal wind component, meridional wind component, wind speed and mean sea level pressure respectively.

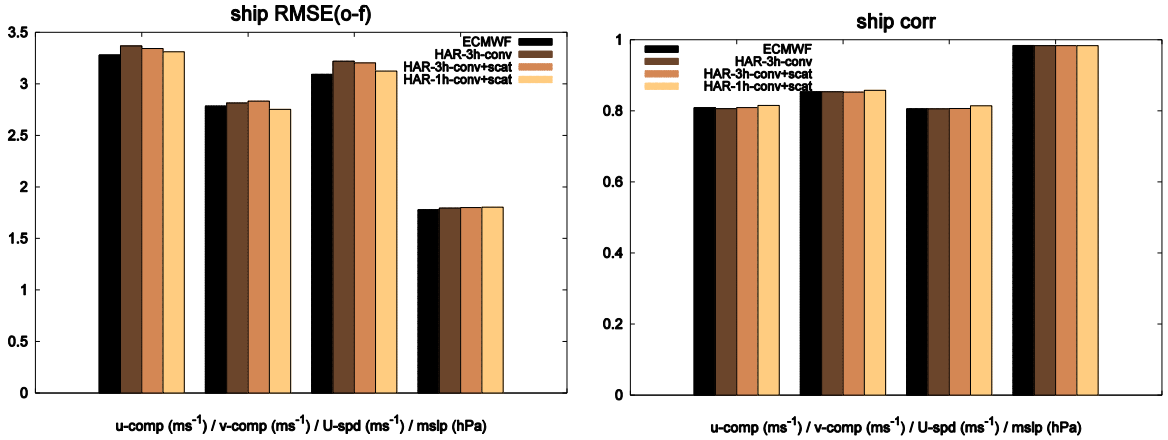

Figure V.30 Same as Figure V.29 but now for all ships.

V.3.3.3 Conclusions and recommendations from the HARMONIE data assimilation experiments

The following conclusions and recommendations follow from the results presented above.

- The time mismatch between observation time of (satellite) observations and analysis time reduces observational impact in a 3D-Var assimilation system because many observations are rejected from the analysis. This is most prominent in high impact weather events with a strong flow, for instance giving a large discrepancy of the location of a front as observed and at analysis time. It was concluded that a 6-hour, but also a 3-h (currently operational) assimilation window is too large for such events. A 1-h window showed significant improved results that is explained by (i) a larger number of used observations in the analysis and (ii) mitigation of time mismatch between observation and analysis time. It was found that HARMONIE model fields from 1-h cycling better fit to pressure and wind observations from buoys and ships. Ultimately, a 4D-Var system will solve the timing issue, but this is still under development in the HARMONIE community.
- HARMONIE better resolves convective processes and small-scale phenomena like squall lines and polar lows than Hirlam and ECMWF. A challenge remains to improve mesoscale model deterministic forecasts, i.e., to use the observational information to get the small-scale phenomena at the right location at the right time in the model simulation. Currently, the additional variance in mesoscale models relative to global models reduces forecast skill, using classical measures like bias and RMSE. In other words, HARMONIE small-scale spatial structures look realistic but are not real, i.e., they do not verify with observations. Within the HARMONIE community, quite some effort is put to solve this issue which includes going from 3D-Var to 4D-Var, a better representation of background error covariances (structure functions), optimal use (weight, thinning, superobbing) of observations in the assimilation and improving the model itself.
- HARMONIE overestimates the wind speed for strong winds exceeding 15 ms^{-1}. First results at the Norwegian Meteorological Institute indicate that a physically consistent coupling of the HARMONIE atmosphere with ocean/wave parameters mitigates HARMONIE ocean surface wind biases due to increased roughness. The physical coupling includes a more sophisticated formulation of ocean roughness, i.e., going from a relation where the roughness is described by wind only, to a formulation where the surface roughness length scale depends on the ocean wave spectrum, also including the effect of wave age and wave steepness. This is work in progress and may be validated with satellite wind and wave data.
- Data assimilation cannot compensate for model deficiencies, such as biases. Successful assimilation relies on bias correction of both the observations and model. The preferred strategy in case model biases cannot be corrected may be to add the bias to the observations, do the assimilation next and correct the bias in a post-processing step. This approach has not been implemented and more research is needed.

Mesoscale data assimilation will profit from more advanced observation operators that take into account the observation footprint size. For instance scatterometer observation footprints typically cover 12.5 to 50 km areas. Yet, they are still treated as point observations which may be a good approximation for global models but less so for mesoscale models, because the footprint is large compared to the mesoscale model grid size.

V.3.4 SWAN performance

The performance of the SWAN-DCSM model is assessed by hindcasting the considered four period using different wind fields. The considered wind fields are:

- The operational HIRLAM wind fields, which are the ones used currently to force the model operationally and have a spatial resolution of about 20 km x 20 km in the earlier periods and about 10 km x 10 km in the more recent periods.
- The wind fields from the operational ECMWF model, which is used to force HARMONIE in the experiments carried out by KNMI and have a spatial resolution of about 25 km x 25 km.
- The HARMONIE wind fields from the experiments carried out by KNMI and which have a spatial resolution of about 2.5 km x 2.5 km.

Because the HARMONIE winds do not cover the whole SWAN-DCSM grid (cf. Figure II.1 and Figure II.2), these have been augmented with the ECMWF winds in order to use them to force the SWAM-DCSM model. An example of such augmentation is shown in Figure V.31.

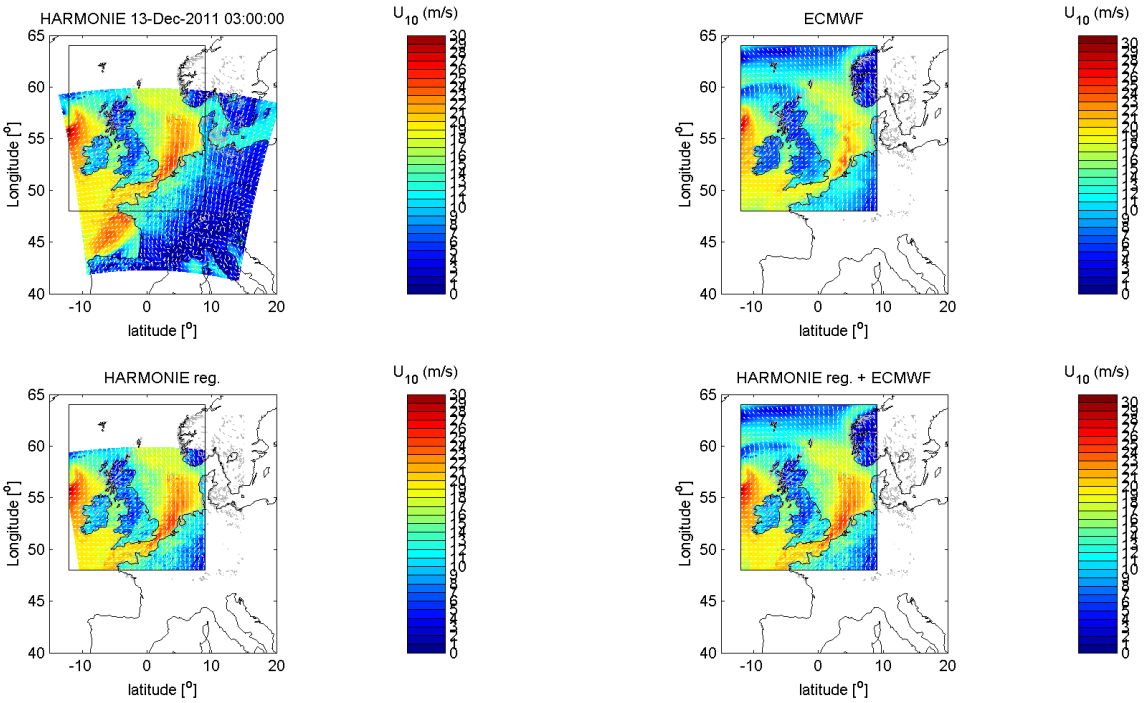

Figure V.31 Augmentation of the HARMONIE wind using the ECMWF wind. Top left panel: Original HARMONIE wind, which is available in a curvilinear grid with a resolution

of 2.5 km x 2.5 km. Top right panel: ECMWF wind in the region covered by the SWAN-DCSM model and linearly interpolated to a regular grid with a resolution of 2.5 km x 2.5 km. Bottom left panel: HARMONIE wind interpolated using the nearest neighbour to a regular grid with a resolution of 2.5 km x 2.5 km covering the region of the SWAN-DCSM model. Bottom right panel: Final field obtained by filling the gaps in the data shown in bottom left panel using the ECMWF data shown in the top right panel.

In the setting up and validation of the operational SWAN-DCSM model a number of whitecapping and bottom friction settings have been assessed. In all SWAN computations reported here the Westhuysen whitecapping formulation and a bottom fiction coefficient of 0.038 were applied. The remaining SWAN settings are equal to those used operationally.

The computed waves at the five in-situ locations shown in Figure B.2.2 have been validated against the available hourly in-situ measurements of significant wave height, mean wave period and mean wave direction and against wave height altimeter measurements of the significant wave height. Because the considered periods are relatively short to compute error statistics from the altimeter data (there are at most a few colocations per period) no statistics with relation to the altimeter data are presented. In all cases where the collocation of model, in-situ and altimeter significant wave height data were possible, the altimeter wave heights were very close to those of the in-situ measurements. The applied wind fields were validated at the five in-situ locations shown in Figure B.2.2 against hourly in-situ measurements (corrected using a Charnock relation to a height of 10 m) and scatterometer data. Again the colocations with the scatterometer data are limited due to the considered short periods. No error statistics of the model results with relation to Scatterometer data are presented, but the data are shown in the time series plots.

V.3.4.1 Period 1

We start by presenting the results for period 1. In this period the SWAN-DCSM model was forced using three wind datasets:

- HIRLAM three hourly data from the operational forecast,
- the HARMONIE hourly data from an experiment run by KNMI (although not presented in the previous section) with scatteromenter data assimilation with an assimilation window of 1 hour,
- ECMWF three hourly data from the operational forecast.

The model results are compared with the observations in the following figures and tables from locations: K13, Euro platform (EPL in Figure B.2.2), L.E. Goeree (LEG in Figure B.2.2), IJmuiden (MUNS in Figure B.2.2) and ELG (ELD in Figure B.2.2). The figures show the time-series of the computed and observed significant wave height, mean wave period, mean wave direction, wind speed and direction. The tables show the bias, RMSE and correlation (R) between the model results and the in-situ observations. For locations Euro platform and IJmuiden wave observations from two measuring devices are available. There are no wind measurements available IJmuiden and ELG and no wave direction measurements available at K13 and L.E. Goeree.

The results show that the model results compare generally well with the observations with the RMSE in H_s, $T_{m-1,0}$ and U_{10} being of at most 0.4 m, 0.7 s and 1.7 m/s, respectively; errors in wind and wave directions are generally of less than 20 degrees. The model results are quite close to each other, with the differences between model results being much less than the differences between the model results and the observations. In general the results of the model forced with the ECMWF winds compare slightly better with the observations than the results of the models forced with the HIRLAM and the HARMONIE winds, although for certain variables at and at certain locations (e.g. H_s at K13, cf. Table V.4) the results of the model forced with the HARMONIE winds are those closer to the observations. The wave height at the peak of the storm are underestimated at the offshore location K13 and underestimated at the other locations.

K13 29/10/2006-03/11/2006		H_s (m)				$T_{m-1,0}$ (s)		
		n	bias	RMSE	R	bias	RMSE	R
in-situ radar	HIRLAM	132	-0.18	0.41	0.97	-0.35	0.63	0.96
	ECMWF	132	-0.33	0.42	0.99	-0.56	0.73	0.97
	HARMORIE (scat. 1h assim.)	132	-0.04	0.34	0.98	-0.23	0.56	0.96
		U_{10} (m/s)				U_{dir} (º)		
		n	bias	RMSE	R	bias	RMSE	R
Anemometer	HIRLAM	132	0.36	1.35	0.95	-10.02	14.88	0.95
	ECMWF	132	0.24	1.29	0.95	-6.31	12.75	0.95
	HARMORIE (scat. 1h assim.)	132	0.77	1.47	0.96	-6.23	12.23	0.95

Table V.4 Error statistics of the modeled wind and waves at K13 platform.

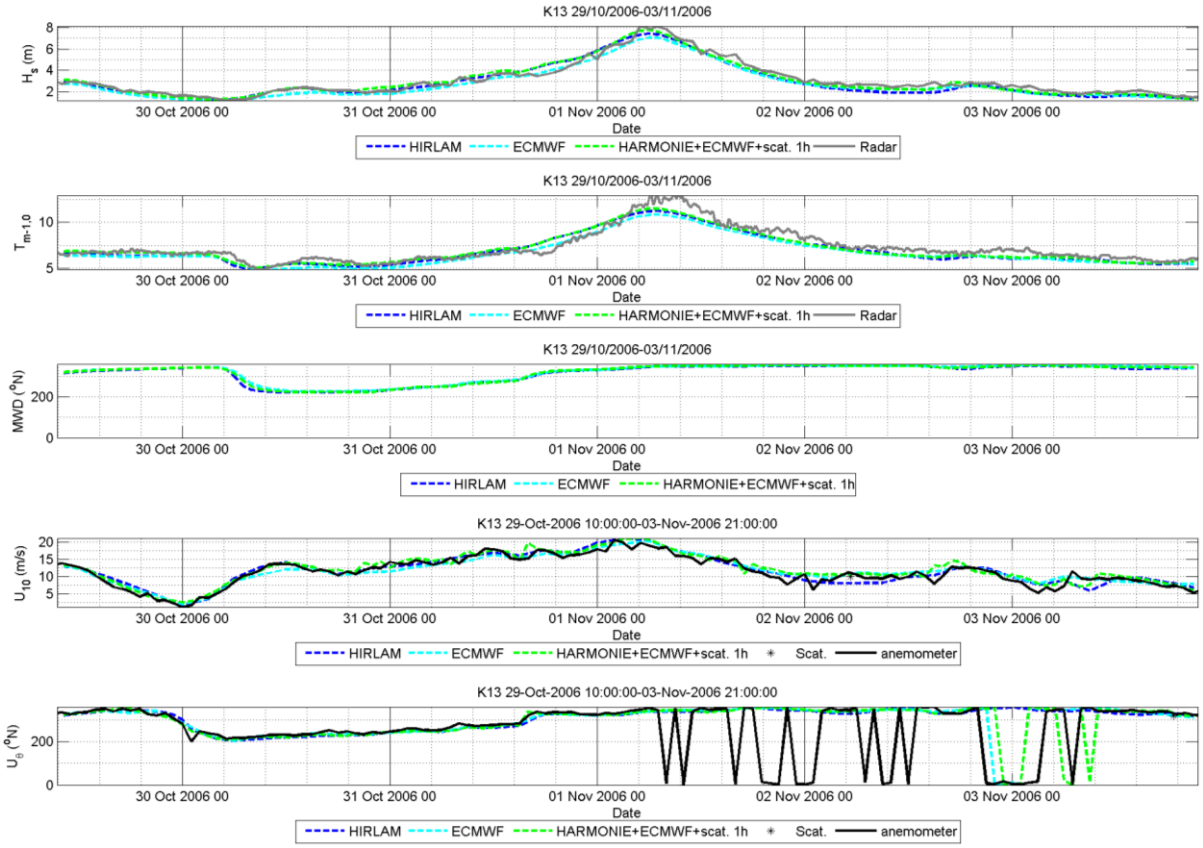

Figure V.32 Comparisons at K13 between the observed and the modeled wind and waves using different forcing winds.

Euro platform 29/10/2006-03/11/2006		H_s (m)				$T_{m-1,0}$ (s)			MWD (°)		
		n	bias	RMSE	R	bias	RMSE	R	bias	RMSE	R
in-situ radar	HIRLAM	132	-0.04	0.34	0.97	-0.22	0.47	0.96			
	ECMWF	132	-0.14	0.29	0.98	-0.33	0.44	0.97			
	HARMORIE (scat. 1h assim.)	132	0.08	0.33	0.98	-0.07	0.39	0.96			
Directional buoy	HIRLAM	132	-0.06	0.34	0.97	-0.24	0.48	0.95	-3.00	14.00	0.92
	ECMWF	132	-0.17	0.29	0.98	-0.35	0.47	0.97	-0.11	11.02	0.94
	HARMORIE (scat. 1h assim.)	132	0.06	0.30	0.98	-0.08	0.40	0.95	-2.72	13.39	0.93
		U_{10} (m/s)				U_{dir} (°)					
		n	bias	RMSE	R	bias	RMSE	R			
Anemometer	HIRLAM	132	0.14	1.63	0.92	-1.88	18.41	0.86			
	ECMWF	132	-0.09	1.47	0.94	-0.65	13.93	0.91			
	HARMORIE (scat. 1h assim.)	132	0.38	1.66	0.92	-1.80	14.86	0.90			

Table V.5 Error statistics of the modeled wind and waves at Euro platform.

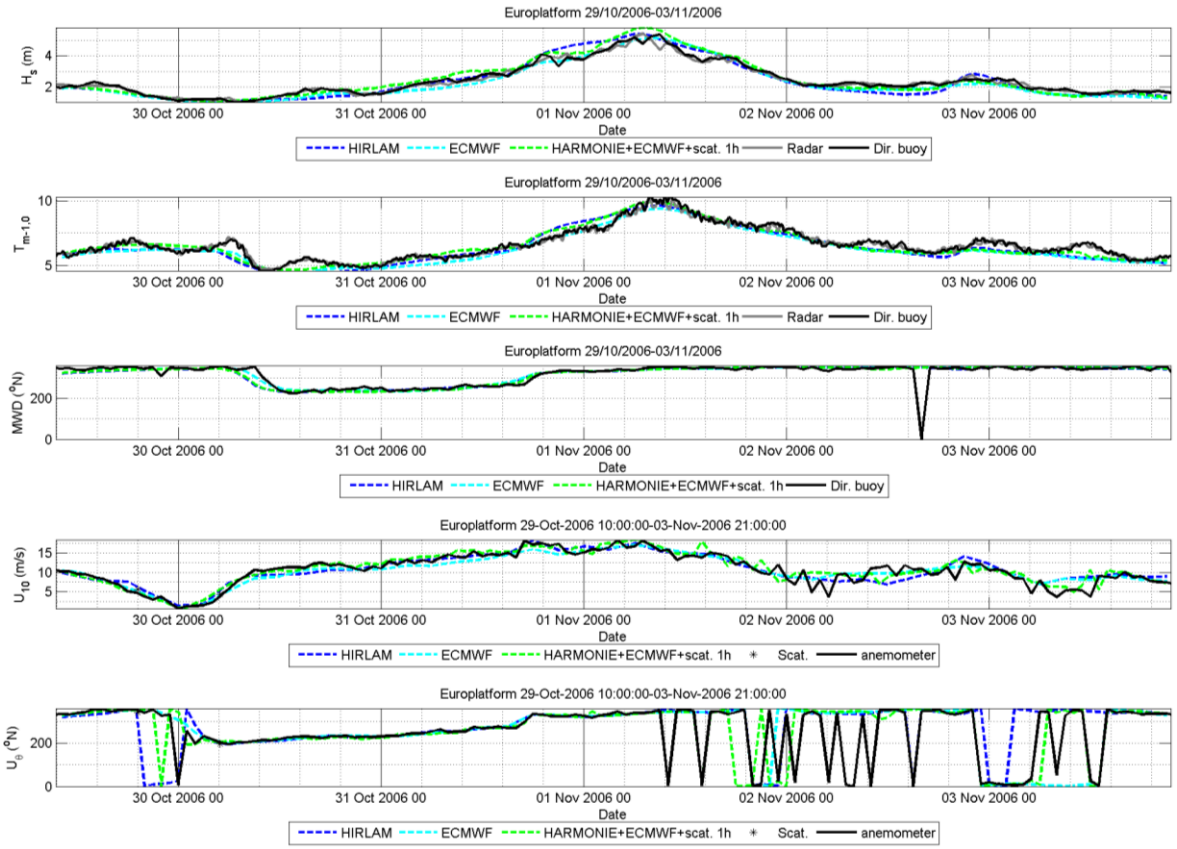

Figure V.33 Comparisons at Euro platform between the observed and the modeled wind and waves using different forcing winds.

L.E. Goeree 29/10/2006-03/11/2006		H_s (m)				$T_{m-1,0}$ (s)		
		n	bias	RMSE	R	bias	RMSE	R
in-situ radar	HIRLAM	132	0.04	0.36	0.97	-0.13	0.47	0.96
	ECMWF	132	-0.02	0.27	0.98	-0.25	0.41	0.97
	HARMORIE (scat. 1h assim.)	132	0.16	0.39	0.97	0.03	0.43	0.96
		U_{10} (m/s)				U_{dir} (º)		
		n	bias	RMSE	R	bias	RMSE	R
Anemometer	HIRLAM	132	0.10	1.41	0.94	-1.81	17.68	0.87
	ECMWF	132	0.30	1.50	0.93	0.99	16.07	0.88
	HARMORIE (scat. 1h assim.)	132	0.39	1.50	0.94	-0.87	21.77	0.84

Table V.6 Error statistics of the modeled wind and waves at L.E. Goeree.

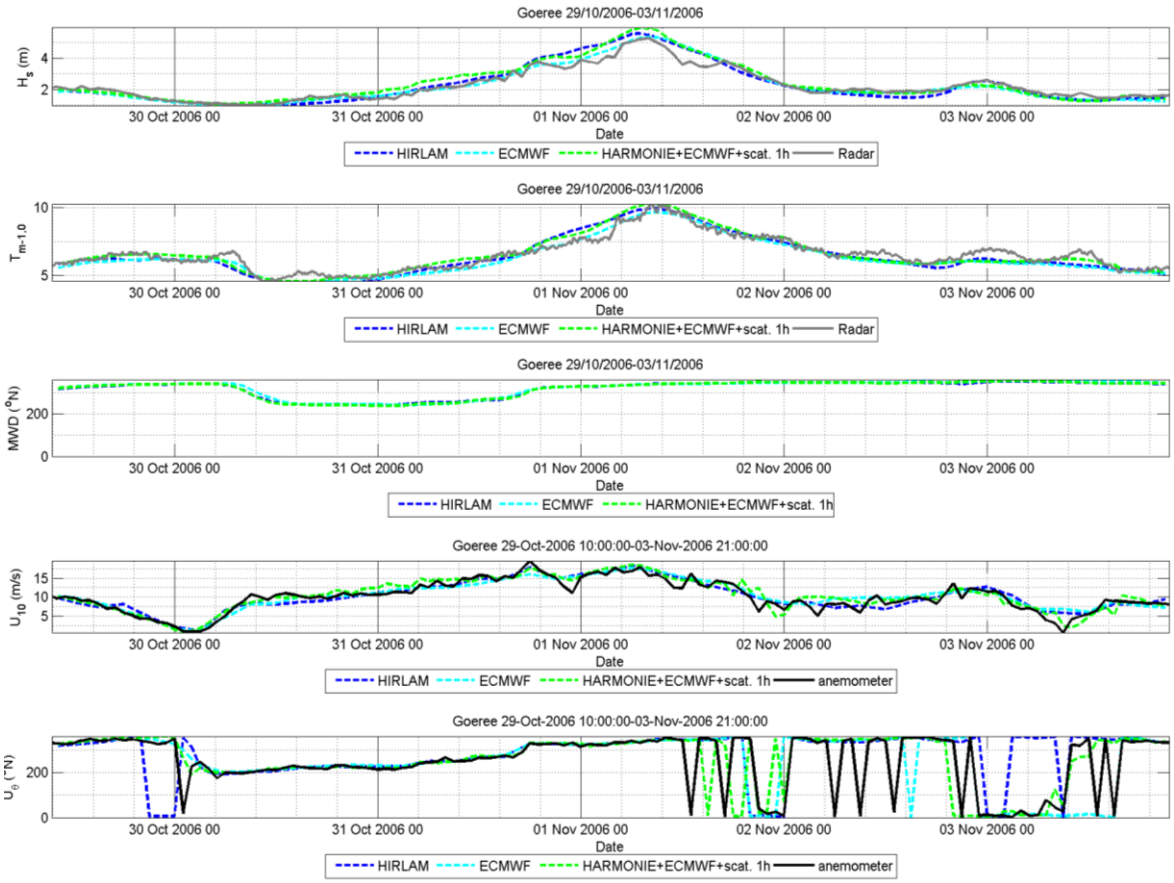

Figure V.34 Comparisons at L.E. Goeree platform between the observed and the modeled wind and waves using different forcing winds.

IJmuiden 28/10/2006-03/11/2006		H_s (m)				$T_{m-1,0}$ (s)			MWD (°)		
		n	bias	RMSE	R	bias	RMSE	R	bias	RMSE	R
Buoy	HIRLAM	131	-0.17	0.35	0.98	-0.39	0.63	0.96			
	ECMWF	131	-0.25	0.33	0.99	-0.56	0.72	0.97			
	HARMORIE (scat. 1h assim.)	131	-0.04	0.32	0.98	-0.23	0.53	0.96			
Directional buoy	HIRLAM	126	-0.25	0.39	0.98	-0.44	0.63	0.97	-3.75	19.46	0.87
	ECMWF	126	-0.31	0.39	0.99	-0.60	0.74	0.97	-1.62	15.71	0.89
	HARMORIE (scat. 1h assim.)	126	-0.11	0.33	0.98	-0.27	0.54	0.97	-3.00	18.53	0.87

Table V.7 Error statistics of the modeled waves at IJmuiden.

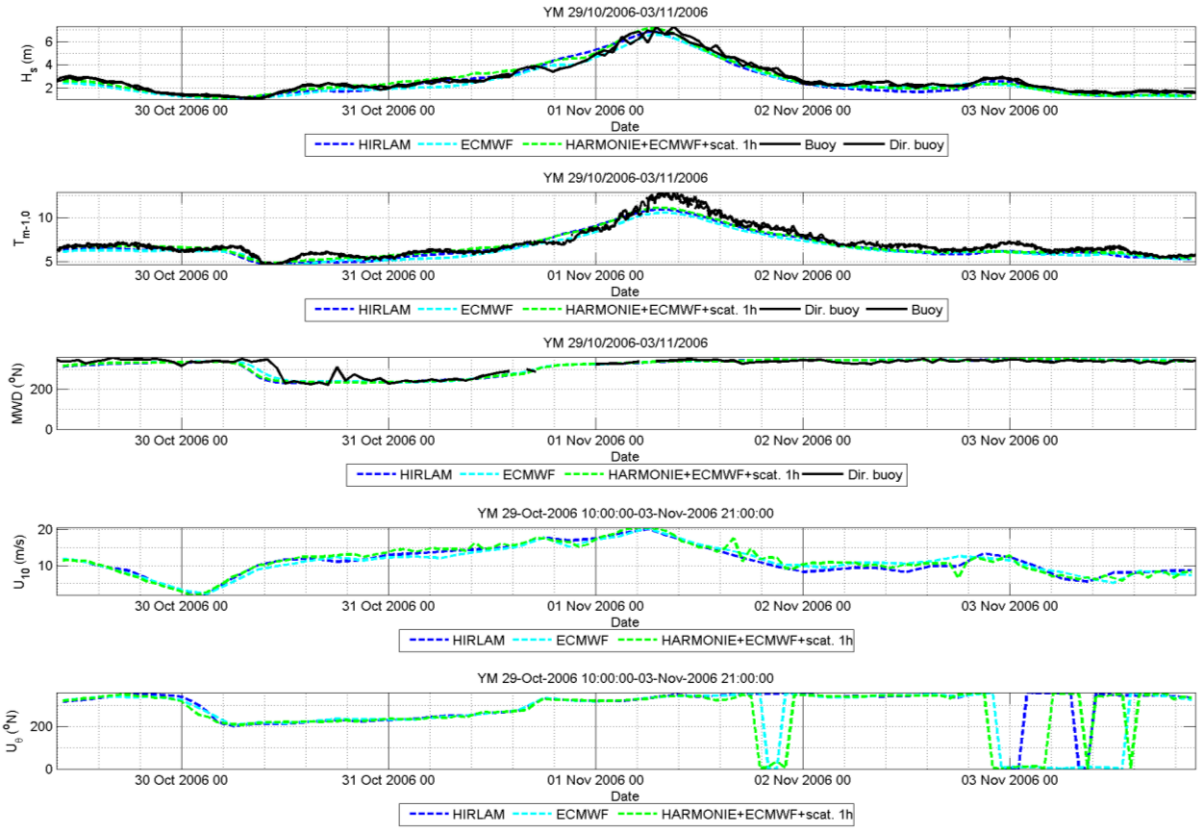

Figure V.35 Comparisons at IJmuiden platform between the observed and the modeled wind and waves using different forcing winds.

ELG 28/10/2006-03/11/2006		H_s (m)				$T_{m-1,0}$ (s)			MWD (°)		
		n	bias	RMSE	R	bias	RMSE	R	bias	RMSE	R
Directional buoy	HIRLAM	132	-0.08	0.37	0.98	-0.30	0.49	0.97	-5.62	19.35	0.90
	ECMWF	132	-0.16	0.33	0.99	-0.47	0.58	0.98	-3.29	16.28	0.92
	HARMORIE (scat. 1h assim.)	132	0.11	0.40	0.99	-0.09	0.39	0.97	-3.62	18.79	0.90

Table V.8 Error statistics of the modeled waves at ELG.

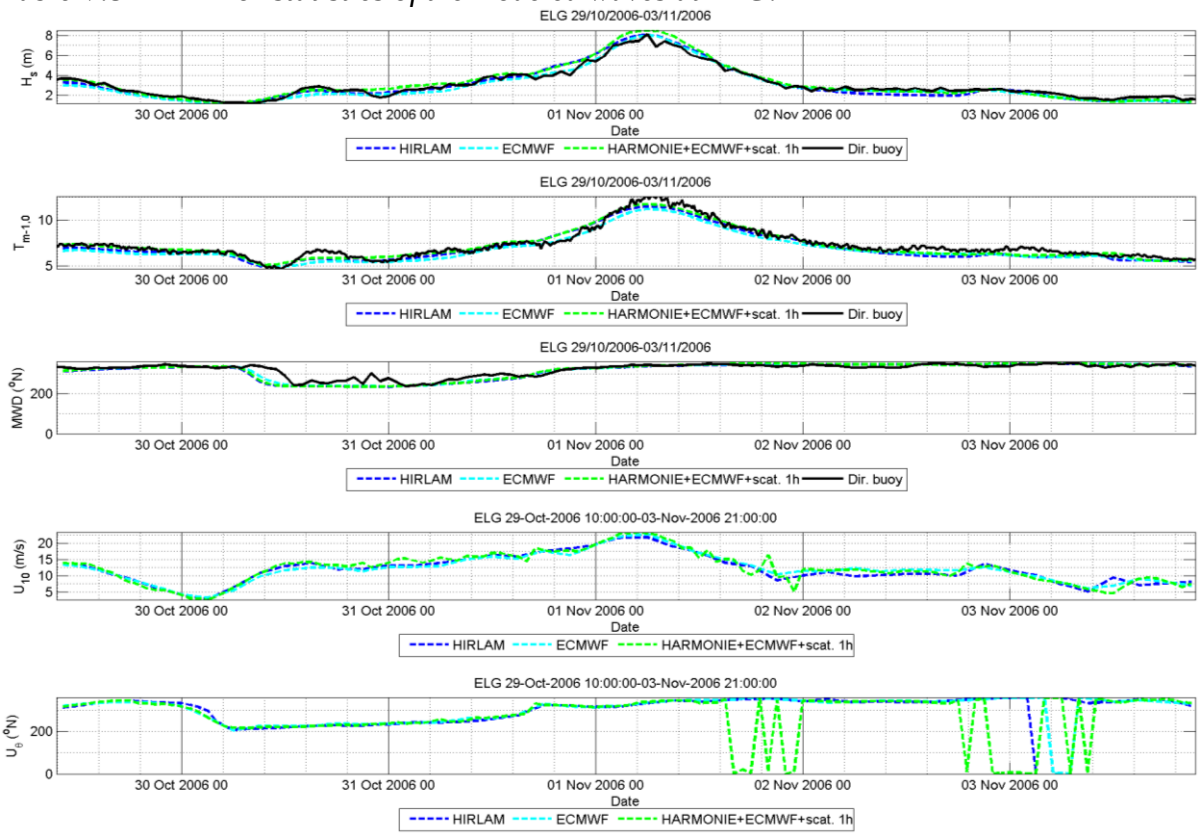

Figure V.36 Comparisons at ELG platform between the observed and the modeled wind and waves using different forcing winds.

V.3.4.2 Period 2

For Period 2 the SWAN-DCSM model was forced using three wind datasets:

- HIRLAM three hourly data from the operational forecast,
- HARMONIE hourly data from an experiment with scatterometer data assimilation with an assimilation window of 3 hours (experiment 3 described in §V.3.3.1),
- ECMWF three hourly data from the operational forecast.

The results of the models are compared with the observations at K13, Euro platform, L.E. Goeree, IJmuiden and ELG in the following figures and tables. For locations K13, Euro platform and IJmuiden wave observations from two measuring devices are available. There are no wind measurements available IJmuiden and ELG and no wave direction measurements available at L.E. Goeree.

As was the case for Period 1, although in Period 2 the errors in the wave direction are higher and those in wind direction lower, the model results compare generally well with the observations. Also, the model results are quite close to each other, with the differences between model results being much less than the differences between the model results and the observations and with the results of the model forced with the ECMWF winds being those closer to the observations. The wave heights at the peak of the storm are to a certain extent underestimated at the offshore location K13 and underestimated at the other locations.

K13 06/11/2007-11/11/2007		H_s (m)				$T_{m-1,0}$ (s)			MWD (°)		
		n	bias	RMSE	R	bias	RMSE	R	bias	RMSE	R
in-situ radar	HIRLAM	136	0.02	0.43	0.94	-0.36	0.73	0.87			
	ECMWF	136	-0.12	0.39	0.95	-0.38	0.71	0.89			
	HARMORIE (scat. 3h assim.)	136	0.12	0.46	0.94	-0.17	0.63	0.88			
Directional buoy	HIRLAM	135	-0.01	0.49	0.92	-0.40	0.80	0.88	-26.96	34.69	-0.15
	ECMWF	135	-0.15	0.46	0.94	-0.43	0.80	0.89	-20.25	28.03	-0.10
	HARMORIE (scat. 3h assim.)	135	0.09	0.51	0.92	-0.21	0.70	0.88	-23.92	33.20	-0.12
		U_{10} (m/s)				U_{dir} (°)					
		n	bias	RMSE	R	bias	RMSE	R			
Anemometer	HIRLAM	136	1.33	1.87	0.92	-7.93	12.21	0.94			
	ECMWF	136	0.74	1.63	0.90	-2.13	9.62	0.94			
	HARMORIE (scat. 3h assim.)	136	1.11	1.84	0.90	-5.54	9.48	0.96			

Table V.9 Error statistics of the modeled wind and waves at K13 platform.

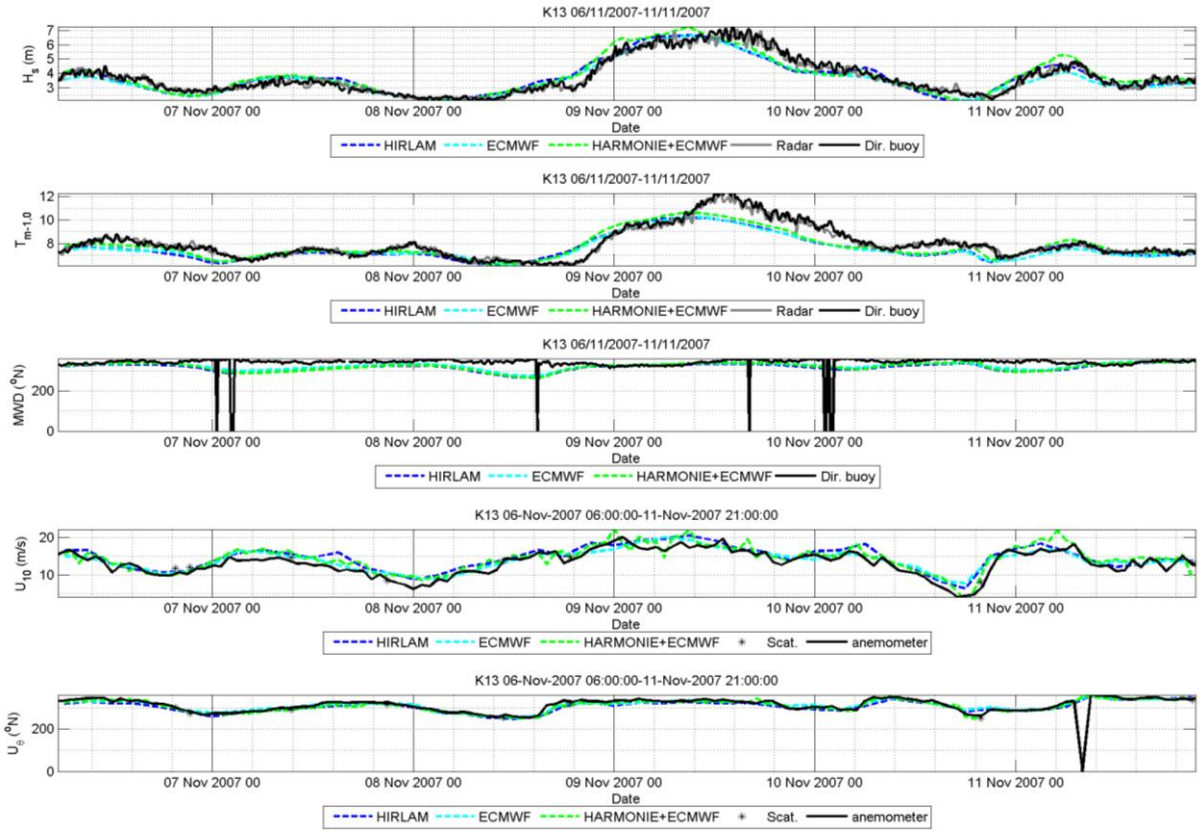

Figure V.37 Comparisons at K13 between the observed and the modeled wind and waves using different forcing winds.

Euro platform 06/11/2007-11/11/2007		H_s (m)				$T_{m-1,0}$ (s)			MWD (º)		
		n	bias	RMSE	R	bias	RMSE	R	bias	RMSE	R
in-situ radar	HIRLAM	136	0.06	0.37	0.94	-0.11	0.38	0.93			
	ECMWF	136	0.00	0.32	0.95	-0.12	0.34	0.94			
	HARMORIE (scat. 3h assim.)	136	0.20	0.39	0.96	0.05	0.35	0.94			
Directional buoy	HIRLAM	28	-0.09	0.28	0.75	-0.31	0.40	0.84	-18.56	25.84	0.64
	ECMWF	28	-0.12	0.20	0.90	-0.37	0.43	0.88	-11.94	19.26	0.60
	HARMORIE (scat. 3h assim.)	28	0.07	0.25	0.81	-0.17	0.30	0.87	-16.24	25.06	0.64
		U_{10} (m/s)				U_{dir} (º)					
		n	bias	RMSE	R	bias	RMSE	R			
Anemometer	HIRLAM	136	0.62	2.02	0.85	-3.45	13.44	0.90			
	ECMWF	136	0.38	1.90	0.87	4.46	13.33	0.92			
	HARMORIE (scat. 3h assim.)	136	0.84	1.81	0.90	0.55	13.15	0.90			

Table V.10 Error statistics of the modeled wind and waves at Euro platform.

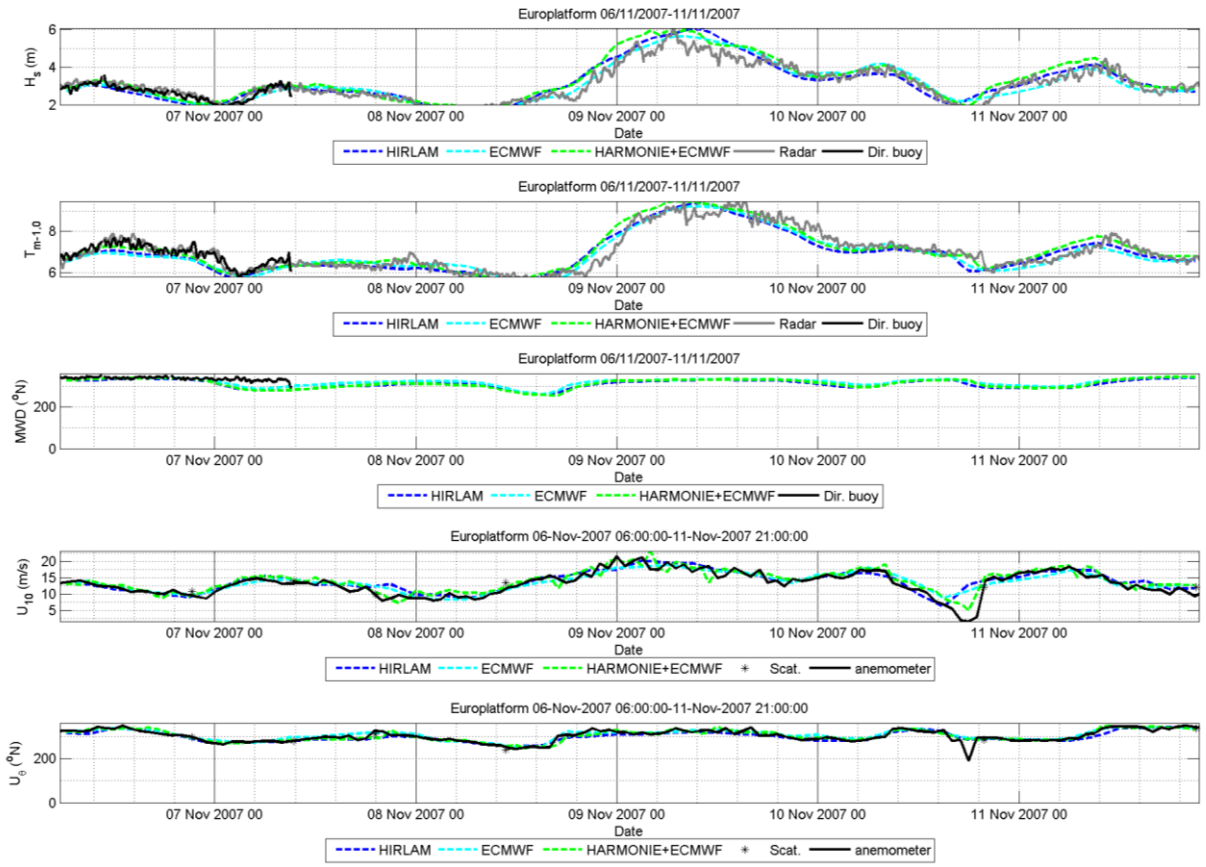

Figure V.38 Comparisons at Euro platform between the observed and the modeled wind and waves using different forcing winds.

L.E. Goeree 06/11/2007-11/11/2007		H_s (m)				$T_{m-1,0}$ (s)		
		n	bias	RMSE	R	bias	RMSE	R
in-situ radar	HIRLAM	136	0.12	0.41	0.93	-0.05	0.35	0.93
	ECMWF	136	0.10	0.34	0.95	-0.07	0.33	0.94
	HARMORIE (scat. 3h assim.)	136	0.24	0.45	0.94	0.12	0.37	0.94
		U_{10} (m/s)				U_{dir} (º)		
		n	bias	n	bias	n	bias	n
Anemometer	HIRLAM	136	0.27	1.73	0.87	-2.06	11.12	0.92
	ECMWF	136	0.52	1.71	0.88	6.75	12.92	0.92
	HARMORIE (scat. 3h assim.)	136	0.60	1.81	0.87	2.99	10.04	0.94

Table V.11 Error statistics of the modeled wind and waves at L.E. Goeree.

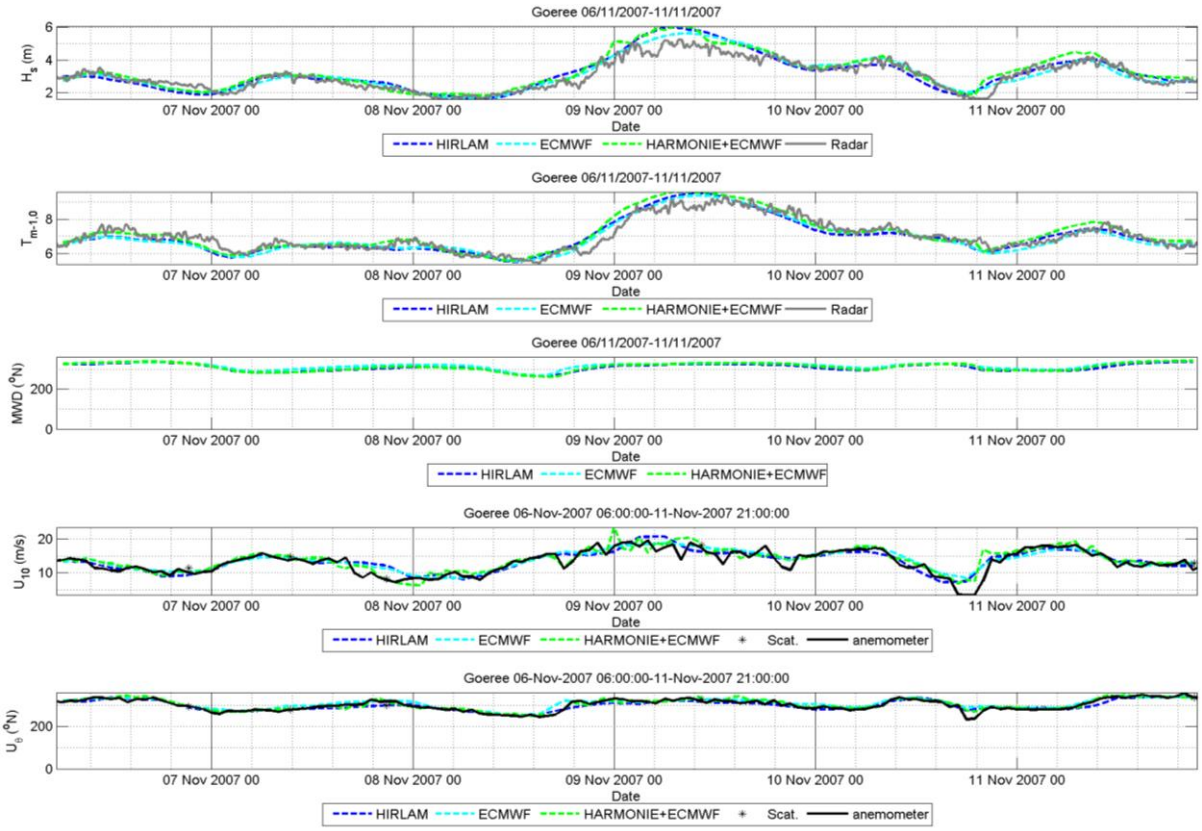

Figure V.39 Comparisons at L.E. Goeree platform between the observed and the modeled wind and waves using different forcing winds.

IJmuiden 06/11/2007-11/11/2007		H_s (m)				$T_{m-1,0}$ (s)			MWD (º)		
		n	bias	RMSE	R	bias	RMSE	R	bias	RMSE	R
Buoy	HIRLAM	129	-0.09	0.46	0.92	-0.60	0.86	0.91			
	ECMWF	129	-0.19	0.42	0.95	-0.64	0.86	0.94			
	HARMORIE (scat. 3h assim.)	129	-0.04	0.44	0.93	-0.42	0.69	0.93			
Directional buoy	HIRLAM	133	-0.17	0.49	0.93	-0.55	0.83	0.90	-28.38	33.91	0.07
	ECMWF	133	-0.26	0.47	0.95	-0.60	0.83	0.93	-21.90	27.36	0.15
	HARMORIE (scat. 3h assim.)	133	-0.10	0.43	0.94	-0.36	0.67	0.92	-26.03	32.84	0.12

Table V.12 Error statistics of the modeled waves at IJmuiden.

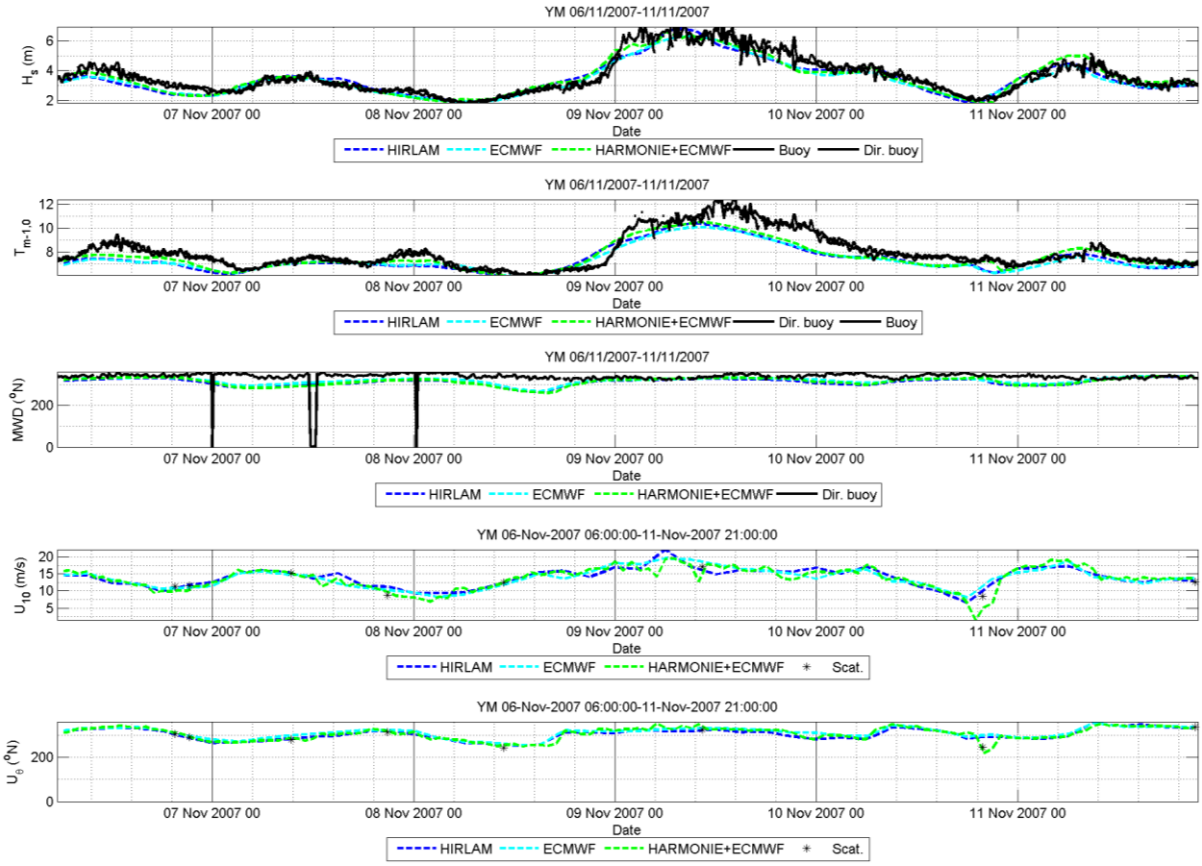

Figure V.40 Comparisons at IJmuiden platform between the observed and the modeled wind and waves using different forcing winds.

ELG 06/11/2007-11/11/2007		H_s (m)				$T_{m-1,0}$ (s)			MWD (º)		
		n	bias	RMSE	R	bias	RMSE	R	bias	RMSE	R
Directional buoy	HIRLAM	136	-0.07	0.48	0.93	-0.46	0.69	0.93	-19.11	25.47	0.20
	ECMWF	136	-0.16	0.38	0.96	-0.51	0.70	0.96	-13.17	19.33	0.30
	HARMORIE (scat. 3h assim.)	136	0.04	0.43	0.94	-0.24	0.52	0.95	-15.33	22.90	0.28

Table V.13 Error statistics of the modeled waves at ELG.

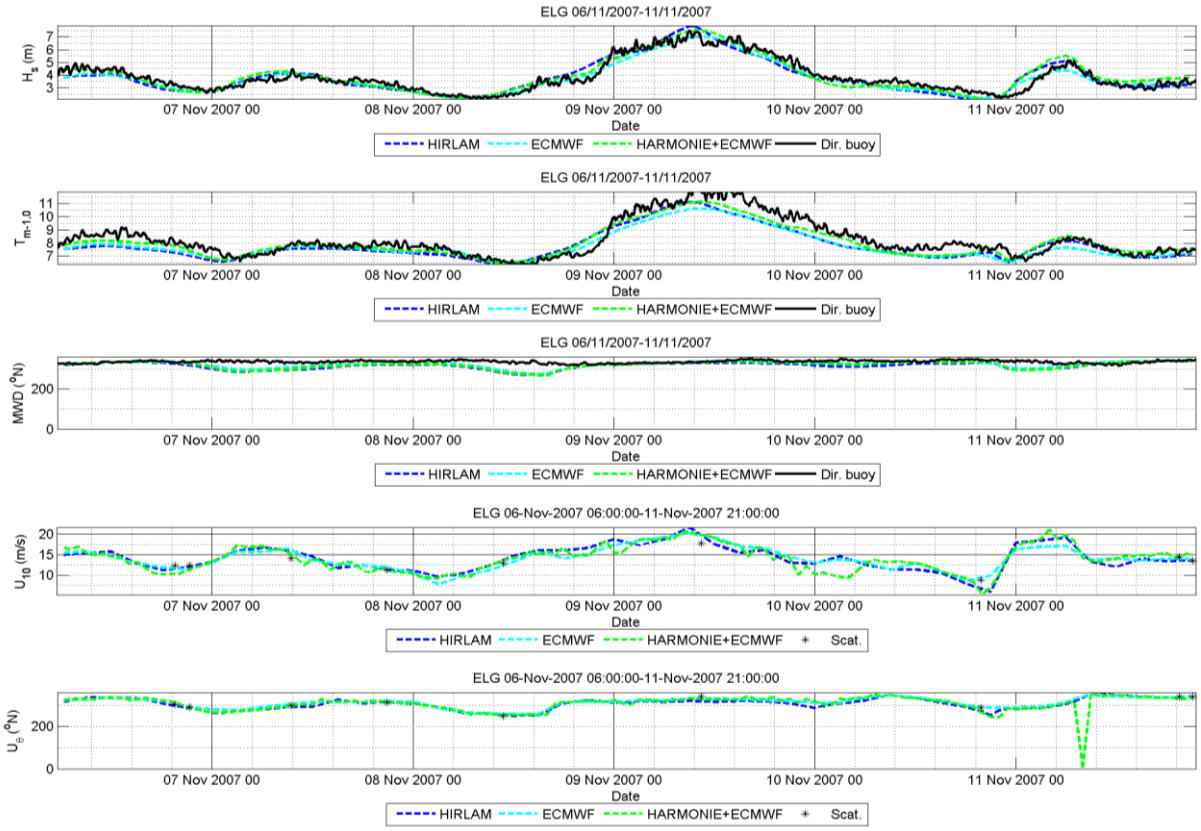

Figure V.41 Comparisons at ELG platform between the observed and the modeled wind and waves using different forcing winds.

V.3.4.3 Period 3

For period 3 only HIRLAM three hourly data from the operational forecast were used to force the SWAN-DCSM model.

The model results are compared with the observations in the following figures and tables.

As also show in the previous periods, the model results compare well with the observations, but underestimate to a certain extent the peak event in the period. In comparison with the performance of the HIRLAM results in periods 1 and 2 the results for this period are closer to the observations. This better performance is partially because the HIRLAM model for this period has a higher resolution than in

the previous periods and partially because the wind and wave conditions are milder in this period.

K13 12/07/2011-17/07/2011		H_s (m)				$T_{m-1,0}$ (s)			MWD (°)		
		n	bias	RMSE	R	bias	RMSE	R	bias	RMSE	R
in-situ radar	HIRLAM	115	-0.07	0.29	0.96	-0.62	1.02	0.68			
Directional buoy	HIRLAM	115	-0.10	0.31	0.96	-0.61	1.03	0.68	0.30	38.67	-0.22
		U_{10} (m/s)				U_{dir} (°)					
		n	bias	RMSE	R	n	bias	n			
Anemometer	HIRLAM	115	0.56	1.52	0.92	-6.16	10.16	0.97			

Table V.14 Error statistics of the modeled wind and waves at K13 platform.

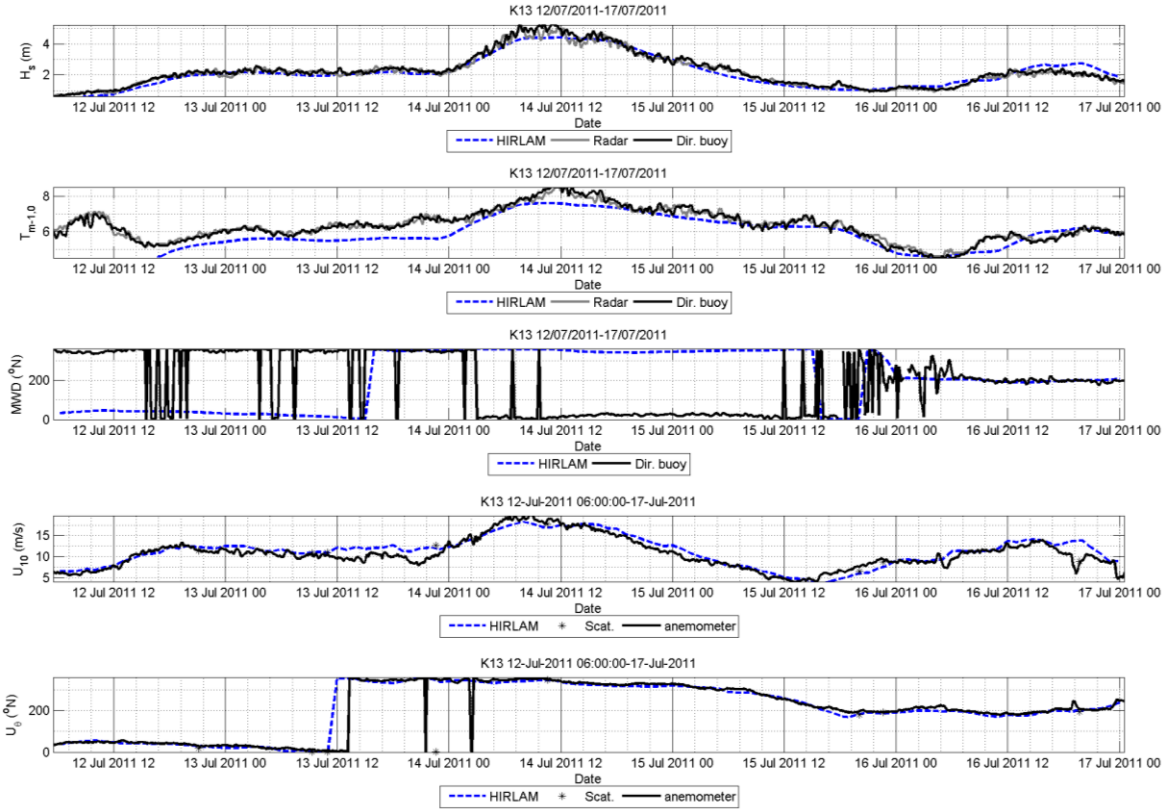

Figure V.42 Comparisons at K13 between the observed and the modeled wind and waves using different forcing winds.

Euro platform 12/07/2011-17/07/2011		H_s (m)				$T_{m-1,0}$ (s)			MWD (º)		
		n	bias	RMSE	R	bias	RMSE	R	bias	RMSE	R
in-situ radar	HIRLAM	115	-0.06	0.26	0.96	-0.23	0.44	0.93			
Directional buoy	HIRLAM	115	-0.05	0.24	0.96	-0.24	0.46	0.92	0.84	22.81	0.72
		U_{10} (m/s)				U_{dir} (º)					
		n	bias	RMSE	R	bias	RMSE	R			
Anemometer	HIRLAM	115	-0.21	0.98	0.96	1.52	7.73	0.98			

Table V.15 Error statistics of the modeled wind and waves at Euro platform.

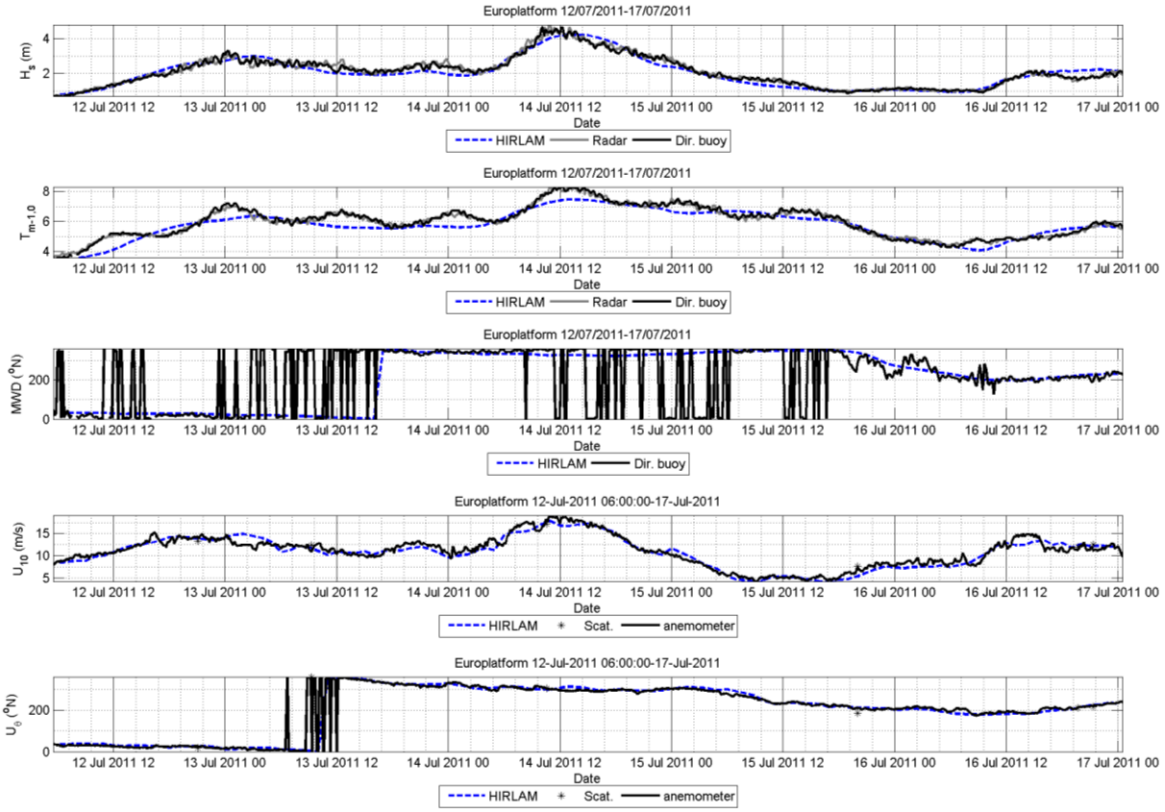

Figure V.43 Comparisons at Euro platform between the observed and the modeled wind and waves using different forcing winds.

L.E. Goeree 12/07/2011-17/07/2011		H_s (m)				$T_{m-1,0}$ (s)		
		n	bias	RMSE	R	bias	RMSE	R
in-situ radar	HIRLAM	115	0.04	0.27	0.96	-0.18	0.42	0.93
		U_{10} (m/s)				U_{dir} (º)		
		n	bias	n	bias	n	bias	n
Anemometer	HIRLAM	115	-0.41	1.29	0.95	-5.57	10.84	0.97

Table V.16 Error statistics of the modeled wind and waves at L.E. Goeree.

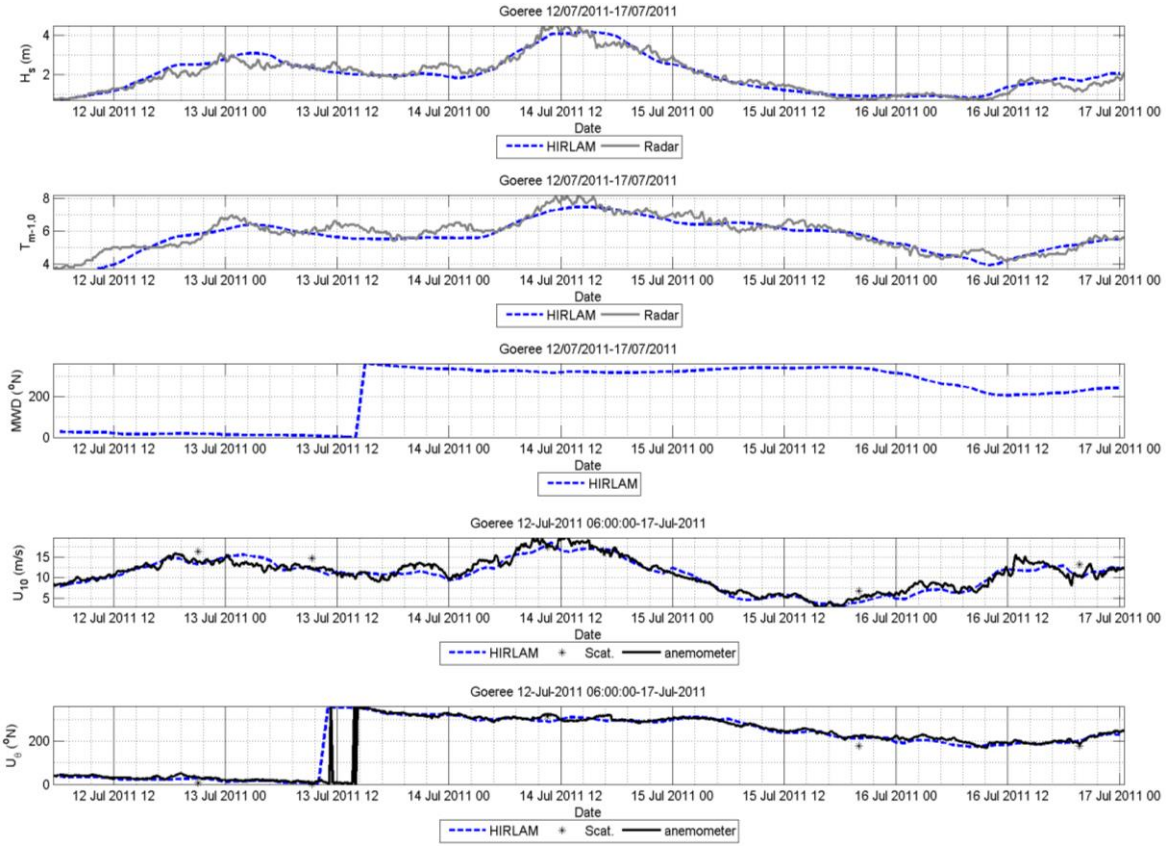

Figure V.44 Comparisons at L.E. Goeree platform between the observed and the modeled wind and waves using different forcing winds.

IJmuiden 12/07/2011-17/07/2011		H_s (m)				$T_{m-1,0}$ (s)			MWD (º)		
		n	bias	RMSE	R	bias	RMSE	R	bias	RMSE	R
Buoy	HIRLAM	114	-0.03	0.29	0.97	-0.38	0.57	0.92			
Directional buoy	HIRLAM	114	-0.01	0.25	0.97	-0.31	0.53	0.92	1.40	22.57	0.70

Table V.17 Error statistics of the modeled waves at IJmuiden.

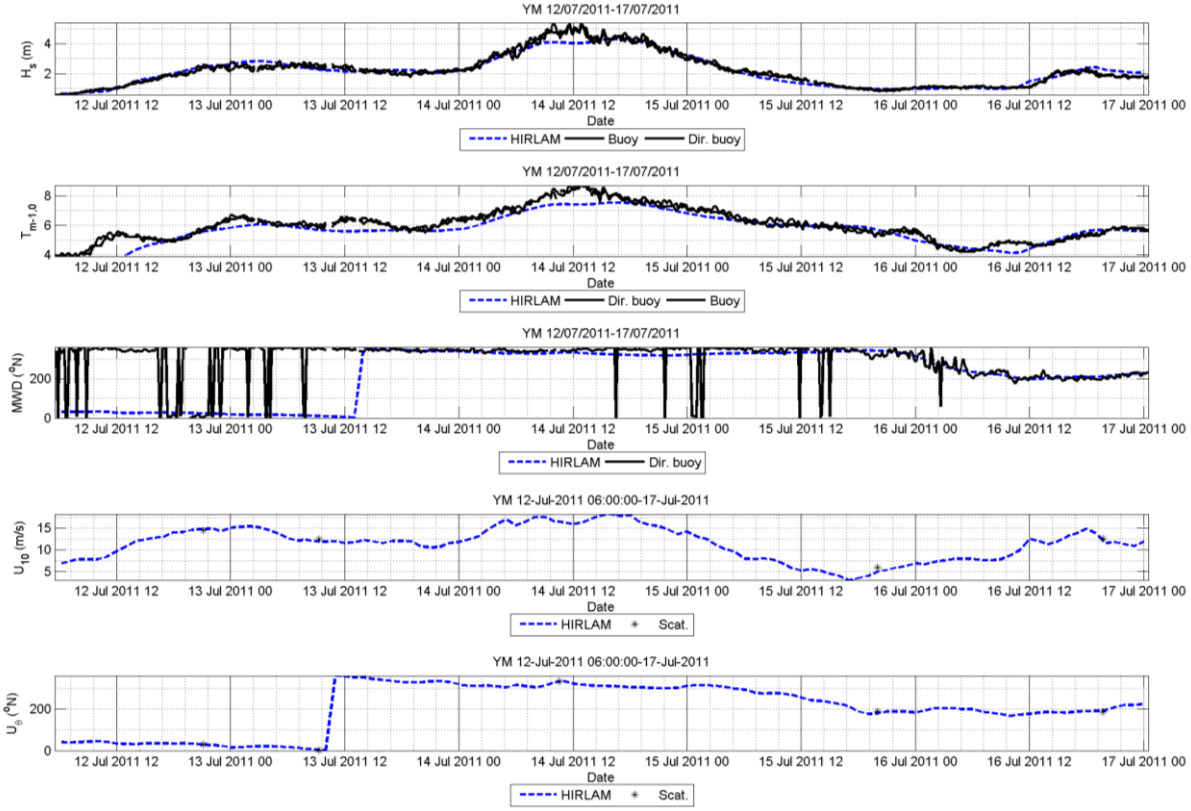

Figure V.45 Comparisons at IJmuiden platform between the observed and the modeled wind and waves using different forcing winds.

ELG 12/07/2011-17/07/2011		H_s (m)				$T_{m-1,0}$ (s)			MWD (°)		
		n	bias	RMSE	R	bias	RMSE	R	bias	RMSE	R
Directional buoy	HIRLAM	113	-0.05	0.35	0.94	-0.39	0.79	0.78	5.01	33.28	0.46

Table V.18 Error statistics of the modeled waves at ELG.

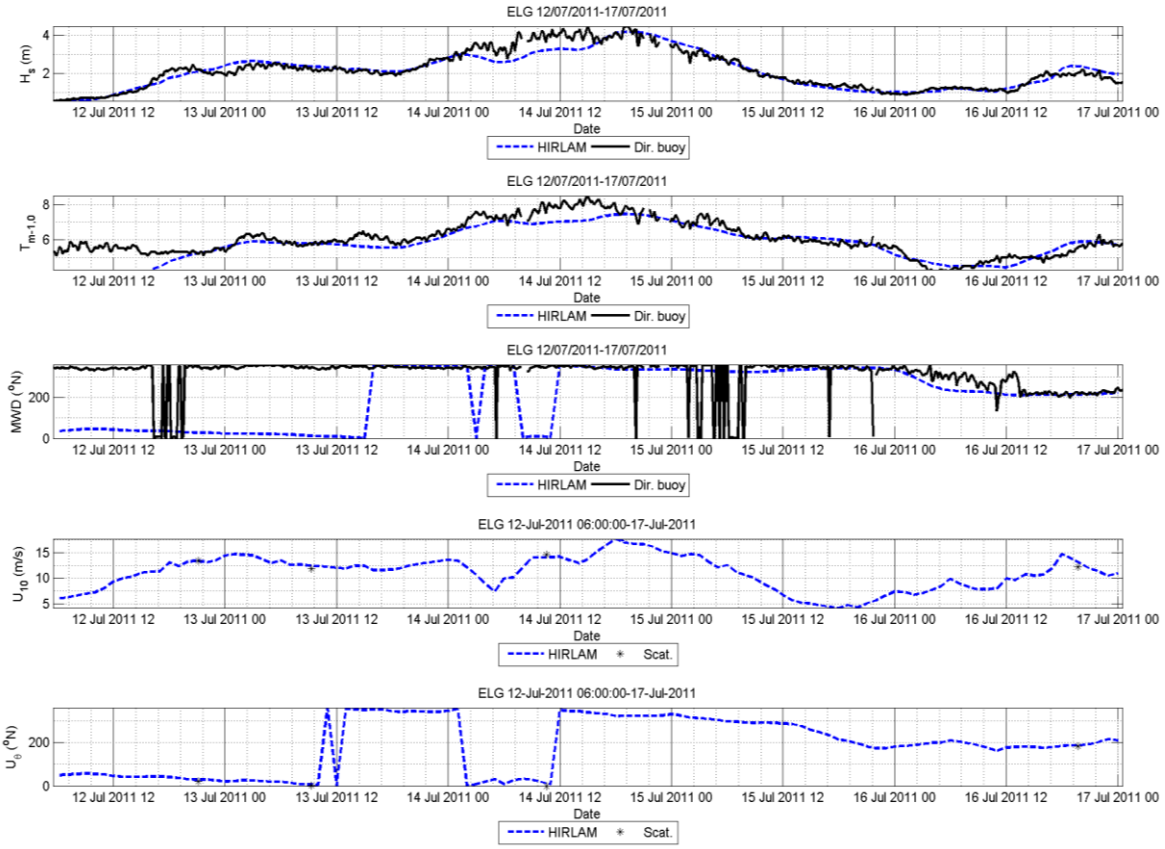

Figure V.46 Comparisons at ELG platform between the observed and the modeled wind and waves using different forcing winds.

V.3.4.4 Period 4

For Period 4 we present results of the forcing of the SWAN-DCSM model with the following fields:

- ECMWF hourly data from the operational forecast,
- HARMONIE hourly data from an experiment with no assimilation of scatterometer surface winds (experiment 1 described in §V.3.3.2),
- HARMONIE hourly data from an experiment with 3-hourly assimilation of scatterometer surface winds (experiment 1 described in §V.3.3.2), and
- HARMONIE hourly data from an experiment hourly assimilation of scatterometer surface winds (experiment 1 described in §V.3.3.2).

Given that the amount of considered HARMONIE experiments we do not show results of forcing the SWAN-DCSM model with the operational HIRLAM fields as done for the other periods.

The model results are compared with the observations in the following figures and tables. This period is much longer than the other considered periods and the much higher number of collocations with the scatterometer data can be seen in Figure V.47 to Figure V.51.

In general, the same conclusions taken for the previous periods can also be taken for this period:

- The model results compare generally well with the observations.
- The model results are quite close to each other, with the differences between model results being much less than the differences between the model results and the observations.
- The model results tend to overestimate the more energetic wave peaks.

However, the results of the model forced with the ECMWF wind compare more noticeably than in periods 1 and 2 better with the observations than those forced with the HARMONIE winds. This is probably because the temporal and spatial resolution of the ECMWF model higher for this period then it was for periods 1 and 2.

K13 07/12/2011-06/01/2012		H_s (m)				$T_{m-1,0}$ (s)			MWD (°)		
		n	bias	RMSE	R	bias	RMSE	R	bias	RMSE	R
in-situ radar	ECMWF	733	-0.09	0.33	0.96	-0.19	0.46	0.93			
	HARMORIE (scat. 3h assim.)	733	0.27	0.51	0.95	0.11	0.48	0.92			
	HARMORIE (scat. 1h assim.)	733	0.23	0.48	0.95	0.09	0.47	0.92			
	HARMONIE (no scat.)	733	0.26	0.51	0.95	0.12	0.48	0.92			
Directional buoy	ECMWF	733	-0.10	0.33	0.96	-0.17	0.48	0.93	-29.0	49.4	0.60
	HARMORIE (scat. 3h assim.)	733	0.25	0.49	0.95	0.13	0.49	0.92	-33.8	55.2	0.55
	HARMORIE (scat. 1h assim.)	733	0.21	0.46	0.95	0.11	0.48	0.92	-34.5	55.2	0.56
	HARMONIE (no scat.)	733	0.24	0.49	0.95	0.14	0.49	0.92	-34.0	55.7	0.55
		U_{10} (m/s)				U_{dir} (°)					
		n	bias	RMSE	R	bias	RMSE	R			
Anemometer	ECMWF	733	0.11	1.22	0.95	-3.3	9.2	0.97			
	HARMORIE (scat. 3h assim.)	733	0.95	1.57	0.96	-6.1	10.5	0.97			
	HARMORIE (scat. 1h assim.)	733	0.81	1.42	0.96	-6.8	10.6	0.98			
	HARMONIE (no scat.)	733	0.90	1.54	0.96	-6.2	12.0	0.96			

Table V.19 Error statistics of the modeled wind and waves at K13.

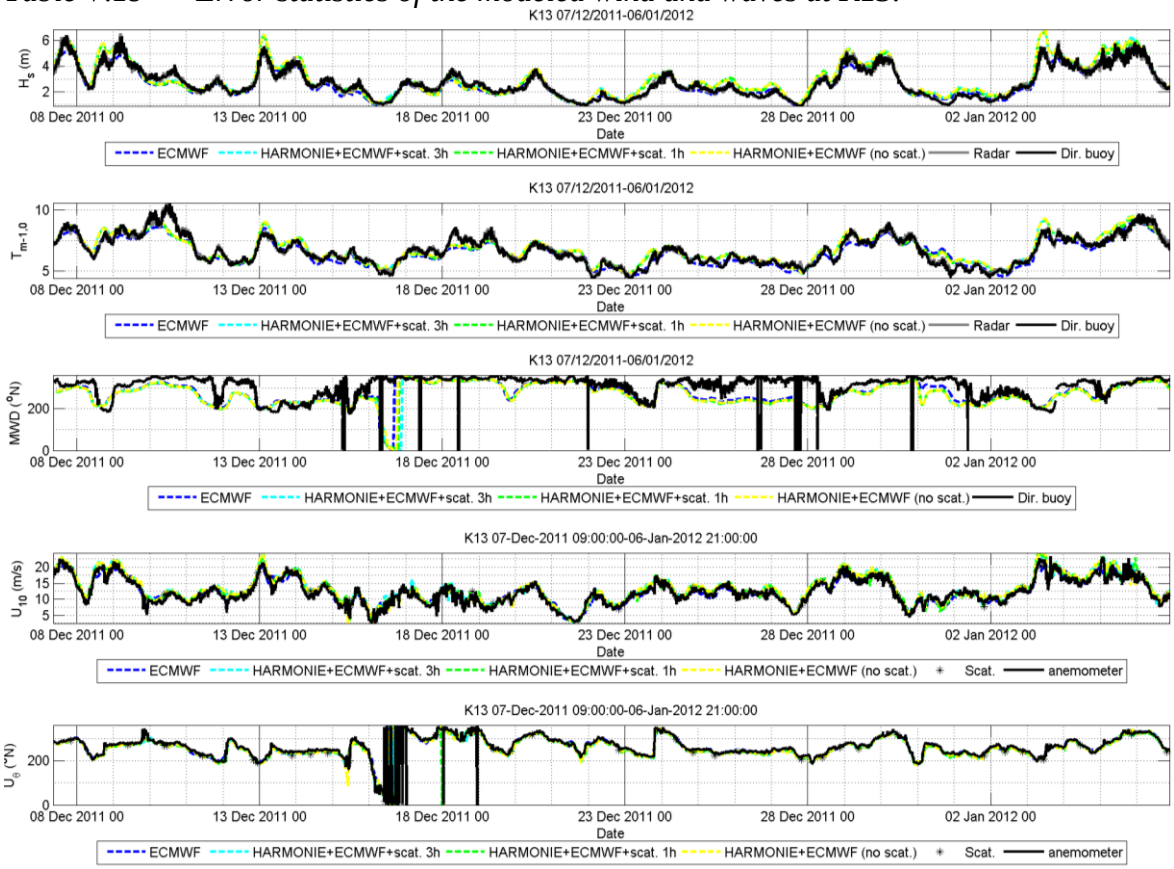

Figure V.47 Comparisons at K13 between the observed and the modeled wind and waves using different forcing winds.

Euro platform 7/12/2011-06/01/2012		H_s (m)				$T_{m-1,0}$ (s)			MWD (º)		
		n	bias	RMSE	R	bias	RMSE	R	bias	RMSE	R
in-situ radar	ECMWF	733	0.01	0.35	0.94	-0.12	0.41	0.91			
	HARMORIE (scat. 3h assim.)	733	0.38	0.60	0.93	0.18	0.49	0.89			
	HARMORIE (scat. 1h assim.)	733	0.39	0.62	0.92	0.18	0.50	0.88			
	HARMONIE (no scat.)	733	0.38	0.59	0.93	0.19	0.49	0.89			
Directional buoy	ECMWF	733	-0.01	0.34	0.94	-0.15	0.44	0.91	-25.4	42.2	0.69
	HARMORIE (scat. 3h assim.)	733	0.35	0.56	0.93	0.15	0.48	0.89	-29.6	46.8	0.65
	HARMORIE (scat. 1h assim.)	733	0.37	0.58	0.93	0.15	0.50	0.89	-29.8	47.0	0.65
	HARMONIE (no scat.)	733	0.35	0.56	0.93	0.16	0.48	0.90	-29.6	47.0	0.65
		U_{10} (m/s)				U_{dir} (º)					
		n	bias	RMSE	R	bias	RMSE	R			
Anemometer	ECMWF	732	-0.14	1.32	0.94	3.8	10.9	0.96			
	HARMORIE (scat. 3h assim.)	732	1.01	1.77	0.93	1.0	10.6	0.96			
	HARMORIE (scat. 1h assim.)	732	1.01	1.80	0.93	0.9	10.5	0.96			
	HARMONIE (no scat.)	732	0.95	1.71	0.94	0.8	10.7	0.96			

Table V.20 Error statistics of the modeled wind and waves at Euro platform.

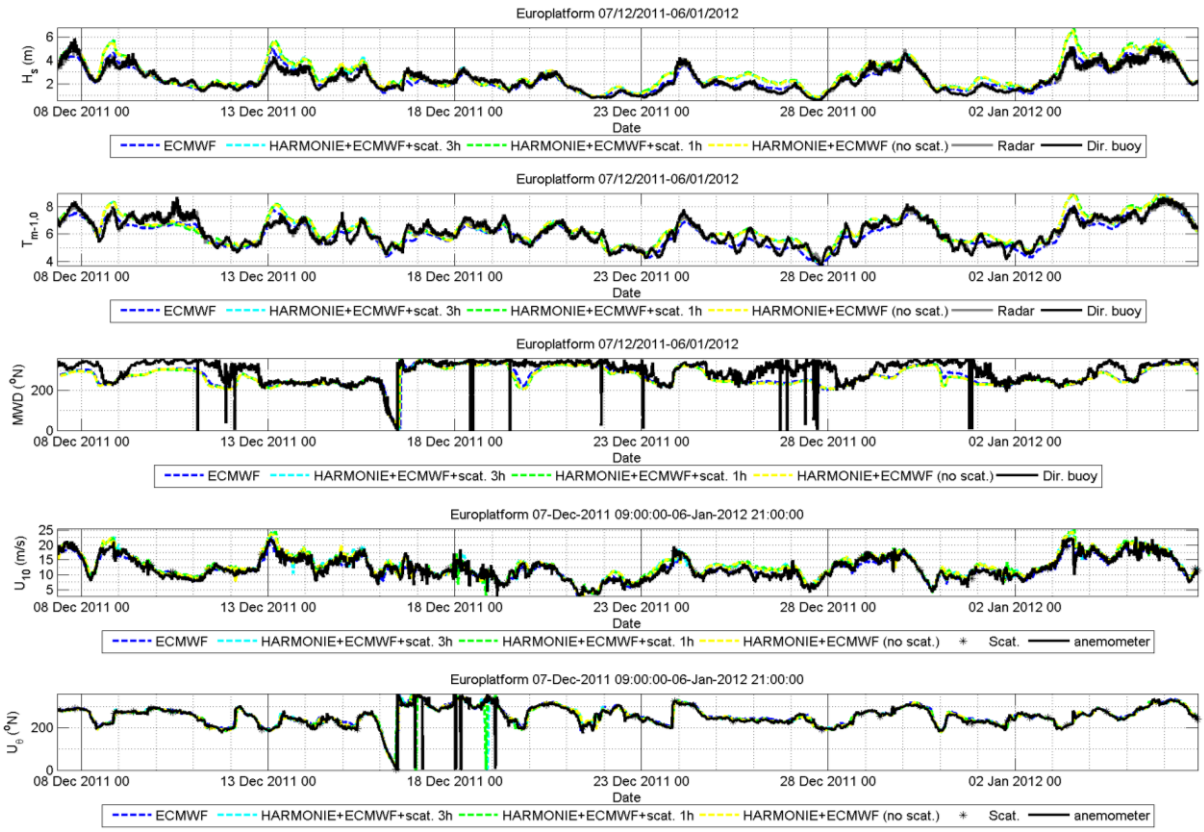

Figure V.48 Comparisons at Euro platform between the observed and the modeled wind and waves using different forcing winds.

L.E. Goeree 7/12/2011-06/01/2012		H_s (m)				$T_{m-1,0}$ (s)		
		n	bias	RMSE	R	bias	RMSE	R
in-situ radar	ECMWF	732	0.12	0.40	0.93	-0.06	0.44	0.90
	HARMORIE (scat. 3h assim.)	732	0.44	0.65	0.91	0.23	0.55	0.88
	HARMORIE (scat. 1h assim.)	732	0.46	0.68	0.90	0.23	0.56	0.87
	HARMONIE (no scat.)	732	0.44	0.65	0.91	0.23	0.55	0.88
		U_{10} (m/s)				U_{dir} (°)		
		n	bias	RMSE	R	bias	RMSE	R
Anemometer	ECMWF	731	-0.13	1.37	0.93	-1.6	10.2	0.96
	HARMORIE (scat. 3h assim.)	731	0.80	1.76	0.92	-5.2	11.4	0.97
	HARMORIE (scat. 1h assim.)	731	0.87	1.79	0.92	-4.9	10.9	0.97
	HARMONIE (no scat.)	731	0.80	1.73	0.92	-5.2	10.8	0.97

Table V.21 Error statistics of the modeled wind and waves at L.E. Goeree.

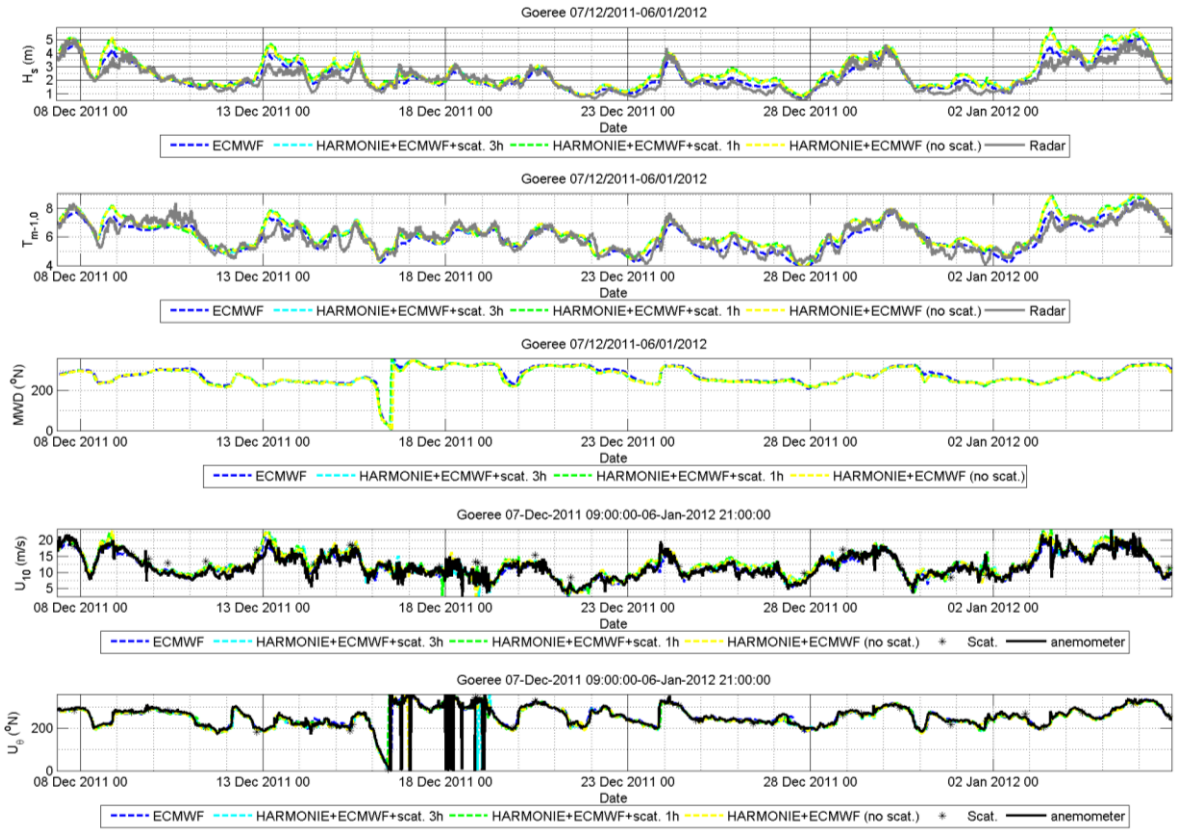

Figure V.49 Comparisons at L.E. Goeree between the observed and the modeled wind and waves using different forcing winds.

IJmuiden 7/12/2011-06/01/2012		H_s (m)				$T_{m-1,0}$ (s)			MWD (°)		
		N	bias	RMSE	R	bias	RMSE	R	bias	RMSE	R
Buoy	ECMWF	639	-0.03	0.35	0.94	-0.28	0.59	0.91			
	HARMORIE (scat. 3h assim.)	639	0.30	0.56	0.91	0.01	0.56	0.88			
	HARMORIE (scat. 1h assim.)	639	0.31	0.58	0.91	0.00	0.58	0.87			
	HARMONIE (no scat.)	639	0.30	0.56	0.91	0.01	0.56	0.88			
Directional buoy	ECMWF	641	-0.04	0.36	0.94	-0.23	0.58	0.89	-38.2	53.0	0.58
	HARMORIE (scat. 3h assim.)	641	0.30	0.56	0.91	0.04	0.55	0.87	-42.6	57.9	0.54
	HARMORIE (scat. 1h assim.)	641	0.30	0.58	0.90	0.03	0.58	0.86	-42.9	58.3	0.53
	HARMONIE (no scat.)	641	0.29	0.56	0.91	0.03	0.55	0.87	-42.6	58.0	0.54

Table V.22 Error statistics of the modeled waves at IJmuiden.

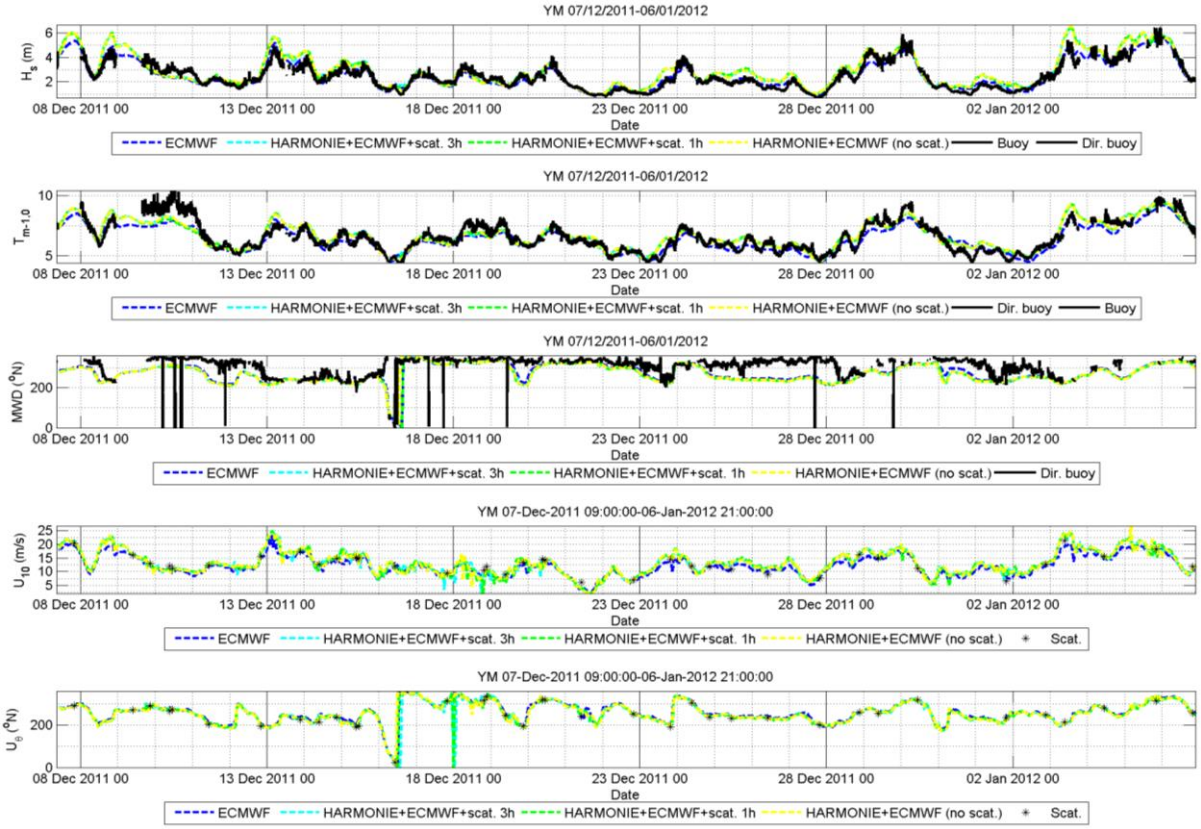

Figure V.50 Comparisons at IJmuiden between the observed and the modeled wind and waves using different forcing winds.

ELG 7/12/2011-06/01/2012		H_s (m)				$T_{m-1,0}$ (s)			MWD (°)		
		n	bias	RMSE	R	bias	RMSE	R	bias	RMSE	R
Directional buoy	ECMWF	666	-0.01	0.36	0.96	-0.18	0.50	0.94	-32.5	47.5	0.56
	HARMORIE (scat. 3h assim.)	666	0.34	0.56	0.95	0.12	0.48	0.93	-35.8	51.3	0.52
	HARMORIE (scat. 1h assim.)	666	0.33	0.56	0.95	0.09	0.48	0.93	-36.3	51.5	0.52
	HARMONIE (no scat.)	666	0.34	0.57	0.95	0.11	0.49	0.93	-35.7	51.2	0.52

Table V.23 Error statistics of the modeled waves at ELG

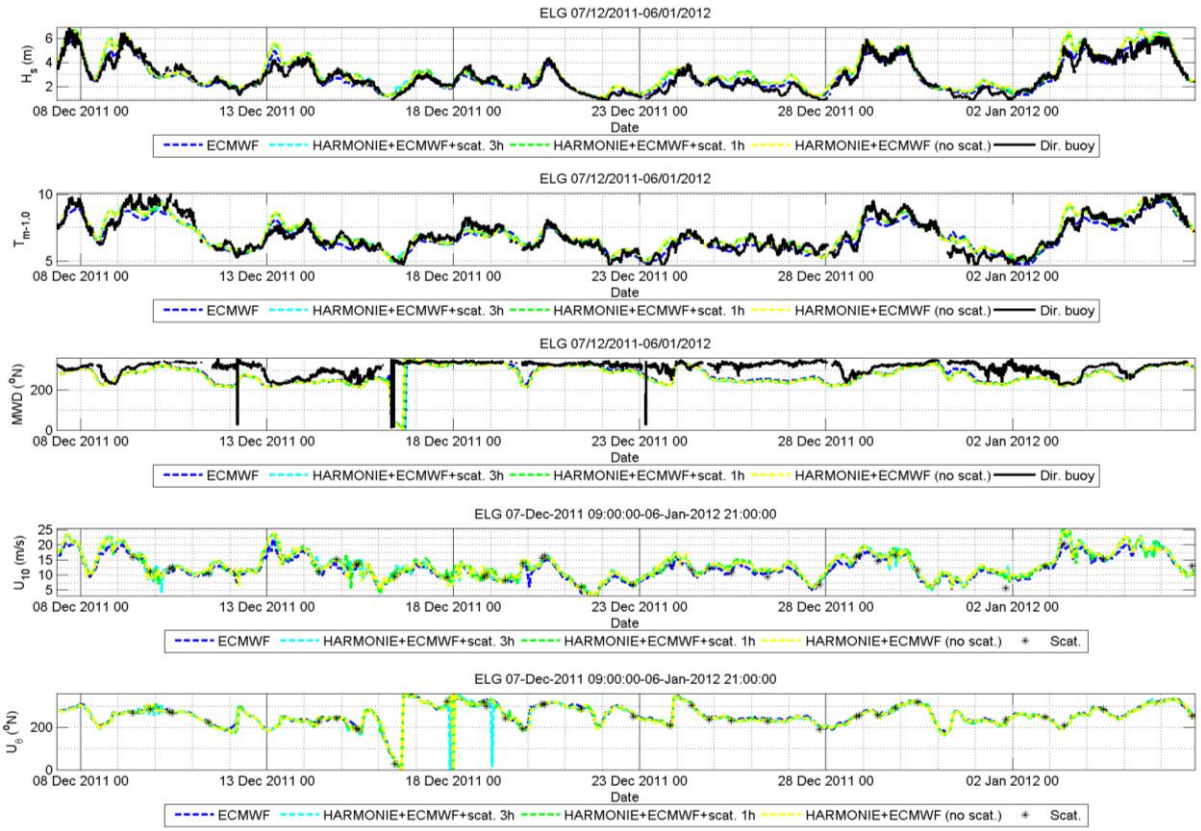

Figure V.51 Comparisons at ELG between the observed and the modeled wind and waves using different forcing winds.

V.3.4.5 Conclusions

The main conclusions that can be taken from this assessment of the SWAN performance is that:

- The SWAN-DCSM model results compare generally well with the observations and the considered wind data compare quite well with the observations.
- The model results using different wind data are quite close to each other, with the differences between model results being much less than the differences between the model results and the observations.
- The SWAN-DCSM errors are larger at the peak of the storms and these tend to be overestimate.

V.3.5 Data assimilation in SWAN

A number of experiments have been carried out by Deltares and KNMI aiming at improving the wave predictions of the SWAN-DCSM model near the coast of the Netherlands. The KNMI experiments, described in Section V.3.3, used assimilation of scatterometer data in their operational high resolution atmospheric model HARMONIE with the 3D-VAR method. These winds have then been used by Deltares to force SWAN-DCSM model, see previous section. The data-assimilation experiments by Deltares involved the direct assimilation of significant wave height measurements in the SWAN-DCSM model, considering uncertainty in the forcing wind and using the HARMONIE wind fields for period 4 and without the assimilation of the scatterometer data as first guess. In all SWAN computations the Westhuysen whitecapping formulation and a bottom fiction coefficient of 0.038 were applied.

The results of these experiments for a subperiod of period 4, the period between the 12th and the 21st of December 2011 are presented next.

V.3.5.1.1 Forcing winds

For the considered period four different wind fields have been received from KNMI and used to force the SWAN-DCSM model in hindcast mode, see §V.3.4.4. These were:

- Fields from the ECMWF model.
- Fields from the HARMONIE model with no assimilation of scatterometer surface winds.
- Fields from the HARMONIE model with 3-hourly assimilation of scatterometer surface winds.
- Fields from the HARMONIE model with hourly assimilation of scatterometer surface winds.

V.3.5.1.2 EnKF settings

Before applying SWAN's OpenDA EnKF implementation to this real case a number of twin experiments using simplified 1D and 2D SWAN models for the North Sea were carried out (Verlaan et al., 2014). The results of these experiments lead to a number of adjustments in SWAN's OpenDA EnKF implementation and lead to a better definition of a number of EnKF settings which have been applied in this study.

The EnKF is sensitive to a number of parameters, such as:

- number of ensemble members;
- assimilated data and their uncertainty; and
- uncertainty specification for forcing wind and boundary waves (control variables).

Although SWAN's EnKF setup can include uncertainty for the open boundary and for the wind forcing, in this application we have only considered it for the wind forcing. The temporal correlation has been set with a scale of 12 hours and a magnitude of 1.0m/s and the spatial correlation has been set as 500km. The two wind components

are treated independently. The noise is specified on the same grid as the wind input. Observations by a directional waverider of H_{mo} have been assimilated every hour at the K13 and Euro platform locations. The standard deviation for errors in the observations was set to 0.2m.

To reduce the computational effort the wind fields have been coarsened from a resolution of 2.5 km x 2.5 km to a resolution of 25 km x 25 km and the SWAN-DCSM computational grid coarsened from a resolution of about 3.6 km x 3.6 km to a resolution of 36 km x 3.6 km. If the assimilation is successful the estimated wind fields can be used to force the high resolution model.

Runs were carried out considering 10, 30 and 100 ensembles. The number of ensembles did not affect the results much but the error statistics of the run with 30 ensembles were slightly better than those of the run using 10 ensembles. The run of the 30 ensemble was carried out is a core-i7 computer with double quad cores. The needed computational time was about 1 hour and 40 minutes per simulation day. This computational time can be reduced if the ensembles are run in parallel, as we have shown in [DR2].

V.3.5.1.3 Results

The results of the experiments are shown in the following figures and tables from locations: K13, Euro platform (EPL in Figure B.2.2), L.E. Goeree (LEG in Figure B.2.2), IJmuiden (MUNS in Figure B.2.2) and ELG (ELD in Figure B.2.2). The figures show the time-series of the computed and observed significant wave height, mean wave period, mean wave direction, wind speed and direction. The tables show the bias, RMSE and correlation (R) between the model results and the observations. For locations K13, Euro platform and IJmuiden wave observations from two measuring devices are available. There are no wind measurements available IJmuiden and ELG and no wave direction measurements available at L.E. Goeree.

In general the comparisons show that the quality of the wind fields is generally high, even that those of the coarser ECMWF model, which show less overestimation than those of HARMONIE. Furthermore, the significant wave height is generally overestimated, especially in the storm at the start of the considered period. In general the EnKF assimilation leads to an improvement of the model results.

Per location the following comments apply:

- **K13** The significant wave height observations from the directional buoy at this location have been assimilated. The positive effect of the assimilation can be seen in a reduction of the RMSE from 0.37 m to 0.21 m when using the first guess wind fields and the ones resulting from the EnKF assimilation. The positive effect is also to be seen in the statistics for the data that were not assimilated. However, although EnKF wind speed and mean wave direction results compare better with the observations than the other model results that, is not the case for Tm-1,0.

- **Euro platform** The significant wave height observations from the directional buoy at this location have been assimilated and this has led to reduction of the H_{m0} RMSE from 0.51 m to 0.23 m when using the first guess wind fields and the ones resulting from the EnKF assimilation. As was the case for K13, the positive effect of the H_{m0} assimilation is also to be seen in the statistics for the data that were not assimilated. For all variables except for the wind direction the EnKF results compare better with the observations than the other model results.
- **L.E. Goeree** The observations at this location have not been assimilated using EnKF, still the results of the EnKF are those comparing in general better with the observations. The H_{m0} RMSE having decreased from 0.57 m to 0.26m when using the first-guess wind fields and the ones resulting from the EnKF assimilation.
- **IJmuiden** Similar to the case for L.E. Goeree, no observations from this location have been assimilated, but still the results of the EnKF are in general in better agreement with the observations. Note also, the good comparison of the results of the simulation using the ECMWF winds and the observations.
- **ELG** The positive effects of the assimilation of the wave heights at K13 and Euro platform can be seen in the comparisons between the EnKF results and the H_{m0} and MWD observations at this location.

K13 12/12/2011-21/12/2011		H_s (m)				$T_{m-1,0}$ (s)			MWD (º)		
		n	bias	RMSE	R	bias	RMSE	R	bias	RMSE	R
in-situ radar	ECMWF wind	238	-0.15	0.32	0.95	-0.19	0.42	0.87			
	HARMORIE (scat. 3h assim.)	238	0.08	0.40	0.94	0.02	0.41	0.85			
	HARMORIE (scat. 1h assim.)	238	0.06	0.36	0.95	0.01	0.41	0.86			
	HARMONIE (no scat.)	238	0.06	0.40	0.94	0.03	0.41	0.86			
	HARMONIE with ENKF	238	-0.02	0.22	0.96	0.13	0.45	0.83			
Directional buoy	ECMWF wind	238	-0.18	0.33	0.95	-0.17	0.41	0.87	-28.8	41.6	0.69
	HARMORIE (scat. 3h assim.)	238	0.05	0.36	0.95	0.04	0.40	0.86	-32.4	46.4	0.66
	HARMORIE (scat. 1h assim.)	238	0.03	0.33	0.96	0.03	0.39	0.87	-32.0	45.0	0.67
	HARMONIE (no scat.)	238	0.03	0.37	0.95	0.05	0.40	0.87	-32.7	46.7	0.66
	HARMONIE with ENKF	238	-0.05	0.21	0.97	0.15	0.47	0.82	-28.0	37.0	0.74
		U_{10} (m/s)				U_{dir} (º)					
		n	bias	RMSE	R	bias	RMSE	R			
Anemometer	ECMWF wind	238	0.34	1.29	0.95	-4.9	12.1	0.96			
	HARMORIE (scat. 3h assim.)	238	0.80	1.58	0.94	-7.8	13.1	0.96			
	HARMORIE (scat. 1h assim.)	238	0.70	1.34	0.96	-7.1	12.8	0.96			
	HARMONIE (no scat.)	238	0.66	1.50	0.94	-8.2	16.8	0.93			
	HARMONIE with ENKF	238	0.35	1.25	0.95	-6.3	12.6	0.96			

Table V.24 Error statistics of the modeled wind and waves at K13.

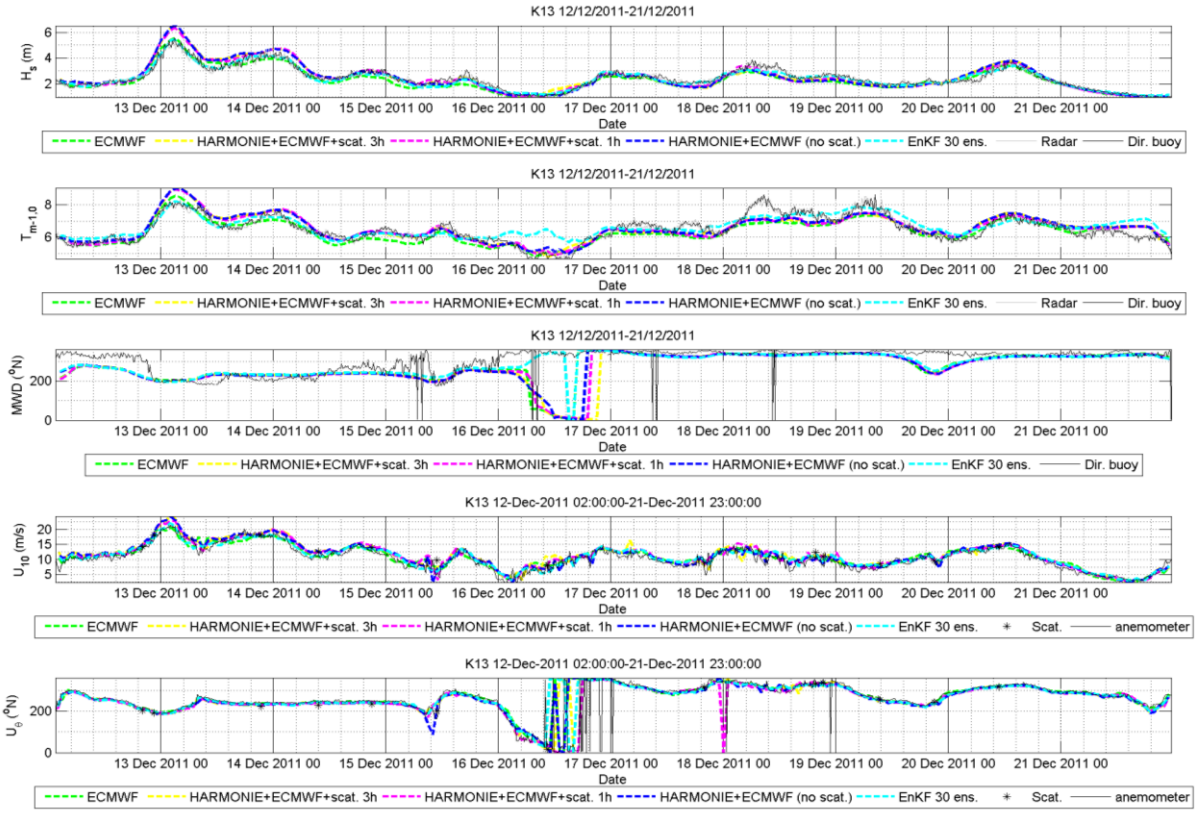

Figure V.52 Comparisons at K13 between the observed and the modeled wind and waves using different forcing winds.

Euro platform 12/12/2011-21/12/2011		H_s (m)				$T_{m-1,0}$ (s)			MWD (º)		
		n	bias	RMSE	R	bias	RMSE	R	bias	RMSE	R
in-situ radar	ECMWF wind	238	-0.02	0.37	0.89	-0.05	0.39	0.80			
	HARMORIE with 3-hourly scat. assimilation	238	0.24	0.51	0.89	0.15	0.43	0.81			
	HARMORIE with hourly scat. assimilation	238	0.24	0.54	0.88	0.15	0.44	0.80			
	HARMONIE (no scat.)	238	0.25	0.52	0.89	0.18	0.44	0.80			
	HARMONIE with ENKF	238	0.07	0.23	0.95	0.10	0.34	0.85			
Directional buoy	ECMWF wind	238	-0.03	0.37	0.89	-0.07	0.41	0.80	-16.8	28.2	0.83
	HARMORIE (scat. 3h assim.)	238	0.23	0.50	0.89	0.13	0.43	0.81	-21.1	32.3	0.81
	HARMORIE (scat. 1h assim.)	238	0.23	0.52	0.88	0.12	0.43	0.80	-21.8	33.5	0.80
	HARMONIE (no scat.)	238	0.24	0.51	0.89	0.15	0.44	0.80	-20.9	31.9	0.82
	HARMONIE with ENKF	238	0.06	0.23	0.95	0.08	0.35	0.84	-19.0	30.3	0.83
		U_{10} (m/s)				U_{dir} (º)					
		n	bias	RMSE	R	bias	RMSE	R			
Anemometer	ECMWF wind	237	-0.18	1.49	0.92	1.7	14.0	0.94			
	HARMORIE (scat. 3h assim.)	237	0.84	1.86	0.92	1.4	13.2	0.95			
	HARMORIE (scat. 1h assim.)	237	0.66	1.87	0.91	1.6	14.0	0.94			
	HARMONIE (no scat.)	237	0.70	1.77	0.92	2.9	13.4	0.95			
	HARMONIE with ENKF	237	0.18	1.44	0.92	1.7	14.0	0.94			

Table V.25 Error statistics of the modeled wind and waves at Euro platform.

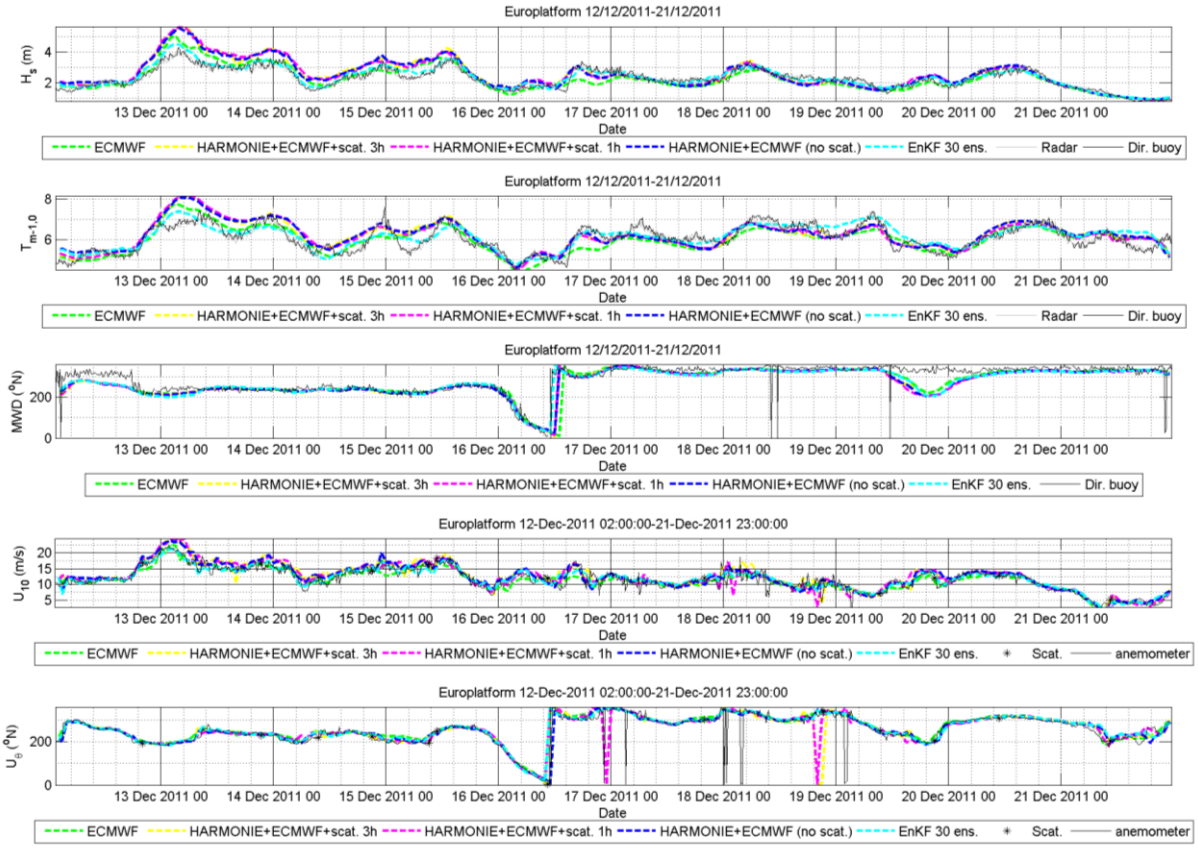

Figure V.53 Comparisons at Euro platform between the observed and the modeled wind and waves using different forcing winds.

L.E. Goeree 12/12/2011-21/12/2011		H_s (m)				$T_{m-1,0}$ (s)		
		n	bias	RMSE	R	bias	RMSE	R
in-situ radar	ECMWF wind	237	0.07	0.44	0.79	0.00	0.43	0.76
	HARMORIE (scat. 3h assim.)	237	0.29	0.56	0.80	0.18	0.48	0.76
	HARMORIE (scat. 1h assim.)	237	0.30	0.59	0.78	0.18	0.49	0.74
	HARMONIE (no scat.)	237	0.30	0.57	0.80	0.20	0.49	0.75
	HARMONIE with ENKF	237	0.02	0.26	0.90	0.16	0.38	0.82
		U_{10} (m/s)				U_{dir} (º)		
		n	bias	RMSE	R	bias	RMSE	R
Anemometer	ECMWF wind	236	0.02	1.55	0.89	0.73	12.04	0.96
	HARMORIE (scat. 3h assim.)	236	0.86	2.09	0.87	-4.83	15.28	0.94
	HARMORIE (scat. 1h assim.)	236	0.89	2.07	0.88	-3.60	12.11	0.96
	HARMONIE (no scat.)	236	0.85	1.97	0.89	-4.07	13.45	0.95
	HARMONIE with ENKF	236	-0.34	1.61	0.89	-1.48	11.98	0.96

Table V.26 Error statistics of the modeled wind and waves at L.E. Goeree.

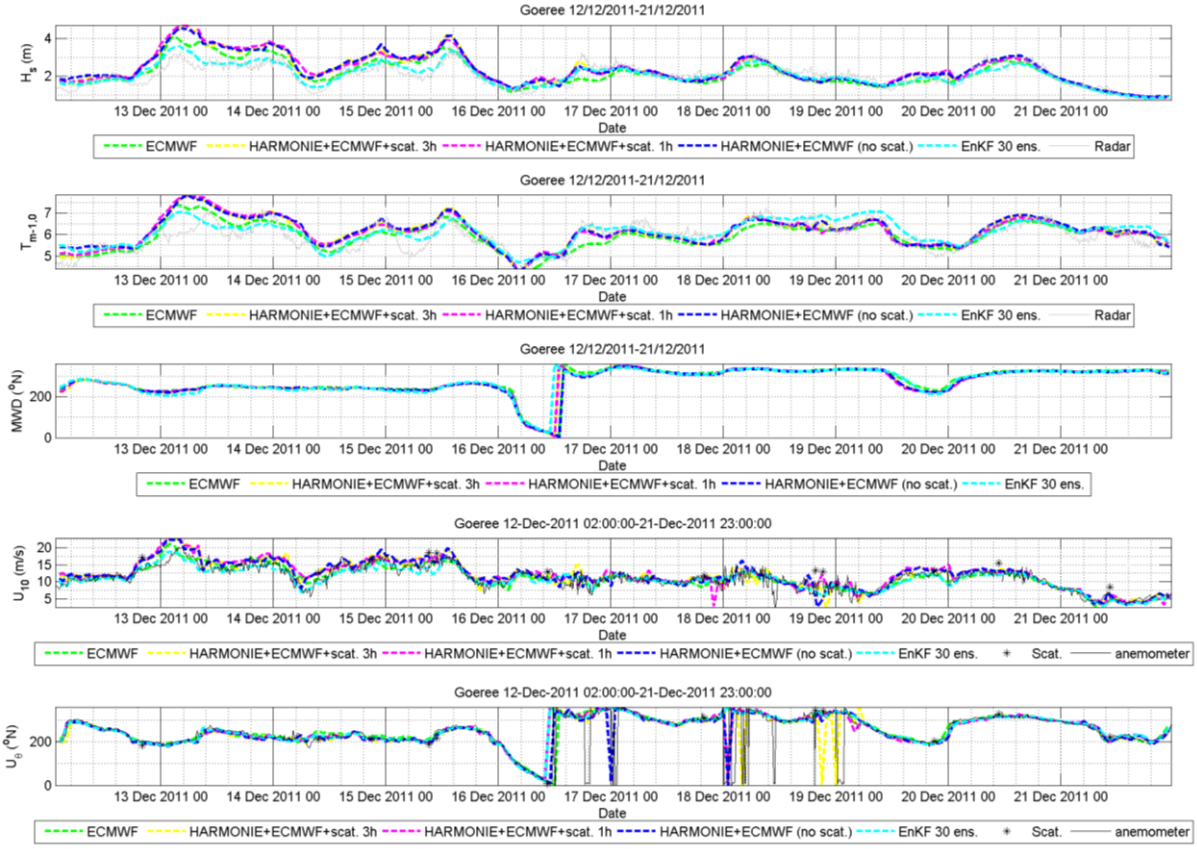

Figure V.54 Comparisons at L.E. Goeree between the observed and the modeled wind and waves using different forcing winds.

IJmuiden 12/12/2011-21/12/2011		H_s (m)				$T_{m-1,0}$ (s)			MWD (°)		
		n	bias	RMSE	R	bias	RMSE	R	bias	RMSE	R
Buoy	ECMWF wind	225	-0.04	0.34	0.91	-0.15	0.45	0.83			
	HARMORIE (scat. 3h assim.)	225	0.21	0.48	0.92	0.05	0.45	0.82			
	HARMORIE (scat. 1h assim.)	225	0.21	0.49	0.92	0.05	0.43	0.83			
	HARMONIE (no scat.)	225	0.20	0.48	0.92	0.04	0.44	0.83			
	HARMONIE with ENKF	225	0.00	0.22	0.95	0.04	0.40	0.85			
Directional buoy	ECMWF wind	226	-0.05	0.35	0.91	-0.18	0.47	0.83	-23.8	36.9	0.77
	HARMORIE (scat. 3h assim.)	226	0.20	0.48	0.91	0.02	0.46	0.81	-27.1	41.1	0.74
	HARMORIE (scat. 1h assim.)	226	0.20	0.49	0.92	0.02	0.45	0.82	-27.0	41.7	0.73
	HARMONIE (no scat.)	226	0.19	0.48	0.91	0.02	0.45	0.83	-26.8	40.2	0.75
	HARMONIE with ENKF	226	-0.01	0.22	0.95	0.01	0.39	0.87	-24.0	36.4	0.78

Table V.27 Error statistics of the modeled waves at IJmuiden.

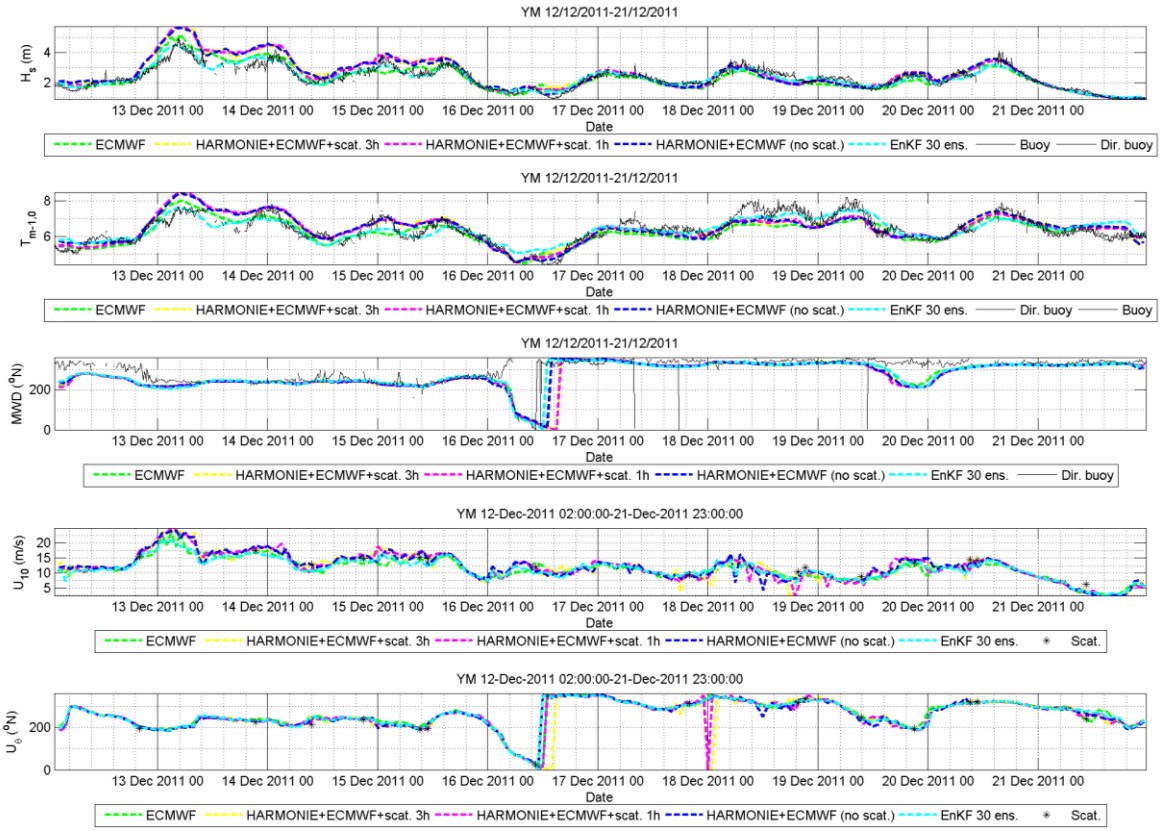

Figure V.55 Comparisons at IJmuiden between the observed and the modeled wind and waves using different forcing winds.

ELG 12/12/2011-21/12/2011		H_s (m)				$T_{m-1,0}$ (s)			MWD (°)		
		n	bias	RMSE	R	bias	RMSE	R	bias	RMSE	R
Directional buoy	ECMWF wind	214	-0.09	0.34	0.92	-0.13	0.40	0.85	-23.2	38.1	0.75
	HARMORIE (scat. 3h assim.)	214	0.20	0.44	0.91	0.10	0.40	0.84	-25.0	40.6	0.73
	HARMORIE (scat. 1h assim.)	214	0.19	0.43	0.92	0.07	0.39	0.85	-25.4	40.7	0.73
	HARMONIE (no scat.)	214	0.18	0.44	0.92	0.09	0.41	0.83	-24.2	38.8	0.75
	HARMONIE with ENKF	214	-0.04	0.29	0.93	0.11	0.43	0.81	-23.5	35.9	0.77

Table V.28 Error statistics of the modeled waves at ELG

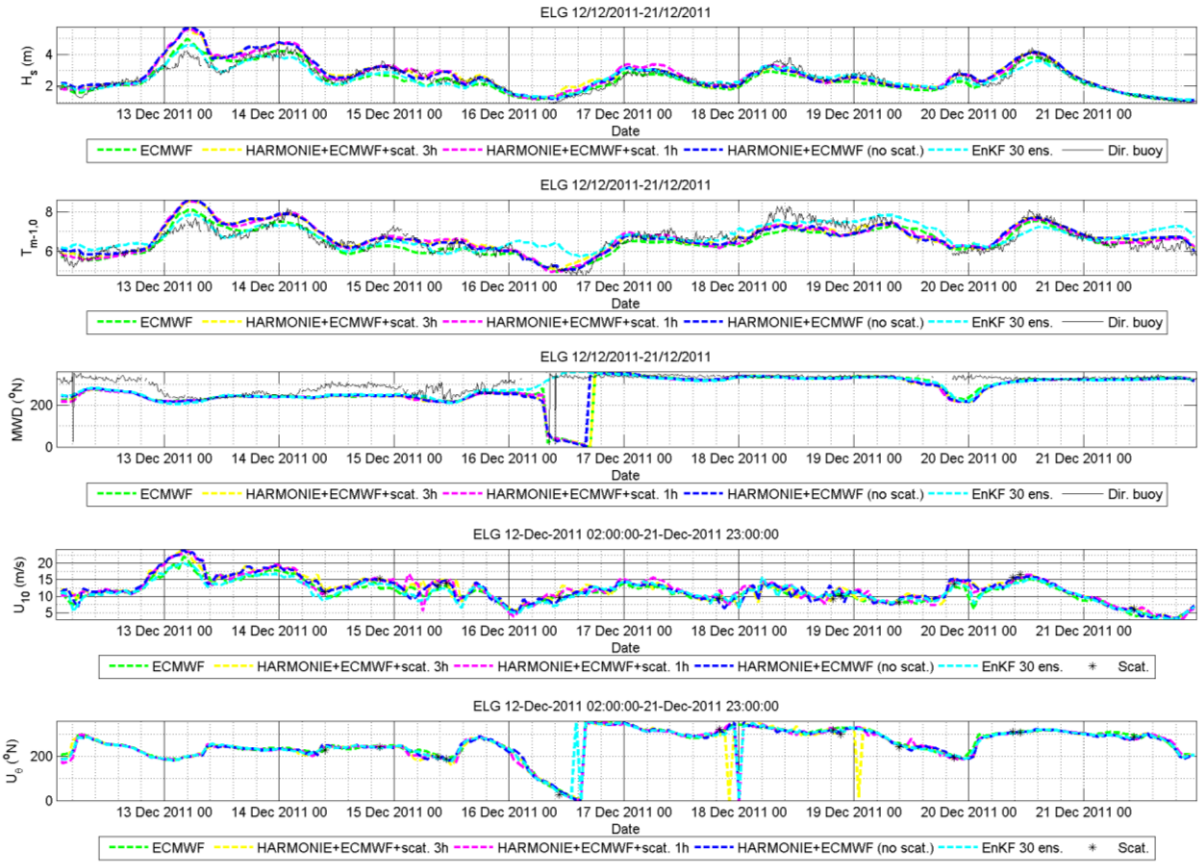

Figure V.56 Comparisons at ELG between the observed and the modeled wind and waves using different forcing winds.

V.3.5.1.4 Conclusions

The assimilation of significant wave height measurements in SWAN-DCSM was shown to be very efficient, leading to improvements in error statistics for variables other than the significant wave height and at locations other than those of the observations used. The obtained improvements of the error statistics are larger than those obtained assimilating scatterometer winds in the atmospheric model. This is mainly because the quality of the wind fields seem already to be very high.

Computational times were kept at acceptable levels by coarsening the grid of the wind fields and the computational grid of SWAN-DCSM.

V.4 German Bight

V.4.1 In Situ Data /Strom Simulations

As representative examples for the validation of the wave model results in the German Bight some comparisons with measurements will be discussed for October 2013. In the end of that month the severe storm Christian afflicted the coasts of Germany with high wind speeds above 30 m/s and significant wave heights of about 8 m. Time series of wind and wave heights at FINO station are given on Figure V.57. At 28th of October during storm Christian the wind speed increases rapidly to 30 m/s causing brake down of several buoys and making impossible to provide measurements for this extreme event.

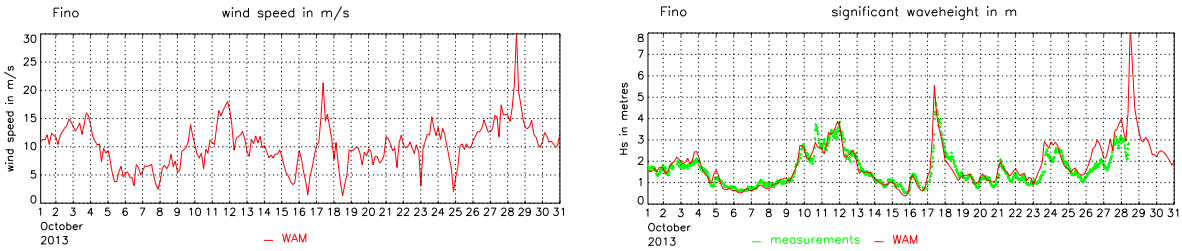

Figure V.57 Time series of wind and wave heights at FINO station (storm Christian).

At Elbe and Helgoland stations (see Figure IV.2 for their coordinates) the wave heights were lower than the ones at FINO station during Christian and they continuously recoded the wave parameters during the storm event. Figure V.58 includes the corresponding comparisons for significant wave heights, Tm_2/T_z-periods and total wave directions at the location Elbe. The agreement between measured and modelled wave parameters is very good. The peak on the 28th of October (3 pm UTC) in H_s of about 6 m and in Tm_2 of about 8 s is well predicted by the wave model.

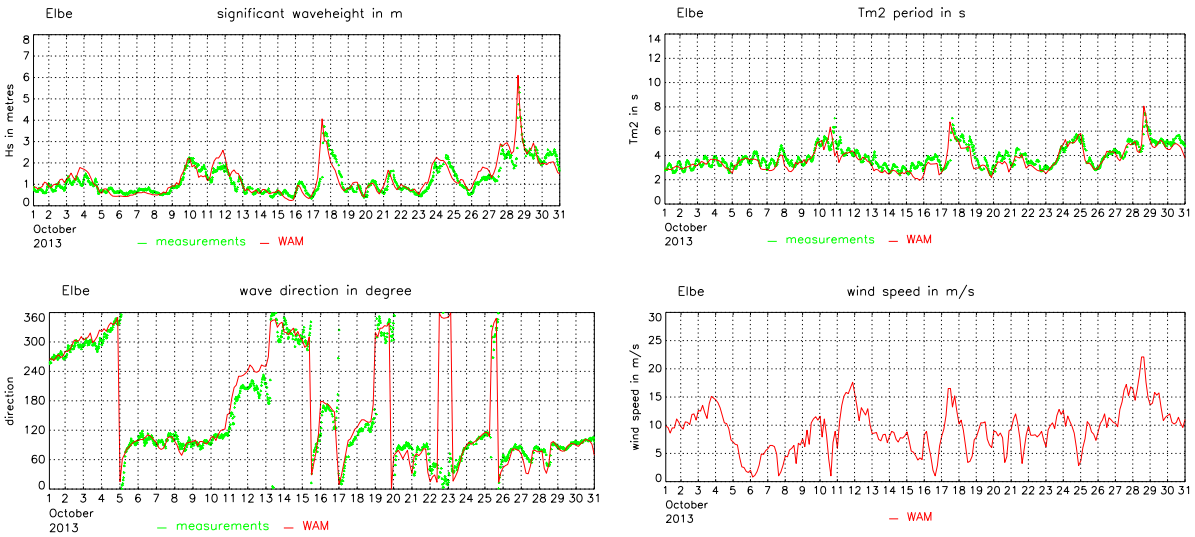

Figure V.58 Time series of measured and computed wave parameters at the location Elbe.

The same is valid for the comparisons done at Helgoland station despite the small underestimation at the peak by the model. The measured peak is higher here (7.7 m) compared with the Elbe station peak. The statistical analysis of the comparisons (see Table V.29) supports the good quality of the nested-model wave simulations for the German Bight area.

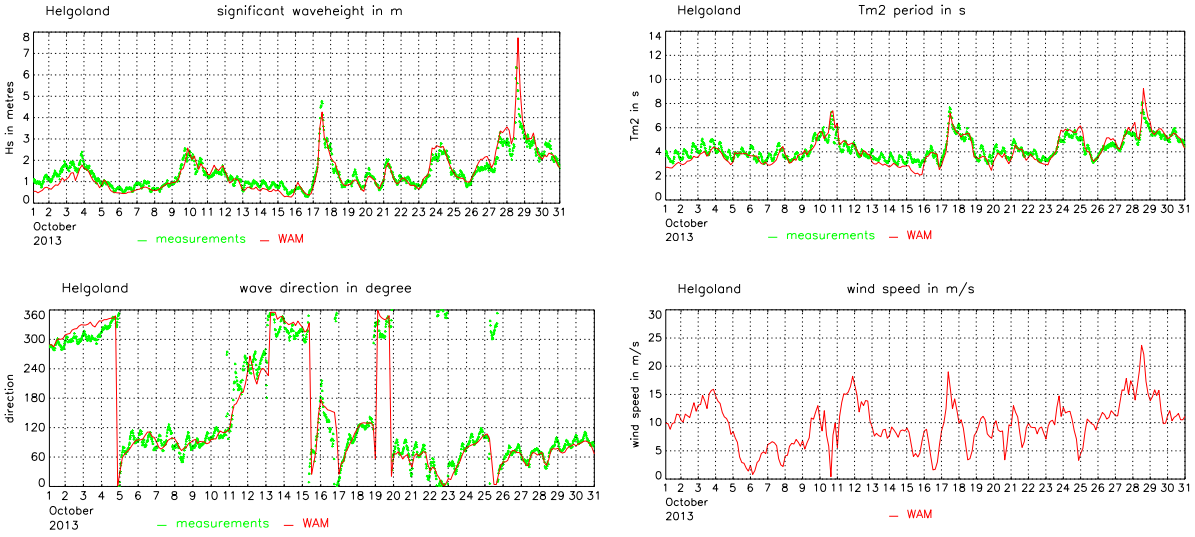

Figure V.59 Time series of measured and computed wave parameters at the location Helgoland.

buoy	number of comparisons	mean of measurements	bias	root mean square error	skill	scatter index
H_s	-	(m)	(m)	(m)	-	(%)
Fino	218	1.59	0.11	0.33	0.86	19
Elbe	247	1.23	0.08	0.31	0.84	25
Westerland	247	1.17	0.14	0.28	0.88	21
Helgoland	247	1.45	-0.03	0.30	0.90	20
Tm_2/T_z		(s)	(s)	(s)		
Fino	218	4.53	-0.15	0.50	0.74	11
Elbe	247	3.92	-0.23	0.52	0.71	12
Westerland	247	4.07	-0.12	0.74	0.74	18
Helgoland	247	4.27	-0.11	0.52	0.80	12
skill : reduction of variance, scatter index : standard deviation*100/mean of the measurements						

Table V.29 Hs statistics for October 2013 at buoys located in the German Bight.

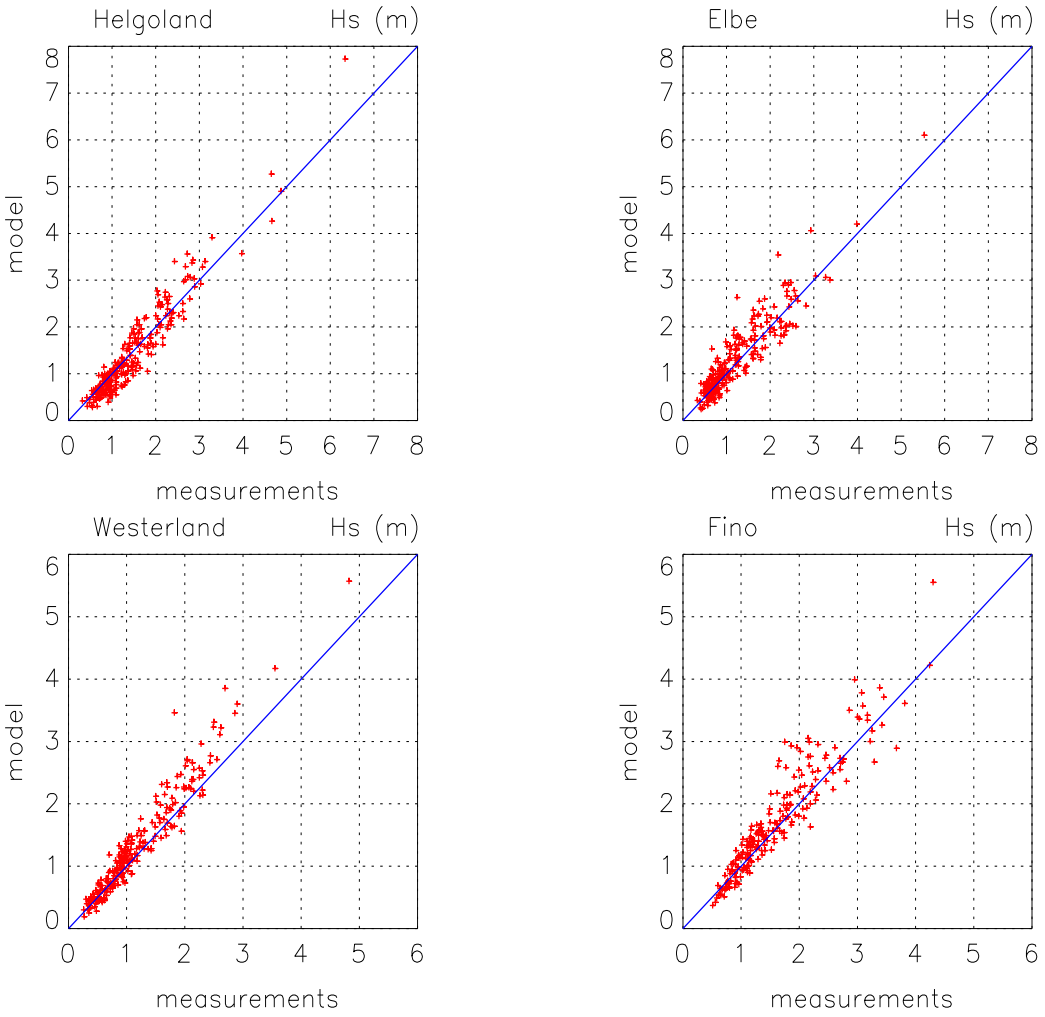

Figure V.60 Scatter plots for measured and computed wave heights for October 2013.

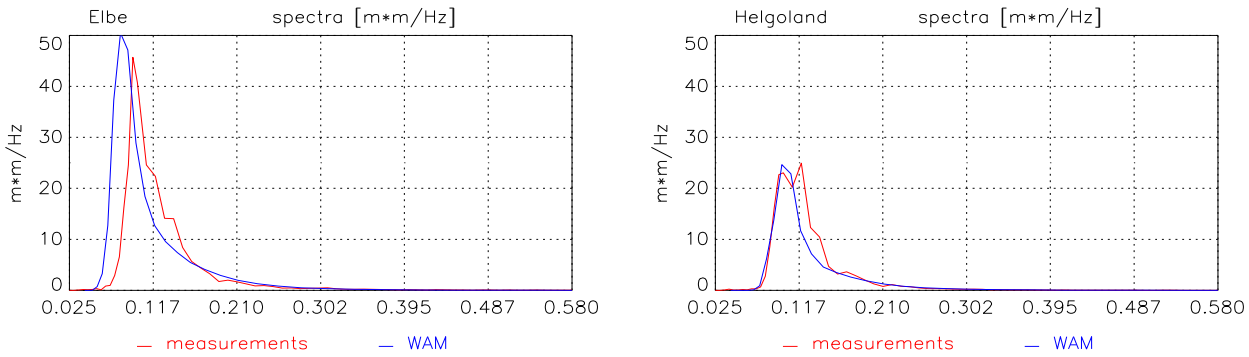

Figure V.61 Comparison of measured and computed one-dimensional wave spectra at location Elbe (left) at the peak of storm Christian on 20131028 15:27 UTC (model results: 15:00 UTC) and at location Helgoland (right) at an intermediate peak on 20131017 11:46 UTC (model results: 12:00 UTC).

V.4.2 Assimilation using Neural Networks – separate tests for boundary value and wind field retrieval

In order to test the newly developed assimilation scheme and with the aim of using it in storm situations two experiments have been performed.

The forecast was re-run to obtain first-guess values using the following to setups by:
1. using the correct wind fields but no boundary values:
2. using the correct boundary values but no wind .

The synthetic HF-radar data together with: (i) correct PC's of wind-fields or (ii) correct PC's of boundary data were applied to the two NN's emulating the adjoint WAM. The NN output (either innovated wind fields or boundary values) was optimised using the Levenberg-Marquardt algorithm described in the previous sections and in [DR2]. Figure V.62 and Figure V.63 show a comparison between NN estimated values and the ones estimated directly from the wave model.

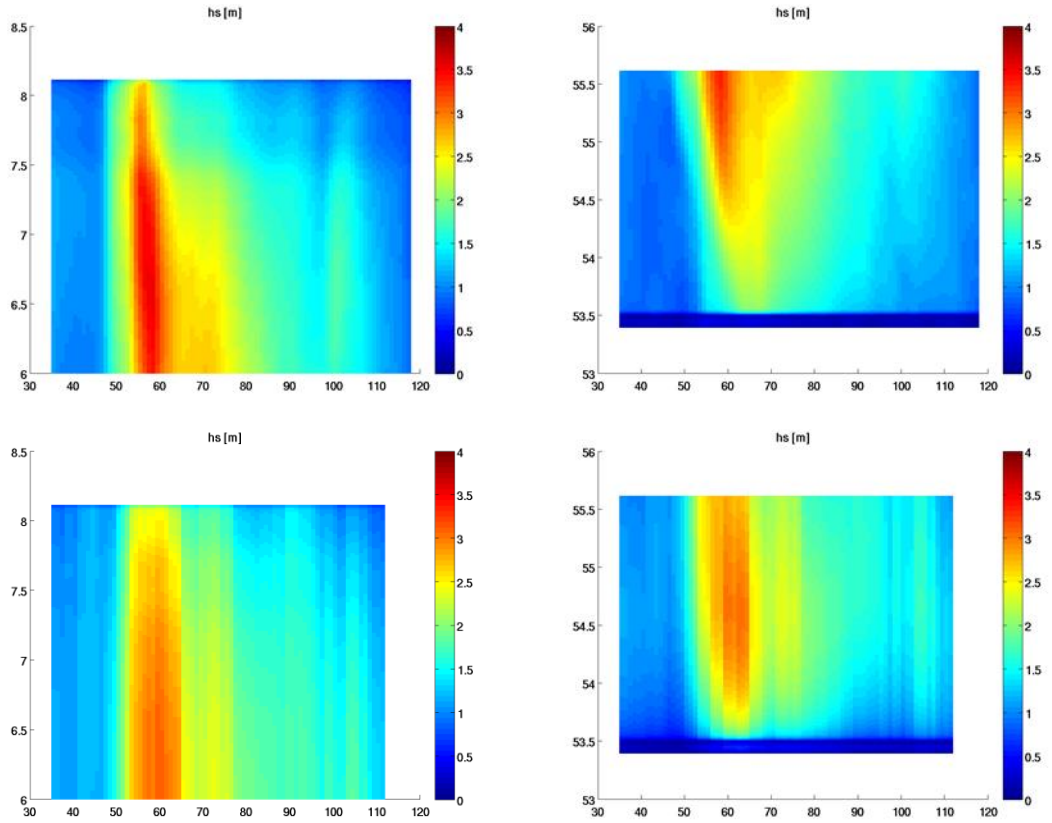

Figure V.62 Boundary values taken from WAM model run (top) and as emulated by Neural Network based assimilation scheme (bottom). Left: significant wave height at Northern boundary, right: at Western boundary. The x-axis is hours since July 12th 12 UTC, y-axis is either longitude or latitude.

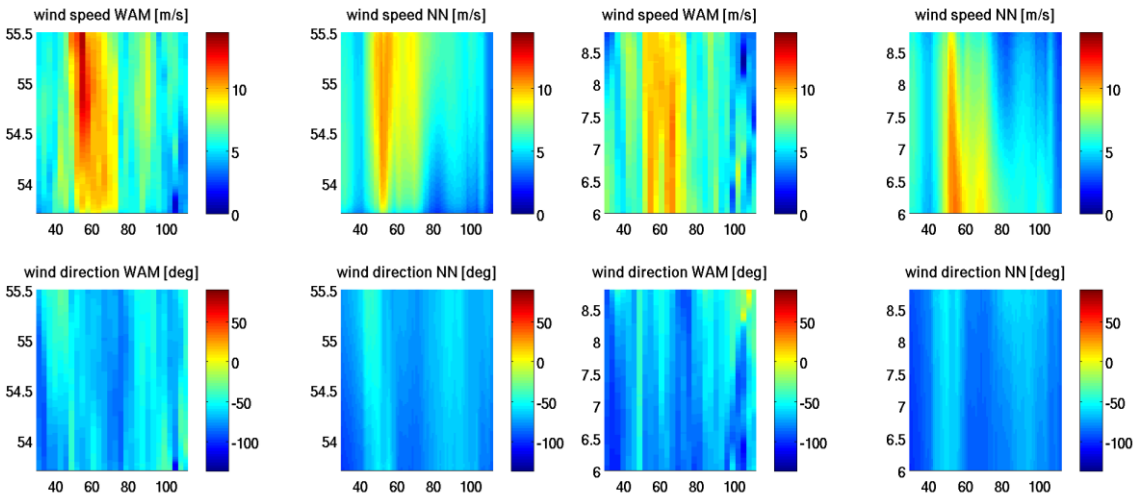

Figure V.63 Same as Figure V.62 but for wind fields (wind speed and direction). Left: profiles along 8 degrees East, right: profiles along 54 degrees North in the German Bight area.

The emulated boundary values match the correct values well over the whole

assimilation period. The storm event (around 60 hours) is slightly underestimated in the East and North and slightly overestimated in the South.

Similar behaviour is observed in the experiment for the emulated wind fields. The wind speed during the storm is underestimated, especially towards the Northern open boundary and the East coast. In addition, the predicted storm duration is also. Emulated wind directions are mainly northern, whereas the correct wind fields contain a (small) eastward component. From the comparisons of the results we can conclude that the overall performance of the NNs data assimilation is very promising.

As next, more advanced experiment, the emulated wind fields and boundary values were used together with either correct boundary values or correct wind fields as input to the NN emulating WAM. The thus obtained wave heights and periods give an estimate of innovations that could be achieved in WAM. The mean of the absolute relative errors in the area where data were assimilated is shown on Figure V.64 and Figure V.65.

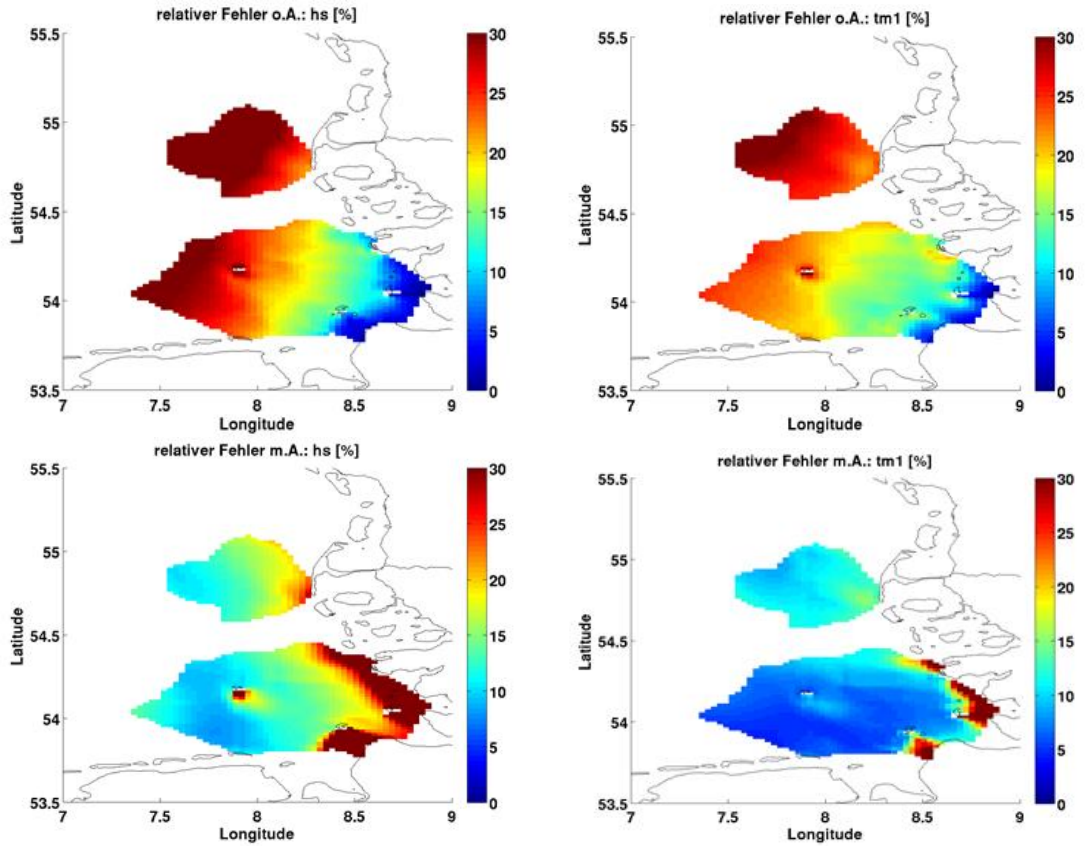

Figure V.64 Mean of the absolute relative errors for significant wave height (left) and m1 period (right). The first guess WAM model run (no boundary values) is on top and below innovations as emulated by Neural Network using correct wind fields and boundary values from assimilation scheme.

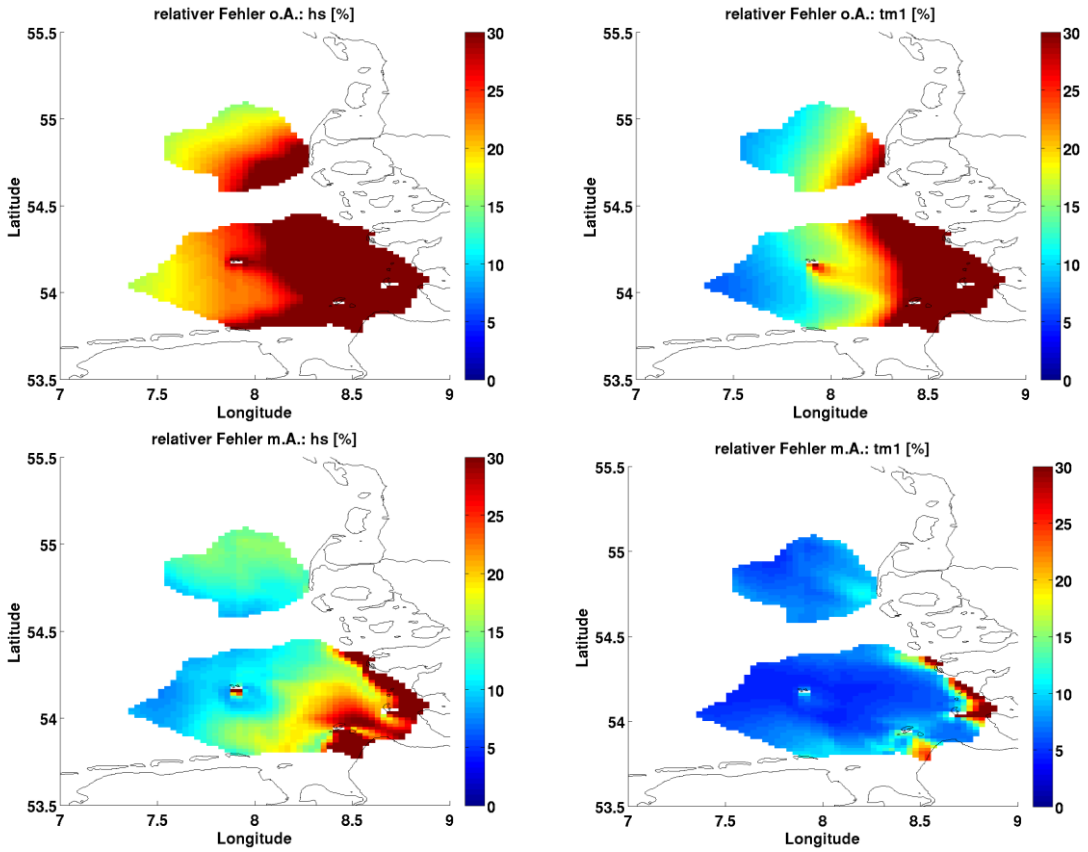

Figure V.65 Same as Figure V.64 but with first guess WAM model run without wind fields and innovations as emulated by Neural Network using correct boundary values and wind fields from assimilation scheme.

Evidently, first-guess errors are largest in the open sea area when boundary values are neglected and largest towards the coast when suppressing wind fields, since the shallow wave state is dominated by local wind. The errors of the innovated wave parameters have been reduced significantly in either case throughout most of the measurement area in particular for tm1 wave period. In summary, the validation of the assimilation scheme gives promising results in the open ocean. It can be supposed that running the wave model with forcing derived by using NN data assimilation method, the large errors in the shallow regions will be diminished.

V.4.3 Assimilation using Neural Networks – first experiment of combined retrieval

After validating the two inverse NN's separately we now present a first experiment of combined retrieval of wind-fields and boundaries.

We used the same data as for the previous experiments. However, the first-guess scenario is more realistic because the shifting of both wind and boundary fields is consistent. The two inverse NN's gave first estimates of improved winds and boundaries. This was iterated until the error $\chi^2$for both nets did no longer decrease. As in the previous chapter an estimate of innovations was calculated using the forward NN. The results are shown in Figure V.66. The errors of significant wave

height decreased throughout the deep water area, only close to the coast the error increased as was expected from the previous experiments. For the tm1 period errors improved only in the Northern area but still are quite small (note the different scales for SWH and tm1).

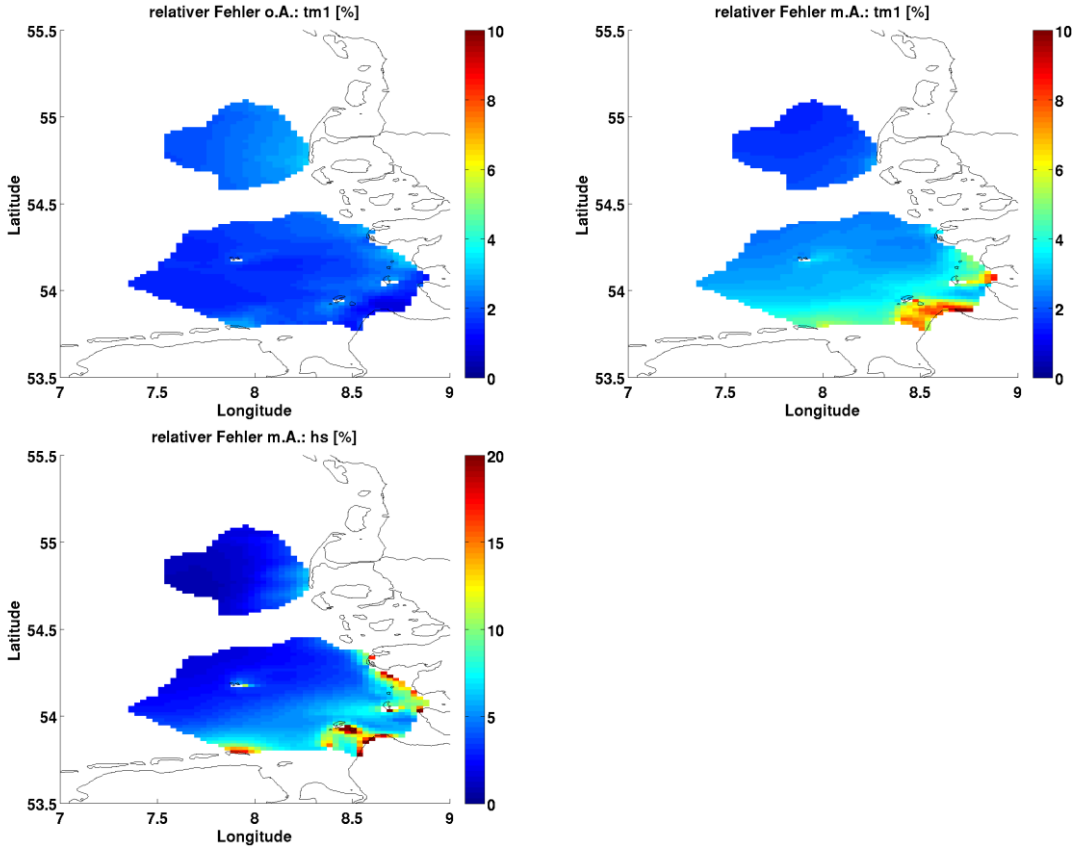

Figure V.66 Same as Figure V.64 and Figure V.65 but with first guess WAM model run with time shifted wind fields and boundary values. The innovations are emulated by combined use of the two inverse Neural Networks.

In Summary, the results of the twin experiments are very promising and confirm the practicability of the newly developed assimilation technique. The method has several advantages compared with other methods: it can be easily implemented for other wave models and regions since it only requires model output and measurements. Additionally, it can be adapted to specific problems (derive improved wind fields and/or boundary conditions or any other model parameter of interest). Data Assimilation using Neural Networks is computational very efficient compared to other advanced (non-local) assimilation strategies. The Neural Network software is freely accessible to any interested user.

V.5 North Atlantic

V.5.1 Introduction

Puertos del Estado and AEMET have worked in two subtasks related with the improvement of coastal wave forecasts: Cross validation of satellite data, in-situ observations and wave forecasts and Comparison of unstructured model versus nesting.

In the first case, Aemet-PdE has applied a triple-collocation method to calibrate and estimate wave heights for the period June 2008- July 2009 in Cantabrian Sea from Pde-WAM model, Jason2 and Cantabrian PdE buoy network. This work is described in section V.4.2.

In regard with the second subtask, two SWAN applications have been developed and compared for the Canary Islands, one based on a standard regular grid and the other one on based on a unstructured grid. Both applications have been compared with buoys from the PdE's buoy network. This work is described in section V.4.3.

V.5.2 Cross-validation of satellite data, in-situ observations and wave-forecasts.

V.5.2.1. Introduction.

Cantabrian WAM data used is forced by analyzed HIRLAM wind fields, provided by AEMET and the model has a spatial resolution of 5'x5' and the time resolution is 3 hours.

The buoy data used in this study come from PdE database. This data has been processed and have passed a quality control. Time resolution is 1 hour.

Buoy	Lat	Lon	Depth
Estaca de Bares Buoy	44.12ºN	7.67ºW	1800 m
Cabo de Peñas Buoy	43.75ºN	6.16ºW	615 m
Santander – IEO Buoy	43.85ºN	3.77ºW	2500 m
Bilbao-Vizcaya Buoy	43.64ºN	3.05ºW	2136 m
Villano-Sisargas Buoy	43.50ºN	9.21ºW	386 m
Cabo Silleiro Buoy	42.12ºN	9.43ºW	600 m

Table V.30 Depth and location of buoys used for triple collocation.

Jason2 significant wave height was obtained from the DEOS radar altimeter data base system (http://rads.tudelft.nl/rads/rads.shtml). All observations for which Hs>18 are neglected. Also observations that deviate more than 4 times the standard deviation of the hourly data from its mean are discarded.

It is important to remark that to use this methodology the three datasets must have uncorrelated errors. This method is explained in Stoffelen (1998), Janssen et al. (2006) and Caires and Sterl (2003).

V.5.2.2. Data collocation

From the Jason2 measurements satellite "super observations" have been formed, by grouping together the consecutive observations crossing a 1.5º by 1.5º latitude-longitude region. The satellite super observation is the mean of these grouped data points after the quality control. These satellite super observations are in 1.5º by 1.5º latitude-longitude region centered at the buoy location.

Due to the difficulty to get data to work with the triple collocation method, the process to obtain the wave model field (which has been interpolated in an hourly resolution) is doing two model counterparts, one referring to the satellite observation X_{alt}, and one referring to the buoy observation. To ensure that the error estimation is not affected by the collocation error, only collocations satisfying a relative difference at most 5% are considered.

The number of observations with the triple collocation has pretty decreased, and there are locations where any location wasn't found.

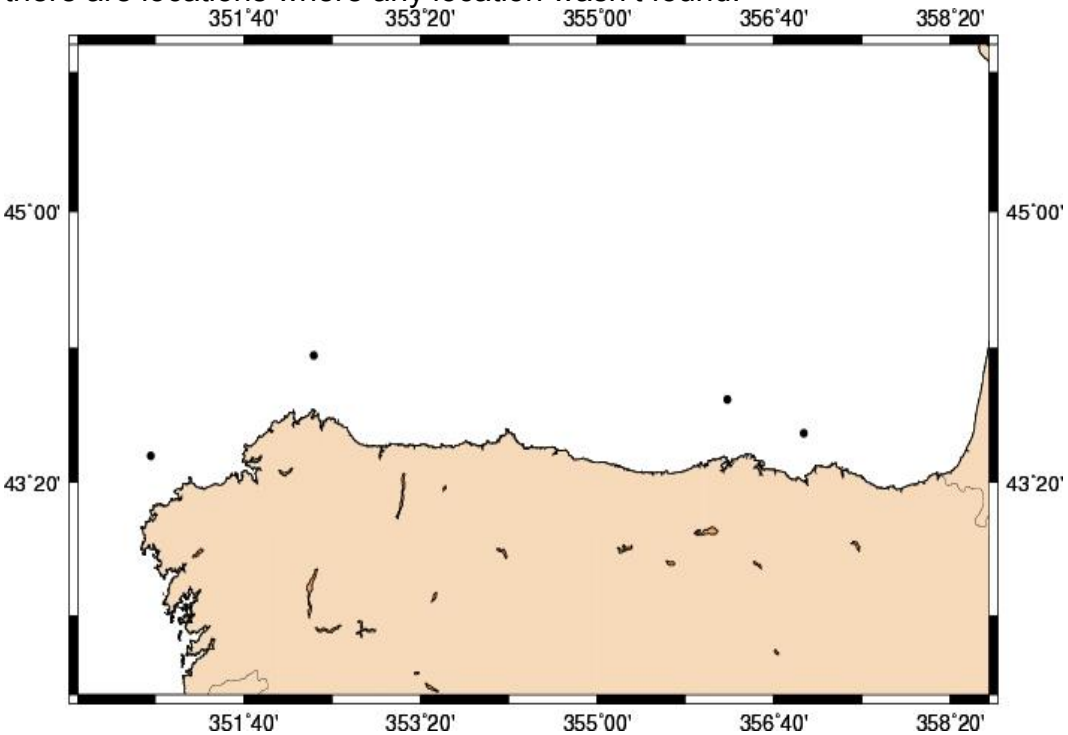

Figure V.67 Number of observation per location for triple satellite, Buoy and WAM model collocation.

V.5.2.3 Error estimation and results

The method used to determinate the respective errors from the three independent estimates of the truth and to calibrate the data by minimization is described in Janssen et al. 2006. Also MyWave-D4.1 explained how this method works:

A triple collocation essentially provided 3 estimates of the truth, X,Y,Z. It is assumed that the measurements depend on truth T in linear fashion:

$X = b_x T + e_x$
$Y = b_y T + e_y$
$Z = b_z T + e_z$

Where e_x , e_y, e_z denote the residual errors and b_x, b_y, b_z are the linear calibration constants. Assuming that the measurement results have uncorrelated errors, and introducing new variables to eliminate the calibration constant (X' = X/$b_x, \ldots$) it is obtained:

$$X' - Y' = e_{x'} - e_{y'}$$
$$X' - Z' = e_{x'} - e_{z'} \quad (7)$$
$$Y' - Z' = e_{y'} - e_{z'}$$

Multiplying the first equation in Eq. (7) above with the second gives the variance error in X' in terms of the variance of X' and the covariance's of X' and Y', X' and Z'. Multiplying the first and the third equation gives the variance error in Y' and the variance error of Z' is obtained by multiplying the second and the third. This leads to:

$(< e_x{}^2 >=< (X' - Y'), (X' - Z') >..)$

The errors are uncorrelated so this approach can be used to estimate the variance of the error in each of them.

The truth is unknown, so only two of the three calibration constants can be obtained. In fact, the relative calibration factors can be computed with respect to a reference and it does no matter statistically which one.

Taking X arbitrary, b_x = 1, b_y=<yz>/<xz> *and* b_z = <yz>/<xy>..

With this method, we have estimated the RMS error of collocated wave datasets. We have applied this approach to the estimation of wave height error in Cantabrian Sea WAM , Jason 2 and PdE buoys network.

We have obtained $b_y = 1.15, b_z = 1.09, e_x = 0.31, e_y = 2.14e-07$ and $e_z = 0.41$.

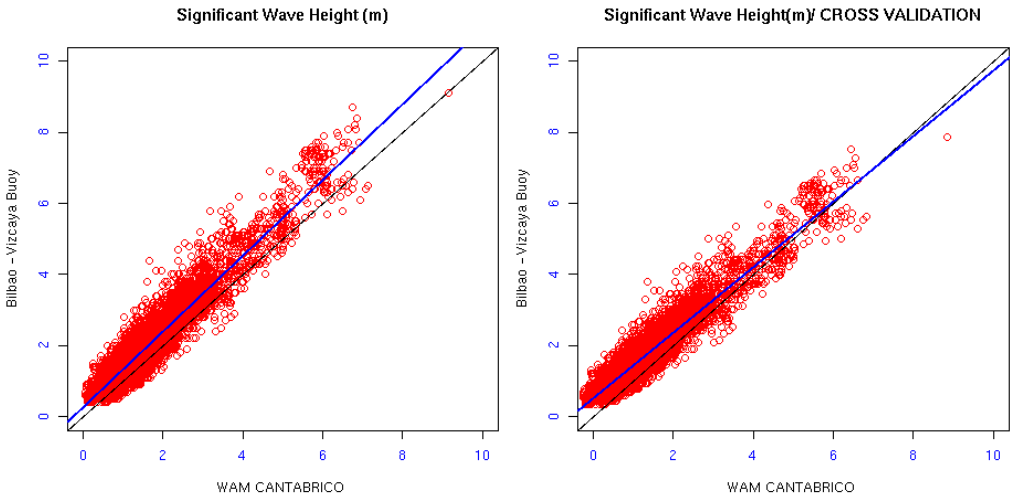

Figure V.68 Scatter diagrams of WAM model data with buoy data for the period June 2008- July 2009 on the right results with data calibrated with the triple collocation method.

Due to the problems to find altimeter samples to form datasets for the period June 2008-July 2009, we have worked with only 29 datasets to apply the triple collocation.

After applying triple collocation method, the comparisons of significant wave height between model and buoy calibrated are better, with the exception of values near zero, where the difference has increased.

V.5.3 Comparison of unstructured model versus nesting

V.5.3.1 Configuration of grids

Aemet-PdE have developed two SWAN applications for Canary Islands, one with a standard regular grid and the other one with an unstructured grid that increases the resolution around each island of the archipelago. These two applications run with boundary conditions provided by PdE's Atlantic WAM application (15'x 15' resolution) and wind fields from the AEMET HIRLAM application (3'x3' resolution).

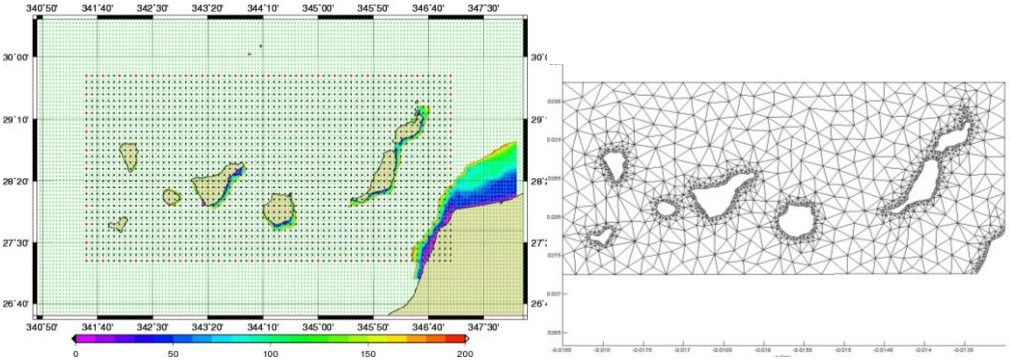

Figure V.69 Nested regular (left) and unstructured (right) SWAN grid of the Canary Islands.

The regular grid has a resolution of 5'X5' which results in 1980 computational grid points.
The unstructured grid has been generated by BatTri, taking into account the resolution of the regular grid, the boundary condition, the coastline provided by the NOAA Coastline Extractor, the imposition of a minimum angle of 25º and a maximum element area of 500km^2 and a refinement mesh imposing $\frac{h}{area} = (\frac{\max(deep)}{\max(area)})$.

The result is an unstructured grid with 1376 computational points and a refinement round the coast.

Due to the complexity of the region with islands and defined on an almost closed rectangle, running unstructured SWAN has not been straight forward. Although from 40.72 version SWAN can theoretically work with unstructured grid, only with the last version (40.91) did we managed to run with the unstructured grid. The grid generated by BatTri did not work directly and some changes in the grid elements were done. We also encountered a problem with the boundary conditions, i.e. the boundary command option SEGMENT to define parametric spectra at the boundary does not work properly, only the option SIDE works.

V.5.3.2. Results and Conclusion

Both applications are operative, the computational time of the unstructured SWAN is 8 minutes and of the SWAN with regular grid is 6 minutes. The models run in Linux 64 bits in a sequential mode on PdE supercomputer. Outputs are in a regular grid with a resolution of 5'. The interpolation of the unstructured SWAN in a regular output is the cause of the unstructured model takes more than regular.

Significant wave height maps and time series are generated in each run. The results have been compared with the PdE buoy network.

Figure V.70 Buoys used for validation.

Buoy	Lat	Lon	Depth
Santa Cruz de Tenerife Buoy	28,46ºN	16,23ºW	56m
Las Palmas Este Buoy	28,05ºN	15,39ºW	30m
Tenerife Sur Buoy	27,99ºN	16,58ºW	710m

Table V.31 Depth and location of buoys used for validation

Significant wave height and mean direction have from regular and unstructured applications have been compared with the three buoys of Canary archipelago. The results show that it is not better the behaviour of the unstructured model.

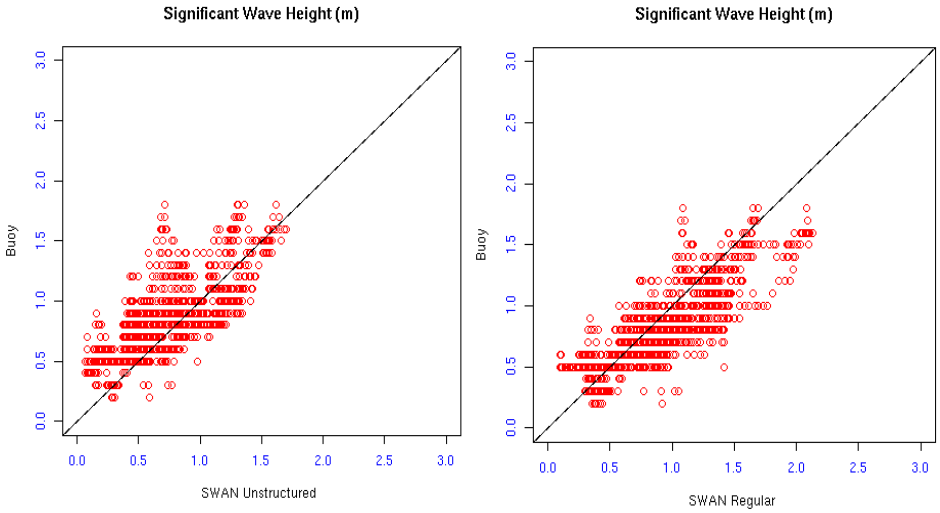

Figure V.71 Significant Wave Height Scatterplots. On the left, unstructured SWAN. Regular model on the right.

Significant Wave Height	Number of data	Correlation coefficient	Slope of regression line	RMSE	Bias	Spread
SWAN Unstructured	1452	0.82	0.65	0.25	-0.1	0.27
SWAN Regular	1452	0.78	0.67	0.27	0.13	0.40

Table V.32 Statistical results for Significant Wave Height.

Mean Direction	Number of data	Correlation coefficient	Slope of regression line	RMSE	Bias	Spread
SWAN Unstructured	1264	0.70	0.89	32.1	16.15	0.14
SWAN Regular	1288	0.83	1.01	28.83	11.49	0.12

Table V.33 Statistical results for Mean Direction.

Results indicate that in this case, SWAN unstructured does not work better than the model with a regular computational grid. A negative bias means that the model underpredicts, but both models have a reasonably overall bias.

Finally, although unstructured grids are a powerful method to work with complicated bottom topography in shallow areas and with an irregular shoreline, it is not always easy to work with them. The target of getting more resolution taking less CPU time has not been achieved in these experiments. Further improvements to the SWAN model are needed to improve the computational speed of the unstructured version.

VI DISCUSSION

Wave forecasts play an important part in the planning and safety in the coastal region, since many activities at and near the coast benefit from advance warning of adverse conditions. While waves generated in deeper water can be modelled adequately on a global scale, these waves undergo large changes when approaching the coast. In mountainous regions, or when there are islands near the coast, the coastal wave conditions are also modified locally by local changes to the wind. For this purpose a number of regional high-resolution coastal wave models are available around Europe. Most of these forecasting systems are based on one of the spectral wave models, WAM, SWAN or WaveWatch (not considered). For accurate forecast of the local wind modification high-resolution meteorological models are applied. Most of these models receive boundary conditions from a large-scale or global wave model, such as the wave forecasts from ECMWF.

Ideally, these regional wave forecasts would be connected by a three-way coupling between waves, hydrodynamics and meteorology, while at the same time assimilating all relevant observations effectively. However, this is far from the current practise. To our best knowledge no forecasting system in the world currently has all these features, though the global systems are ahead of most regional systems in this respect. At this stage of the development, it was considered most effective to improve the use of observations for coastal wave forecasting, with a number of different applications, with different wave models, different observations and different techniques.

In the following paragraphs we first discuss the results of the individual applications before making an attempt to integrate the results:

1. Satellite observations of surface winds over water are now routinely available and generally of high quality. In MyWave the processing of the raw data was improved to provide valid data closer to the coast, which is highly relevant for coastal wave forecasting. Experiments were performed to assimilate scatterometer winds into a high-resolution HARMONIE meteorological model. These experiments encountered some technical issues that were all resolved. The assimilation of scatterometer observations did improve the accuracy of the results at analysis time, but unfortunately the impact was quickly lost during the forecast. We believe that this is caused by a more fundamental issue: the high-resolution HARMONIE model generates features at a scale comparable to or smaller than the resolution of the scatterometer, which does not lead to satisfactory results for the assimilation with the 3D-VAR method. Perhaps, spatial filtering techniques or the use of an ensemble can improve this, but clearly there is a need for further research.
2. The high-resolution HARMONIE winds were used subsequently to force a regional SWAN wave model. It was shown that assimilation of the scatterometer wind observations did improve the accuracy of the wave model runs, but the impact was not very large. The impact can probably be improved

further in the future by improvements of the assimilation of scatterometer into the HARMONIE model.

3. In another experiment, in-situ observations of waves by wave buoys and radar were assimilated into a SWAN model of the same region. The well-known EnKF data-assimilation, here as implemented in the OpenDA toolbox, was used to perform the assimilation. In these experiments, the full 4D spectral wave energy density was corrected directly by the assimilation. A big advantage of this approach is that many more observation types, such as wind-speed and direction, wave-direction, wave-period and wave-spectra, can in principle be assimilated. Moreover, the method attempts to correct other aspects of the wave spectrum in a consistent way. It was shown for example that a higher observed wave-height also creates increments that increase the wind speeds and wave-period. Disadvantages of this approach are the need to run an ensemble of models; and the large amount of spectral data that needs to be adjusted during the analysis. These drawbacks were partially countered by the use of parallel computing and the use of a reduced spatial resolution. The results are very promising and are currently being considered for pre-operational trial runs in the wave forecasting system. Additional research is needed to study the impact of various other observation types. One interesting experiment would be the assimilation of the scatterometer winds into the wave model instead of the meteorological model. This can potentially result in a greater impact than in the meteorological model.
4. HF radar is another observation type that was studied. An innovative data-assimilation method, based on Neural Networks (NNs), was developed. The method uses two steps. In the first step the wave observations are used to estimate the boundary condition and wind input. In the second step, the NN-model predicts the waves at the observation locations with an iterative method. Important advantages of the NN-method are that it can in principle be applied to a wide range of observations and models, that it is easy to implement and the computational efficiency during the operational phase. Disadvantages are that the operational phase needs to be preceded by a training phase containing sufficient and homogeneous data. Moreover, the training phase needs to be updated whenever one wishes to include new observations.
   Unfortunately, the HF-RADAR wave observations were of insufficient quality to be assimilated. It was decided to continue the experiments with synthetic observations. Clear positive impacts of the data-assimilation were shown for two stormy periods. These promising results need to be followed up by further experiments with real observations in the future, before operational use can be contemplated.
5. Validation of model accuracy against more than one type of observations can provide additional information about the accuracy of model and observations. Traditionally, models are evaluated against observations that are assumed to represent the truth. However, with more and more accurate models, it is increasingly useful to account for errors in the observations. The use of multiple observation datasets can provide further insight in this. Here the triple-collocation technique was applied that assumes that the errors of the different observations and the model are uncorrelated and uncorrelated with

the signal as well. Results for the Adriatic show marked differences in accuracy of significant wave height measured by different satellites, where Saral-Altika is more accurate than Jason-2 and Cryosat. Also the error estimates for in-situ observations vary per location, which larger relative errors for more sheltered locations with on average smaller wave heights. This can be explained by larger representativity errors compared to the model and satellite or by the smaller signal amplitude. Care must be taken to verify the assumption of uncorrelated errors. The altimeter wave height for example gave inconsistent results against lead-time, which is an indication that the assumptions were violated.

6. Wind waves undergo large changes when approaching the coast while the situation is much more homogeneous in the open ocean. Unstructured grids can be adapted in a more flexible manner to provide the right accuracy both near the coast as in deep water. One unstructured model was developed for the Canary Islands. Although it was possible to create an unstructured grid that had higher coastal resolution, sufficient resolution in deep water and still fewer grid-cells than the structured grid model, no increase in accuracy or computational performance was found. Some possible causes for these results are: a larger number of iterations for the unstructured solver, too large changes in size between adjacent grid-cells, or too large changes in incidence angle of the waves between adjacent grid-cells for the unstructured grid model. Further research is needed to identify the real causes and test various remedies.

The experiments described above clearly show that a synthesis of a fully three-way coupled high-resolution ocean-atmosphere-wave model that can assimilate all relevant observations is not within reach. Still, progress has been made on a number of aspects working towards this synthesis. Since, it may still take considerable time to reach this fully coupled assimilative system; one also has to consider the intermediate steps towards this goal. On this path several approaches were studied to assimilate new observation types, to speed-up the assimilation process and to increase our knowledge of the errors present in todays' forecasting systems. These approaches have varying stages of maturity and are by no means exhaustive. We recommend further research to further increase our understanding and eventually design fully coupled assimilative forecasting systems.

VII DISSEMINATION AND IMPACT

VII.1 Dissemination

The results of this workpackage have been disseminated in a number of ways. In this and in the previous deliverables a large extent of the work is reported. Access to the project deliverable is, therefore, important and should be supported.

Besides reporting our study in the deliverables our results have been disseminated in a number of meetings and conferences and through publication. Currently a number of papers are in preparation or have already been submitted to journals.

Besides dissemination of scientific results through publications, it is also important that the applied and developed software is made available. All of the software used for modelling and data-assimilation in this report is available for other researchers. The following list shows where to obtain access to the software:

1. WAM wave model including OI data-assimilation → https://github.com/mywave/WAM/
2. SWAN wave model → http://swanmodel.sourceforge.net/.
3. HARMONIE → http://www.hirlam.org/index.php/hirlam-programme-53/access-to-the-models.
4. OpenDA data-assimilation toolbox → http://www.openda.org.
5. Neural Network tools → contact Kathrin Wahle at HZG Germany for a copy.

VII.2 Impact

The results of this study have led to a number of new insights and opportunities in the forecasts of coastal waves and winds. For instance:

- The improved processing of the raw Scatterometer data has lead to the availability of valid wind data closer to the coast, which is highly relevant for coastal wave forecasting.
- The EnKF wave assimilation results are very promising and are currently being considered for pre-operational trial runs in the wave forecasting system.

VIII CONCLUSIONS

The main goals of this work package have been to explore new methodologies in data assimilation, improve the use of near shore remote sensing data and connect large-scale forecast to near shore forecasts.

Data-assimilation has seen a strong development of new methods recently. Application of these new insights mainly from meteorology and oceanography to wave-forecasting can improve the amount of information extracted from observations. Furthermore, recently new techniques were developed to improve the processing of scatterometer winds near the coast.

Regional wind and wave forecasts for the considered study areas have been compared with: scatterometer winds, altimeter wave heights, wave-buoy observations and in-situ wind observations to make a realistic assessment of the accuracy of each, to identify inconsistencies and to suggest potential improvements. Special attention has been given to particularly difficult areas as the Northern Adriatic Sea. Here the surrounding mountains make the wind forecast particularly challenging, while the proximity of coastlines stresses the satellite capability.

Unstructured grids can be more easily adapted to increase resolution locally than structured grids, which makes this approach very attractive for coastal wave-forecasting. Here the unstructured-grid approach is compared to the more traditional nesting of refined local structured-grids.

In the framework of the MyWave project we have applied innovative data-assimilation techniques with the aim of improving near shore North Sea wave forecasts. The considered approaches were a) 3D-VAR assimilation of coastal scatterometer winds in HARMONIE; b) EnKF assimilation of wave observation in SWAN and c) NN assimilation of wave observation in WAM. As reported, the results of the first trials using mainly synthetic data have led to promising results. In accordance with the project planning, we shall now move on to applying these techniques for assimilation of real wind and wave data considering a number of relevant North Sea storms.

REFERENCES

S. Caires and A.Sterl, 2002: Validation of ocean wind and wave data using triple collocation

Baas, P., 2014: *Final report of WP1 of the WTI2017-HB Wind Modelling Project*. KNMI Scientific Report; WR 2014-02 (http://www.knmi.nl/bibliotheek/knmipubWR/WR2014-02.pdf), August 2014.

Behrens, A., Günther, H., 2009 : Operational wave prediction of extreme storms in Northern Europe, Natural Hazards, Volume 49, Issue2 (2009), Page 387 – 399 (DOI 10.1007/s11069-008-9298-3

Bidlot, J., P. Janssen and S. Abdalla, 2005: A revised formulation for ocean wave dissipation in CY29R1. MEMORANDUM RESEARCH DEPARTMENT of ECMWF, April 7, 2005 File: R60.9/JB/0516

Bishop, C.M., 1995. *Neural Networks for Pattern Recognition*. Clarendon Press, Oxford.

ECMWF, 2011: IFS DOCUMENTATION – Cy37r2 Operational implementation 18 May 2011 PART VII: ECMWF WAVE MODEL (via http://www.ecmwf.int/research/ifsdocs/ CY37r2/IFSPart7.pdf).

Figa-Saldaña, J., J. J.W. Wilson, E. Attema, R. Gelsthorpe, M. R. Drinkwater, and A. Stoffelen, 2002: The advanced scatterometer (ASCAT) on the meteorological operational (MetOp) platform: A follow on for the European wind scatterometers, Can. J. Remote Sens., 28(3), 404–412, doi:10.5589/m02-035

Günther, H., S. Hasselmann, P.A.E.M. Janssen, 1992: The WAM Model Cycle 4.0. User Manual. Technical Report No. 4, Deutsches Klimarechenzentrum, Hamburg, Germany. 102 pages.

Haykin, S., 1994: Neural networks: a comprehensive foundation. Prentice Hall PTR.

Hersbach, H. and P.A.E.M. Janssen, 1999: Improvements of the short fetch behavior in the WAM model. J. Atmos. Ooceanic Techn., 16, 884-892.

Janssen, P. A.E.M, S. Adballa, H. Herbach, and J.- R. Bidlot, 2006: Error estimation of Buoy, Satellite, and Model Wave Height Data.

Komen, G.J., L.Cavaleri, M. Donelan, K. Hasselmann, S. Hasselmann and P.A.E.M. Janssen, 1994: Dynamics and modelling of ocean waves. Cambridge University Press, Cambridge, UK, 560 pages.

Monbaliu, J., R. Padilla-Hérnandez, J.C. Hargreaves, J.C. Carretero Albiach, W. Luo, M.

Portabella, M., and A. Stoffelen, 2004: A probabilistic approach for SeaWinds data assimilation, Q. J. R. Meteorol. Soc., 130, pp. 127–152, doi: 10.1256/qj.02.205.

Sclavo, and H. Günther, 2000: The spectral wave model WAM adapted for applications with high spatial resolution. Elsevier Coastal Engineering 41, pp 41-62.

Sakov, P., G. Evensen and L. Bertino, 2010: Asynchronous data assimilation with the EnKF. Tellus A, 62.

Schiller, H., 2007. Model inversion by parameter fit using NN emulating the forward model - Evaluation of indirect measurements, Neural Networks, 20 (4), Computational Intelligence in Earth and Environmental Sciences, pp. 479-483.

Stoffelen, A., 1998: Toward the true near-surface wind speed: Error modeling and calibration using triple collocation, J. Geophys. Res., 103(C4), 7755–7766, doi:10.1029/97JC03180.

Stoffelen, A. and D. Anderson, 1997: Scatterometer Data Interpretation: Measurement Space and Inversion, J. Atmos. and Oceanic Technol. 14, 1298-1313.

Verhoef, A., Portabella, M., Stoffelen, A., 2012: High-Resolution ASCAT scatterometer Winds near the coast, IEE Trans. On GeoSc. and Rem. Sens., vol. 50, No. 7.

Verhoef, A., and A. Stoffelen, 2011: ASCAT coastal winds validation report, OSI SAF Report, SAF/OSI/CDOP/KNMI/TEC/RP/176

Vogelzang, J., A. Stoffelen, A. Verhoef, and J. Figa-Saldaña (2011), On the quality of high-resolution scatterometer winds, J. Geophys. Res., 116, C10033, doi:10.1029/2010JC006640.

Vogelzang, J., A. Stoffelen, A. Verhoef, J. de Vries and H. Bonekamp, 2009: Validation of two-dimensional variational ambiguity removal on SeaWinds scatterometer data, J. Atm. Oceanic Technol., 7, 26, 1229-1245, doi:10.1175/2008JTECHA1232.1

WAMDI Group. The WAM Model–A Third Generation Ocean Wave Prediction Model. Journal of Physical Oceanography, 18, 1775-1810, 1988.